



NUMERICAL INVESTIGATION ON DYNAMIC RESPONSE OF BUS STRUCTURE BY OPTIMIZING THE FRAME SIZE

By

TEWODROS GAMEA

A thesis submitted as partial fulfillment for the degree of Master of Science in
Mechanical and Electrical Engineering (Automotive engineering)

to

Department of Mechanical Engineering

Addis Ababa Science and Technology University

MAY 2021

CERTIFICATION

This is to certify that the thesis prepared by Mr. Tewodros Gamea Workachew entitled "numerical investigation on dynamic response of bus structure by optimizing the frame size" and submitted as partial fulfillment for the degree of Master of Science complies with the regulations of the university and meets the accepted standards concerning originality, content, and quality.

Signed by examining board:

External Examiner

Dr. Anteneh Mohammed. signature, date
(Anteneh) 19/12/2013

Internal examiner:

Dr. Dinku Seyoum signature, date
(Dinku) 19/12/2013

Chairperson:

Mezid A. signature, date
(Mezid) 19/12/2013

DGC chairperson
Elias Gebremichael Habte
Head, Department of
Mechanical Engineering

signature, date

Collage Dean/Associate Dean for GP:

signature, Date

CANDIDATE'S DECLARATION

I hereby declare that this thesis entitled "*Numerical Investigation on Dynamic Response of Bus Structure by Optimizing the Frame Structure*" was prepared by me, with the guidance of my advisor. The work contained herein is my own except where explicitly stated otherwise in the text, and that this work has not been submitted, in whole or in part, for any other degree or professional qualification.

Tewodros Gamea:

Student Name



Signature

30/10/13

Date

This is to certify that the above statement made by the candidates is correct to the best of our knowledge and belief. This thesis has been submitted for examination with our approval.

Bisrat Yoseph (Ph.D.):

Principal Advisor



Signature

30/10/13

Date

APPROVAL PAGE

Title:

NUMERICAL INVESTIGATION ON DYNAMIC RESPONSE OF
BUS STRUCTURE BY OPTIMIZING THE FRAME STRUCTURE

Student Name:

Towodros Gamea Workachew

Signature, Date:

[Signature] 30/10/13

Approved by the examining committee members:

	Name	Academic Rank	Signature	Date
Advisor:	<u>Dr. Bisrat Yoseph</u>	<u>Assistant prof.</u>	<u>[Signature]</u>	<u>30/10/13</u>
Co-Advisor:	_____	_____	_____	_____
Examiner: (int)	<u>Dr. Dincal Seyoum</u>	<u>(PhD)</u>	<u>[Signature]</u>	_____
Examiner: (ext)	<u>Dr. Anteneh M.</u>	<u>Associate prof.</u>	<u>[Signature]</u>	<u>19/10/13</u>
Chairperson:	_____	_____	_____	_____
DGC Chairperson:	<u>Elias Gebremichael Habte</u>	<u>Head, Department of</u>	<u>[Signature]</u>	_____
Associate Dean for	<u>Mechanical Engineering</u>	_____	_____	_____
Graduate	_____	_____	_____	_____

ABSTRACT

This research presents the numerical investigation of the dynamic response of bus structure by optimizing the frame size. The study is very important to fill the gap in the area of vehicle structure response due to maneuverability. Here it is aimed to optimize the weight of bus body structure by evaluating its stress and deformation. The study worked at Bishoftu bus model ZK6118HGA, modeled with solid work 18 and analysis has been done with ANSYS 19.0. Braking left corner, and right cornering test has been performed. Optimization has been done by replacing oversized RHS (rectangular hollow section) with lower-sized RHS. The improved structure was also investigated with the cornering and braking tests. The weight of the improved structure is significantly lower than the original structure. The study revealed that the weight of the bus body structure was reduced by 93.58 kg. Which is about 3.07% of the whole structure weight. The procedure used for the analysis is validated using analytical calculations on simply supported overhanging beam comparing to software verification.

Keywords: Braking, deformation, left cornering, optimization right cornering, steel structure, stress.

ACKNOWLEDGEMENT

First of all, I would like to thank God for the endless blessings and gifts.

I would like to thank Dr. Bisrat Yoseph for his scientific and technical guidance and support throughout this research, without his continuous corrections and constructive comments this project wouldn't have been successful. I am grateful to all staff of the Bishoftu automotive industry.

I would also like to thank my father Gamea workachew, my mother Almaz Kassa, my sister Sina, my brother choye, and my beloved Novia for their love, understanding, support, and encouragement.

Last but certainly not least, I would like to thank all of my friends for their encouragement, and support with different materials and ideas.

TABLE OF CONTENT

CERTIFICATION	I
CANDIDATE’S DECLARATION	II
APPROVAL PAGE	III
ABSTRACT.....	IV
ACKNOWLEDGEMENT	V
TABLE OF CONTENT	VI
LIST OF FIGURE.....	IX
LIST OF TABLE	XIII
NOMENCLATURE	XV
1 CHAPTER ONE INTRODUCTION.....	1
1.1 Background.....	1
1.2 Bishoftu Automotive Engineering Industry.....	3
1.3 Statement of The Problem	4
1.4 Research Objective	5
1.4.1 General Objective	5
1.4.2 Specific Objective.....	5
1.5 Significant (Outcomes) of the Study.....	5
1.6 Scope of The Study	5
1.7 Limitations of The Study	6
2 LITERATURE REVIEW	7
2.1 Fundamental concept	7
2.1.1 Vehicle Fixed Coordinate System	7

2.1.2	Earth Fixed Coordinate System.....	7
2.1.1	Mechanics of Vehicle	8
2.2	Review of Literatures.....	9
2.2.1	Analysis of original bus bodies	9
2.2.2	Analysis of the improved bus structure	10
2.3	Summary of Literature Reviews	13
2.4	Research Gap	13
3	MATERIALS AND METHODOLOGY.....	15
3.1	Mathematical Model of Bus Structure	15
3.1.1	For static loading condition	15
3.1.2	Dynamic Modelling of the Vehicle	21
3.2	Numerical modeling.....	25
3.2.1	Bus geometry	25
3.2.2	Finite element meshing of the bus body structure	29
3.2.3	Inputs for Finite Element Analysis	31
3.2.4	Boundary Conditions used in the analysis.....	32
3.3	Boundary conditions of the Modified structure	36
3.4	Research Methodology	36
3.5	Data Collection	39
4	RESULTS AND DISCUSSION.....	43
4.1	Validation of the method used	43
4.1.1	Deflection of the beam	43
4.1.2	Bending moment.....	45
4.1.3	Verification of manual analysis of the beam with ANSYS Workbench	49

4.2	Dynamic analysis of original bus structure.....	52
4.2.1	Braking Load Condition.....	52
4.2.2	Cornering Load.....	55
4.3	Dynamic analysis of improved bus structure.....	63
4.3.1	Braking load condition	63
4.3.2	Cornering load condition	67
4.4	Comparison of the original structure and improved bus structures.	75
4.4.1	Mass of the structure.....	75
4.4.2	Braking loading condition	78
4.4.3	Right cornering.....	80
4.4.4	Left cornering	83
5	CONCLUSION AND RECOMMENDATION	85
5.1	Conclusion	85
5.2	Recommendation	86
	REFERENCE.....	87
	APPENDIX-A.....	92
	APPENDIX-B.....	105

LIST OF FIGURE

Figure1. 1 Bishoftu bus model ZK6118HGA.....	2
Figure1. 2 Workflow of Bishoftu automotive industry	4
Figure 2. 1 vehicle reference system [10].....	8
Figure 3. 2 Horizontal structure member.....	18
Figure 3. 3 Free body diagram of braking[49].....	23
Figure 3. 4 bus cornering [50].....	24
Figure 3. 5 solid work model of Bishoftu bus model.....	27
Figure 3.6 model imported to ANSYS workbench.....	30
Figure 3.7 ANSYS meshed structure.....	31
Figure 3.8 Braking boundary condition	33
Figure 3.9 braking loads and boundary condition.....	33
Figure 3.10 boundary condition for right cornering	34
Figure 3.11 right cornering loads and boundary condition.....	34
Figure 3.12 boundary condition for left cornering.....	35
Figure 3.13 loads and boundary conditions for left cornering	35
Figure 3.14 Analysis flow chart diagram.....	38
Figure 3.15 Bishoftu Bus left side frame structure	39
Figure 3.16 Bishoftu Bus right side frame structure.....	40
Figure 3.17 Bishoftu Bus Roof side frame structure	40
Figure 3.18 Bishoftu Floor side frame structure	40
Figure 3.19 Bishoftu bus Front side frame structure	41
Figure 3.20 Bishoftu bus Rear side frame structure.....	41

Figure 4.1 Passenger door side structure showing members which use the same RHS ..	28
Figure 4.2:-Driver side door structure showing members which use the same RHS.	28
Figure 4.3 Reaction force on the beam	43
Figure 4.4 Load applied on the beam.....	46
Figure 4.5 RHS from solid work welding profile	47
Figure 4.6 RHS cross-section	48
Figure 4.7 shear force diagram	48
Figure 4.8 the meshed structure of the beam	49
Figure 4.9 equivalent stress distribution	50
Figure 4.10 normal stress distribution at the upper and bottom periphery of the beam	51
Figure 4.11 deformation of the beam.....	51
Figure 4. 12 normal stress of original structure for braking load case.....	53
Figure 4.13 von-misses stress of original structure for braking load case	53
Figure 4.14 total deformation of the original structure for braking load case	54
Figure 4.15 directional deformation of the original structure for the braking load case.	54
Figure 4.16 shear stress (XY plane) of the original structure for the braking load case.	55
Figure 4.17 normal stress of original structure for the right cornering load case	57
Figure 4.18 von-misses stress of original structure for right cornering load case	57
Figure 4.19 total deformation of the original structure for the right cornering load case.	58
Figure 4.20 directional deformation of the original structure for right cornering load case.	58
Figure 4.21 shear stress (XY plane) of the original structure for the right cornering load case.....	59

Figure 4.22	normal stress of original structure for the left cornering load case	61
Figure 4.23	von –misses stress of original structure for the left cornering load case	61
Figure 4.24	total deformation of original structure for left cornering load case.....	62
Figure 4.25	directional deformation of the original structure for the left cornering load case.....	62
Figure 4.26	shear stress (XY plane) of the original structure for the left cornering load case.....	63
Figure 4.27	normal stress of improved structure for braking load case.....	64
Figure 4.28	von-misses stress of improved structure for braking load case	65
Figure 4.29	total deformation of improved structure for braking load case	65
Figure 4.30	directional deformation of improved structure for braking load case	66
Figure 4.31	Shear stress (XY plane) of improved structure for braking load case.....	66
Figure 4.32	normal stress of improved structure for the right cornering load case	68
Figure 4.33	von-misses stress of improved structure for right cornering load case	69
Figure 4.34	total deformation of improved structure for the right cornering load case..	69
Figure 4.35	directional deformation of improved structure for the right cornering load case.....	70
Figure 4.36	shear stress (XY plane) of improved structure for the right cornering load case.....	70
Figure 4.37	normal stress of the original structure for the left cornering load case	72
Figure 4.38	von- misses stress of improved structure for the left cornering load case...	73
Figure 4.39	total deformation of improved structure for the left cornering load case	73
Figure 4.40	directional deformation of improved structure for the left cornering load case.	74

Figure 4.41 shear stress (XY plane) of improved structure for the left cornering load case.	74
Figure 4. 42 stress comparison of the original structure with improved structure.....	80
Figure 4.43 displacement comparison of the original structure with an improved one..	80
Figure 4. 44 right cornering stress comparison of the original structure with improved structure.....	82
Figure 4.45 right cornering displacement comparison of the original structure with improved structure	82
Figure 4. 46 left cornering stress comparison of the original structure with improved structure.....	84
Figure 4.47 left cornering displacement comparison of the original structure with improved structure	84

LIST OF TABLE

Table3. 1 Material properties RHS (rectangular hollow section) structure	26
Table3.2 Solid work model of improved structure	29
Table3. 3 Total weight of the bus	32
Table3.4 Self structure weight of bus body	42
Table 4.1 deflection of the beam.....	45
Table 4.2 summary result of bus structure during braking	55
Table 4.3 Summary table of stress and displacement for right cornering.....	59
Table 4.4 Summary table for left cornering.....	60
Table 4.5 Summary table for displacement and stress values for braking load case after improvement.	67
Table 4.6 Summary table for displacement and stress values for the right cornering load case after improvement.	71
Table 4.7 Summary table for displacement and stress values for left cornering load case after improvement.	72
Table 4.8 Previous RHS used and New RHS used.....	75
Table 4.9 Total length of RHS 80X40X2mm used in driver door side structure	75
Table 4.10 Total length of RHS 60X52X2mm used in driver door side structure	76
Table 4.11 Total length of RHS 80X40X2mm used in passenger door side structure ...	76
Table 4.12 Total length of RHS 75X50X2.5mm used in passenger door side structure.	77
Table 4.13 Total length of RHS 70X50X2mm used in passenger door side structure....	77
Table 4.14 Total length and weight of the Original structure.....	77
Table 4.15 Total length and weight of the Modified structure	78

Table 4.16 Comparison of displacement and stress values of the original structure with modified braking load case	78
Table 4.17 Comparison of displacement and stress values of the original structure with modified on the right cornering load case.....	80
Table 4.18 Comparison of displacement and stress values of the original structure with modified on left cornering analysis.....	83

NOMENCLATURE

AISI	American iron and steel institute
APCs	Armed Person Carriers
CAD	computer-aided design
CAE	Computer-Aided engineering
DIN	Deutsches Institute for Normung
FEA	finite element analysis
FBD	Free Body Diagram
ISO	International Standard Organization
MFFD	mean fully developed deceleration
RHS	rectangular hallow section
SUVs	sports utility vehicle
SAE	society of automotive engineering

1 CHAPTER ONE

INTRODUCTION

This chapter covers the background of bus structure, Statement of Problem, General and Specific objectives, Scope, limitation, and outcomes of the study. Finally gives the outline of the Thesis work.

1.1 Background

As the population increased significantly, the transportation system becomes progressively incontrollable. Bus, a road vehicle designed to carry many travelers, is used to transport passengers to reach their destination. To give the finest service to passengers good and strong bus is required. The increasing demand for public transportation forces responsible governments to find a solution. To meet the need and simultaneously save foreign currency, local fabrication has been strongly supported. Bishoftu automotive engineering industry is one of the military institutions which is found under the ministry of national defense industry sector has a bodybuilder. Vehicle structure used in the industry depends upon the application and end-user requirements. The vehicle structure must be assessed for various loading patterns to simulate real-time application. It is critical to assess these various design configurations and arrive at the optimized design.

Over the last decades, the transport sectors are accountable for the consumption of a large percentage of oil reserves worldwide[1]. Moreover, it accounts for a large contribution to total greenhouse gas emissions. For energy reduction and environmental protection application of lightweight methods in the automotive industry is helpful. A small reduction in overall weight will result in huge operational cost savings. For conventional combustion vehicles, it is stated that 6-8% of fuel consumption and 4% of emission could be saved for every 10% mass reduction[2]. The current trend in bus design is to reduce weight to minimize fuel consumption. Optimization techniques applied for structural design are a major research area to reduce the overall weight of vehicles without compromising the safety of the passengers[3]. Design experts usually try to maintain all required structural parts and elements, which may increase the production cost and the product price.

Moreover, the increase in weight leads to weight increase and thereby an increase in fuel consumption of the bus[4]. The structural analysis involves the determination of the force and displacements of the structures or components of a structure and assessing its stability and safety. The structural analysis includes the determination of the forces and displacements of the structures or components of the structure and assessing its stability and safety[5]. In the process of designing a selection of material and or designing the components that make up a table, the structure is involved. The bus body (compartment) structure is generally fabricated from welded beams of the rectangular cross-section which makes up the six sides and is covered by sheet metal.

The bus body structure can be considered as a rectangular box, mainly consists of six major parts: the front part, the top part, rear part, left part, right part, and the floor.



Figure1. 1 Bishoftu bus model ZK6118HGA

Recently the major challenges faced by the automobile and transportation industry are fuel efficiency and environmental pollution which are indirectly related to weight and thus by reducing weight is one of the solutions to overcome these problems. Lighter vehicles require less energy to move and can retain the desired performance characteristics while making use of a lighter, smaller, less polluting engine[6]. Further, the use of a large number

of components adds up unnecessary weight to the body and impacts the overall efficiency. The inspiration of this research is to reduce the weight of the bus structure by working finite element analysis, structural analysis, and weight-reducing techniques to optimize the size of various beams and elements of the body structure. The dynamic analysis of the braking system is defined from the dynamic boundary condition and it is almost similar to the static distribution of the static weight and acceleration. The dynamic behavior of structure during braking is the analysis of the longitudinal dynamics of the bus how ever, The main part of the cornering load lies on the side frame while the car turns left most of the mass shifts to the right side in a lateral direction since a portion of the load is applied on the right side of the frame lateral force and self-aligning torque transient response should be studied.

1.2 Bishoftu Automotive Engineering Industry

Bishoftu Automotive Engineering Industry (BAEI) is one of the military institutions which is found under the Ministry of National Defense Industry sector. The increasing demand for public transportation forces responsible governments to find a solution. To meet the need and simultaneously save foreign currency, local fabrications have been strongly supported. As a result, there are bus body builders in Ethiopia, mainly located in Bishoftu, 45 km to the southeast of Addis Ababa, the capital city of the federal democratic republic of Ethiopia. The bus body on imported regular trucks, mostly single and double cabin Isuzu engine pickups, SUVs, city buses, cross country buses, heavy-duty trucks, and military vehicles like a tank, bush car, APCs (Armed Person Carriers), and bush ambulances. And mainly based on vehicle body repair experience. Most, do not have any designs, and worse, none have any design analysis which ought to be a requirement for the certification for these vehicles.

Further, the use of a large number of components with the false assumption “any strong structure is good” adds up an unnecessary weight to the body and impacts the overall efficiency. The motivation of this research is to propose a dynamic analysis response and recommended further weight optimization to find the improved structure of a locally built bus. By analyzing the strength behavior of the bus structure during static and dynamic loading, providing data for improvement has to be made.



Figure1. 2 Workflow of Bishoftu automotive industry

1.3 Statement of The Problem

All Bishoftu city bus body structures are imported from china the only assembly is done at BAEI, no document on analysis of structural integrity or optimization of the basic design is available. Hence there is a requirement to carry out suitable analysis to optimize the existing bus body design thereby optimizing the weight of the bus body structure without compromising the integrity and safety of the structure. This will also lead to reducing production costs of the bus. Depends on prior research upon the optimization techniques based on the static analysis of bus structure that lacks dynamics stress response, this fulfills deformation and stress response due to braking and cornering maneuvers. Efficient, sustainable, and environmentally friendly transport systems require several challenges to be addressed to meet many requirements in terms of transport performance, comfort, safety, energy consumption and costs, quality and reliability as well as environmental impacts. Conventional design of bus bodies has more weight and which will affect the carrying capacity, performance, and resulting in higher fuel consumption. Braking and cornering are the most prevailing dynamic loads which have a great impact on the structural design of the vehicle. Therefore, Identifying and analyzing the dynamic behaviors of the bus is crucial.

1.4 Research Objective

1.4.1 General Objective

The general objective of this research is to analyze the dynamic behavior of bus structure during braking and cornering.

1.4.2 Specific Objective

- Geometrical modeling of Bishoftu City bus (MODEL ZK6118HGA) structure.
- Evaluate the dynamic behavior of bus structure during cornering and braking numerically.
- Modify the existing bus body structure by testing the longitudinal performance and handling characteristics.

1.5 Significant (Outcomes) of the Study

The study is very important to address the gap in the dynamic analysis of the bus. beyond the academic benefit, the optimization of buses tends to improve the fuel efficiency and emission rate to the atmosphere. For the safe range of design, the manufacturer studies the requirement to optimize the structure and get better profit over the modified structure.

1.6 Scope of The Study

Generally, the study worked on numerical investigation of bus structure. the dynamic analysis has been work on the bus frame skeleton during braking and cornering. The sample used to work for the study is the Bishoftu bus with model ZK6118HGA. The bus geometry was constructed with SOLIDWORK and analysis has done with ANSYS 19 workbench tool. The two loading conditions were analyzed with cornering and braking boundary conditions by which stress and deformation of the structure were obtained. Finally, some of the RHS frame structures were replaced with lesser dimensions and achieved weight optimization. Further analysis has been done with the improved bus structure based on the above two loadings.

1.7 Limitations of The Study

The study was carried out with limited resources available in the college in terms of software and computers. The major limitations of the study are:

- Lack of latest software suitable for this kind of work
- Lack of high performance of the computer.

2 LITERATURE REVIEW

2.1 Fundamental concept

2.1.1 Vehicle Fixed Coordinate System

The vehicle motions are well-defined as a right-hand orthogonal coordinate system (the vehicle fixed coordinate system) that originates at the C.G.(center of gravity) and travels with the vehicle. SAE defines this as X-forward used on the longitudinal plane of symmetry, Y-lateral used the right side of the vehicle. Z- Downward to the vehicle. Vehicle movements are defined as a right-hand orthogonal coordinate system (the vehicle's fixed coordinate system) originating from the center of gravity and traveling with the vehicle. SAE defines this as X-forward used on the longitudinal symmetry plate, Y-lateral used on the right side of the vehicle. Z- Down concerning the vehicle[7, 8]. Taking Body (Vehicle) frame of reference, B (X, Y, Z) and Originated at C.G (C) of the vehicle which is moving along the vehicle. Vehicle Fixed Coordinate System (Originate from C.G, C) have 3-Axes Follows the “Right Hand” Rule which is x-Axis - Longitudinal, y-Axis – Lateral, and z-axis – Vertical with roll, pitch, and yaw orientation respectively.

2.1.2 Earth Fixed Coordinate System

Vehicle attitude and trajectory through the case of maneuver are defined to right hand orthogonal concerning axis system fixed on the earth. It is selected to coincide with a right-hand orthogonal axis system fixed on the earth and to coincide with the vehicle fixed coordinate system at the point where the maneuver is stated[9]. The coordinates are X-forward travel-travel to the right, Z-vertical travel (positive downward). The relation of the vehicle fixed coordinate system to the earth fixed coordinate system is defined by Euler angles. Euler angles are determined by a sequence of three-angle rotation. Beginning at the earth fixed system, the axis system is first rotation in yaw (around z-axis), then in pitch (around the y axis) to line up with the vehicle fixed coordinate system.

Taking Global frame of reference, G (OX, Y, and Z) and Originated at the fixed ground location (O), which is not moving along the vehicle

The three-angle obtained are the Euler angles. It is necessary to adhere strictly to the defined sequence of rotations because the resultant attitude will vary the order of rotations. In the figure below the position and orientation of the vehicle coordinate frame B (Cxyz) is measured to a grounded fixed coordinate frame G (OXY Z). Analysis of the vehicle motion is equivalent to expressing the position and orientation of B (Cxyz) in G (OXY Z).

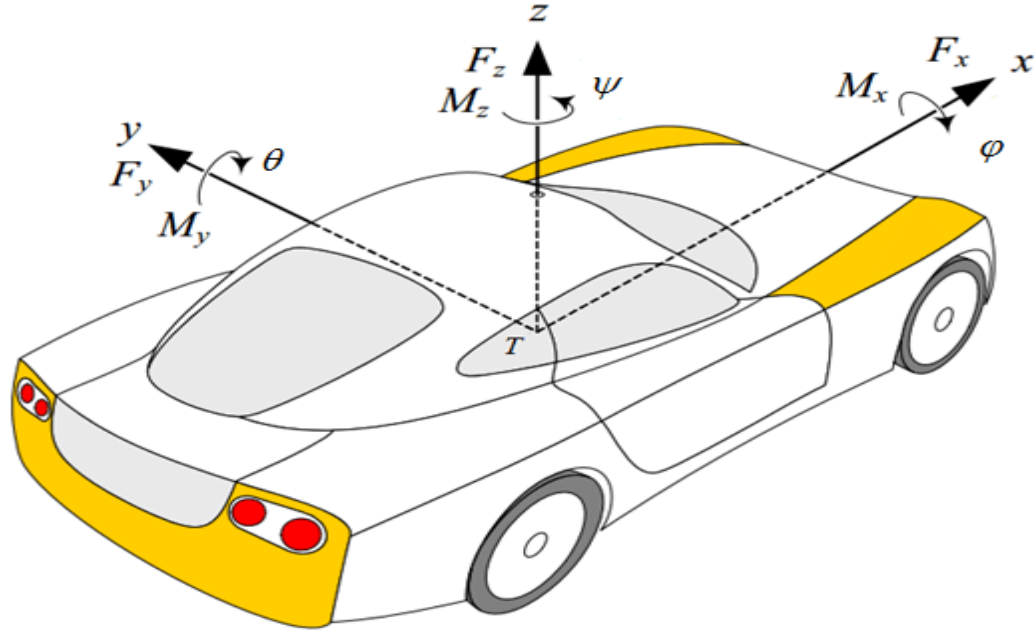


Figure 2. 1 vehicle reference system [10]

2.1.1 Mechanics of Vehicle

Vehicle mechanics involve the static and dynamic condition of the component. All external loads are subjected to both static and dynamics. The static load includes the weight of structure and passengers and luggage. Load resulting from road bump excitation[11] and aerodynamic forces[12] are considered dynamic loads.

The static analysis is concerned with the determination of the response of the model/vehicle to study load whose value remains unchanged with time. The response of the vehicle is express in terms of stress, strain, and displacement to develop a mathematical model for the structure. It is better to study each structure independently. At any given instant of time, a vehicle is subjected to a single force acting at some location and in some direction. This

so-called external or applied force maintains the velocity or causes an acceleration of the vehicle. This force is made up of tire, aerodynamic, and gravitational components. These different components are governed by different physical laws and it is not convenient to deal with this single force. To study the vehicle performance it is necessary to define axis systems to which all the variables, such as acceleration, velocity, and many others can be referred to. Throughout this thesis, the axis systems used in vehicle dynamics modeling will be according to SAE J670[13].

2.2 Review of Literatures

This section explains several reviewed literature and different software that has been used in the analysis of bus body structure by various researchers. The works of literature studied and reviewed include books, articles, research papers, and documents available on the internet. Many types of research have been carried out in the analysis and optimization of different bus body structures. Moreover, static and dynamic analysis of the bus body including its chassis, engine, frame structure as well as interior and exterior structure has been studied[14].

2.2.1 Analysis of original bus bodies

The ease of the vehicle system depends on the optimal design of the part and running condition. Several types of research worked on automotive specialization among them engine system[15], power transmission[16], vehicle chassis design and simulation[17], stationary and rotary part design and manufacturing[18], tire dynamics, and over all system dynamics[8, 19]. All of the above specifications lied on the material selection and optimization, system dynamics, strength analysis temperature, and aerodynamics analysis. Different scholars worked on the optimal design of the vehicle body[12, 20, 21].

Numerical idealization on the real scenario of vehicle system has the boundary and initial condition which is based on static and maneuvering time with different loading and constraining schemes which consider the action of gravitational acceleration, braking at upper deceleration limit of vehicle, cornering maneuver, and side torsions due to uneven road surfaces. It is stated that the bus which runs on an uneven road could be subjected to torsion[22].

There were different methodologies to construct the most precise data collection and interpretation. Specifically, bus structure strength analysis could predict through different styles. Modal analysis was considered to be the best way to excerpt the structure resonance frequencies and spatial descriptions such as normal nodes frequencies and shapes[23]. Most of the literature used Structural analysis to test and evaluate the strength and deformation as a design constraint. These finite element methods are implemented via Abaqus, Ansys, and linear programming of Matlab[24, 25]. Dynamic maneuvers have been approximated through a quasi-static approach and finite element method. Verification of the method was done by fully experimental and quasi-experimental tests[26]. The conducted experimental analysis on the dynamic analysis of the truck and compare it with a numerical value of cornering load case and braking load case. In this work, the experimental strain measurement during braking and cornering maneuver is made in the loaded truck to identify high-stress condition areas. On the numerical investigation, mean fully developed deceleration (MFFD) was simulated to define the braking boundary condition and cornering acceleration to simulate cornering maneuver.

The bus-body structure is designed based on safety criteria such as vehicle registration regulation, the strength of the bus structure under various driving conditions, bending and torsion requirement, and rollover testing. Multivariate functions are formulated to determine the correlations of structural responses with changes in geometric parameters[27]. Lots of research worked on optimizing the chassis and frame structure of bus body, oversized structures were considered as unwanted parts[28, 29].

2.2.2 Analysis of the improved bus structure

Most optimization techniques resulted in a positive economic impact without losing rigidity and stiffness of the system structure. The body structure is partitioned into seven components based on stress distribution, load path, and deformation characteristics of the benchmark model under prescribed load cases. A parametric study of the thickness variations of the cores and faces of the sandwich structures reveals the levels of significance of changing each design parameter on the specific stiffness's, specific frequencies, and specific side deformation of the bus. Reduced size has been achieved with a different optimization technique.

Different scholars used a different methodology to achieve a weight-reduced structure. Generally, two classes of methods are used such as substitute the sub structure with completely different material and with the same material but reduced size. The composite material was the main constituent for the replacement of the frame structure and chassis of the bus. To reduce the weight of the chassis structure, lightweight materials (carbon fiber composite) were used to replace the full steel chassis to be composite-steel chassis[24, 29–31]. An existing vehicle chassis frame of a Mahindra Bolero vehicle is taken for chassis frame with three different composite materials namely, Carbon/Epoxy, E-glass/Epoxy, and S-glass /Epoxy subjected to the same pressure as that of a steel chassis frame. Uniquely AISI 4130 Chromoly steel for the frame design[21, 32, 33].

From the above paragraph, newly selected material for the replacement is discussed, however, the replacement was examined with various methods. Several works of literature studied the modeling and analysis of medium bus structure and evaluate comparative evaluation of two body side structure. In the study first analysis of structural strength and stiffness for low order vibration modes was carried out [34, 35]. The effect of different structures on the strength rigidity and material use efficiency were examined. Moreover, sensitivity studies and structural optimization were performed to reduce body weight without losing overall strength and rigidity

Some kinds of literature presented a procedure in numerical simulation for improving the structural features of a bus frame with a synchronized decrease in the mass by multi-material optimization whereas added with sensitivity and robustness analysis. Topology optimization was done by taking torsional, bending stiffness, and frequency as design constraints to design identified space of the bus. In addition design optimization is conducted for a newly developed aluminum-steel electric bus body structure[30, 33-36].

It is believed that experimental analysis is more accurate than the above numerical idealization methods. Other literature carried out an experiment and numerical investigation on truck chassis with different mode and frequency for optimizing the weight by replacing with composite material. Experimental results were used in conjunction with the finite element to predict the dynamic characteristic of truck chassis such as the natural frequency and corresponding mode shape[26, 37].

Various literature obtained different results on deformation and stress. Lan et al. found that stress levels lower than 10 Mpa on the sides, the roof, the front, and rear pans. Besides, it is obtained that torsional rigidity does not change significantly after the removal of some of the supporting members between longitudinal beams. Chinta and Vengopal [38] concluded that better results are obtained by reducing the thickness and also using composite materials than the original model and conventional steel. Foucault et al.[9] verified experimental test and bodyweight reduction was found to be 5.7%. Zhang et al.[39] find out the optimized frame bending, the full-load braking condition, and the full-load torsional operating condition stresses decreased by 44.499%, 23.364%, and 31.303%, respectively. The bending stiffness of the improved structure is higher compared to the original structure. Sudirja et al.[40] concluded that hybrid bolted composite-steel chassis structure, the total weight of the chassis reduces by about 22.7 % relative to the complete steel chassis structure, thus it could be presumed to prolong the mileage of electric vehicles by an additional 20 %. Mohd Khalid Ahmed et al.[41] stated that, for the similar load carrying capacity Composite material with heavier vehicle chassis, the weight reduced with a range between 73%-40%. Natural frequencies of polymeric composite heavy vehicle chassis are 32% - 54% higher than steel chassis and 66 -78% stiffer than steel chassis. In the structural analysis the Stress. Filho et al.[29] concluded that the optimized structure presented an increase of 75% in torsional stiffness, an increase of the height of the center of gravity of only 30mm, an increase of 6% in the total mass.

Method of validation for the above results stated mathematically and physically. The verification process was done by theoretical calculation and computational methods. Since analytical calculations are limited to simple problems, computational methods are becoming more and more popular methods of predicting physical processes, especially with the rapid advancement of computing technology. Ansys and Abaqus software were used to analyze structural and modal analysis for the analysis of stress and deformation Stress, strain, and modal analyses of this frame structure to validate the safety factor of the structural design. sensitivity and robustness analysis were also verified multi-material optimization to produce the new bus model. Moreover, the SAE rules book was used to validate the entire design parameters optimization and simulation analysis. For the analysis used above, experimental tests were proven as a tangible validation method.

2.3 Summary of Literature Reviews

Optimization was done by different scholars with different methodology, it develops substantial theory along with the vehicle mathematical models and boundary conditions. The above researchers analyze the vehicle bodies based on two categories such as modal analysis and structural analysis. The modal analysis studies stress and deformation of the structure by considering its natural frequency, mode, and vibration response, whereas structural analysis considers the mechanical loads and conditions to the obtained structural response. On the other hand, an experimental investigation was done for validating the ideal numerical investigation. Analyzing the structural frame by replacing the parts partially or fully with alloy and composite materials was another focusing area on the previous works of literature. Further studies were carried out by applying different optimization methods for the entire bus structure[42, 43]. The entire optimization process needs static and dynamic analysis, through static analysis the parameter like torsion and bending constant were obtained using boundary conditions and modal analysis development. From those researches the optimization process made in the body frame structure of bus model ZK6118HG[44]. Improvement was carried out by analyzing structure for bending load and torsional stiffness analysis has been done for existing structures and improved one for both smooth roads and bump case. Many optimization techniques simulate the real condition by different engineering software including CATIA [41], SOLIDWORK [45], etc. And further analysis has been done through ANSYS [46] and ADAMS [47] software to compare von misses stress and shear stress.

2.4 Research Gap

The literature reviewed shows that the study on the frame structure of the bus body studied under both static and dynamic analysis through structural and modal analysis as discussed before. The static structural analysis of the bus frame mainly applied the static load of the bus including the self-weight of the bus body. In most studies, the authors concentrate only based on bump cases in addition to static structural to obtain the dynamic response of the structure so that torsional load is studied. The main dynamic loads such as cornering and braking have not been addressed properly. The dynamic analysis was considering the boundary condition from maneuvers such as braking and cornering. Static distribution of

static weights and acceleration, braking, cornering, displacement direction magnitude was observed during the dynamic analysis of bus structure.

3 MATERIALS AND METHODOLOGY

This chapter covers vehicle kinematics, kinetics, and mathematical modeling for the vertical and horizontal beam of the structure. The mathematical model covers both the static and dynamic models of the vehicle system. This chapter also discusses the methodology that describes the method followed in the general analysis and improvement of the weight of the bus structure based on the bending load and torsional stiffness.

3.1 Mathematical Model of Bus Structure

3.1.1 For static loading

condition Vertical Members of the

Elements

The vertical components are subjected to compression load and moment of force at both endpoints, hence the members will be forced to lose stability which might exhibit bending and deflection.

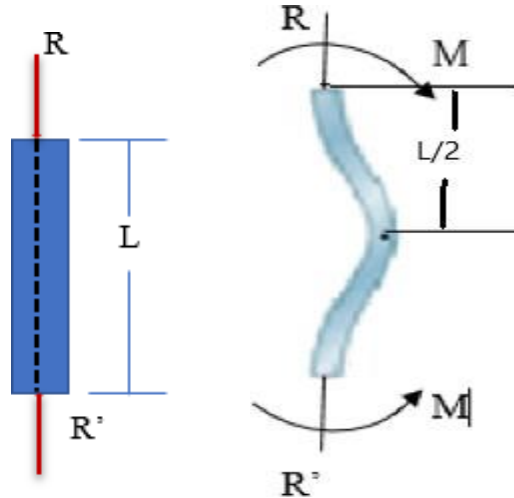


Figure 3.1 Vertical structure member

As it is observed in the above Figure 3.2 the bending is toward +X direction. This requires a negative moment for the reaction. Hence,

$$M = -RX \quad (3.1)$$

It is known that,

$$\frac{d^2x}{dz^2} + \frac{R}{EI}x = 0 \quad (3.2)$$

The solution is: $X = A \sin \sqrt{\frac{R}{EI}} Z + B \cos \sqrt{\frac{R}{EI}} Z$

Where A and B are constants of integration and must be determined from the boundary condition of the problem. We evaluate them using the following condition:

$X=0$ at $Z=0$ and $Z=L$ this gives $B=0$ and $X = A \sin \sqrt{\frac{R}{EI}} L$

The trivial solution of no buckling occurs with $A=0$ however if $A \neq 0$ then $\sin \sqrt{\frac{R}{EI}} L = 0$

The equation is satisfied by $\sqrt{\frac{R}{EI}} L = n\pi$

Where $n=1, 2, 3$, solving from R where $n=1$ gives the critical load.[48]

$$R_{cr} = \frac{\pi^2 EI}{L^2}$$

Using the relation $I = Ak^2$ where A is the area and k the radius of gyration. Enable us to rearrange $R_{cr} = \frac{\pi^2 EI}{L^2}$ in to the more convenient form of $\frac{R_{cr}}{A} = \frac{\pi^2 E}{\left(\frac{L}{k}\right)^2}$.

Where $\frac{L}{k}$ is called the slenderness ratio. The ratio rather than the actual column length will be used in classifying columns according to length categories. The member we are working for has both ends fixed. As the Figure above shows inflection point is at D a distance of $L/4$

from end A (Figure 3.2).

$$\sigma_{CR} = \frac{R_{cr}}{A} = \frac{16\pi^2 EI}{\left(\frac{L}{k}\right)^2} \quad (3.3)$$

This equation retested critical stress in the member with the square of the length of the vertical structural members during column analysis. The critical stress is inversely proportional with the square of the slenderness ratio (ratio of the length to the radius of Gyration) the combination of the equation

$$\sin \sqrt{\frac{EI}{R}} \quad L=0 \text{ and } \sigma_{CR} = \frac{R_{cr}}{A} = \frac{16\pi EI}{\left(\frac{L}{k}\right)^2} \quad (3.4)$$

Helps to determine the safety factor of the member by considering the yielding stress of the materials. This helps us to conclude whether our member fails or not.

Horizontal members of the structure

Statically indetermination structure can be solved by using different techniques. However singularity function is the best technique to integrate the equation using a computer program.

Double integration of the moment equation yields the deflection equation. The definition of singularity function referees the quantities $(x-a)$ if $(x < a)$. The figure 3.3 shows a beam supported by reaction R_1 and R_2 and loaded by the concentrated force F_1 , F_2 and F_3 if the beam is cut at the same section located at $x=x_1$ and the left-hand portion is removed as a free body, an internal shear force v and bending moment M must act on the cut surface to ensure equilibrium. The sheer force is obtained by summing the force on the isolated section. The bending moments of the force to the left of the section taken about an axis through the isolated section the sign convention used the bending moment and shear force are as shown in figure 3.3.

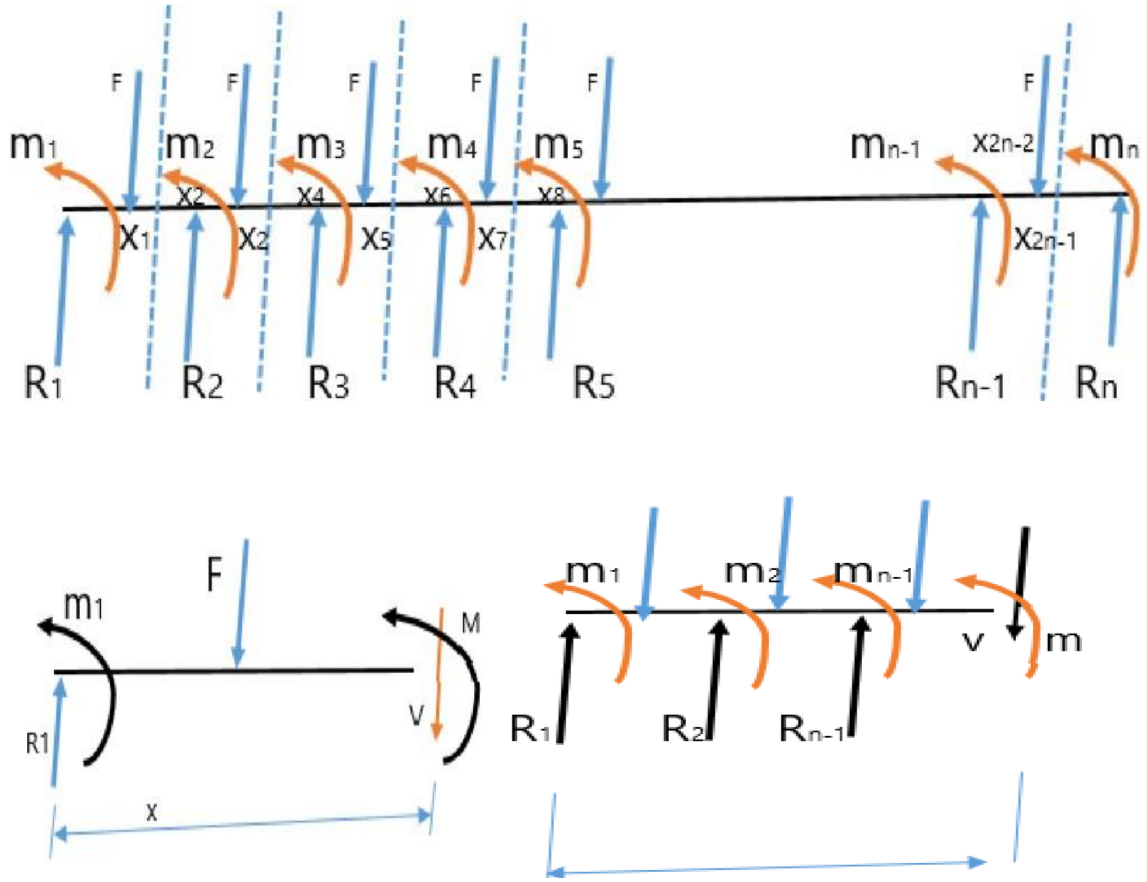


Figure 3. 2 Horizontal structure member

$\sum M_o = 0$ for section 1;

$$M + m_1 + F(x - x_1) - R_1 x = 0 \quad (3.5)$$

$\sum M_o = 0$ for section 2;

$$M + m_1 + m_2 + F(x - x_1) + F(x - x_3) - R(x - x_2) = 0 \quad (3.6)$$

For section, we can generalize by a mathematical notation which divided by using a concept of arithmetic progress, where the n th term is determined from $a_1 + (n-1)d$ [48] where d is a common difference and a_1 the initial value.

$\sum M_o = 0$ for section n

$$m_1 + m_2 + \dots + m_n + F(x - x_1) + F(x - x_2) \dots + F(x - x_{2n-1}) - R_{1x} - R_{2(x-x_2)} - R_{3(x-x_4)} \dots - R_{n(x-x_{(2n-2)})} = 0 \quad (3.7)$$

From equation (3.6) solving for M, the following representation can be obtained.

$$M = \sum_{n=1}^i R_n(x - x_{(2n-2)}) - \sum_{n=1}^i F(x - x_{(2n-2)}) - \sum_{n=1}^i m_n(x - x_{(2n-2)}) \quad (3.8)$$

But From the mechanics of materials, we know [27].

$$EI \frac{d^2 y}{dx^2} = M$$

Rewriting equation yields

$$EI \frac{d^2 y}{dx^2} = M = \sum_{n=1}^i R_n(x - x_{(2n-2)}) - \sum_{n=1}^i F(x - x_{(2n-2)}) - \sum_{n=1}^i m_n(x - x_{(2n-2)}) \quad (3.9)$$

$$EI \frac{dy}{dx} = y = \frac{1}{2} \sum_{n=1}^i R_n(x - x_{(2n-2)})^2 - \frac{1}{2} \sum_{n=1}^i F(x - x_{(2n-2)})^2 + \sum_{n=1}^i m_n(x - x_{(2n-2)}) + c_1 \quad (3.10)$$

Upon double integration we obtain

$$EI y = \frac{1}{6} \sum_{n=1}^i R_n(x - x_{(2n-2)})^3 - \frac{1}{6} \sum_{n=1}^i F(x - x_{(2n-2)})^3 - \frac{1}{2} \sum_{n=1}^i m_n(x - x_{(2n-2)})^2 + c_1 x + c_2 \quad (3.11)$$

Where c_1 and c_2 are integration constants.

To determine the constant of the integration boundary condition will be used as $x=0, y=0$, hence from equation (3.10) have the value of $c_2=0$ nothing that all have the value of in the bracket are negative equations and therefore are equal to zero.

Letting now $x=L, y=0$. In equation (3.9) we write C_1 by

$$c_1 = \frac{1}{6} \sum_{n=1}^i F(x - x_{(2n-2)})^3 + 3 \sum_{n=1}^i m_n (L - x - x_{(2n-2)})^2 - \sum_{n=1}^i Rn(L - x - x_{(2n-2)})^3$$

By substituting and rearranging the expression for c_1 , we can rewrite the equation as

$$\begin{aligned} EI \frac{dy}{dx} = y = & \frac{1}{2} \sum_{n=1}^i Rn(x - x_{(2n-2)})^2 - \frac{1}{2} \sum_{n=1}^i F(x - x_{(2n-2)})^2 + \sum_{n=1}^i m_n (x - x_{(2n-2)}) + \frac{1}{6L} \sum_{n=1}^i F(x - x_{(2n-2)})^3 + \\ & 3 \sum_{n=1}^i m_n (L - x - x_{(2n-2)})^2 - \sum_{n=1}^i Rn(L - x - x_{(2n-2)})^3 \end{aligned} \quad (3.12)$$

Then the Deflection equation becomes

$$\begin{aligned} EI y = & \frac{1}{6} \sum_{n=1}^i Rn(x - x_{(2n-2)})^3 - \frac{1}{6} \sum_{n=1}^i F(x - x_{(2n-2)})^3 - \\ & \frac{1}{2} \sum_{n=1}^i m_n (x - x_{(2n-2)})^2 + \frac{x}{6L} \sum_{n=1}^i F(x - x_{(2n-2)})^3 + \\ & 3x \sum_{n=1}^i m_n (L - x - x_{(2n-2)})^2 - x \sum_{n=1}^i Rn(L - x - x_{(2n-2)})^3 \end{aligned} \quad (3.13)$$

From the boundary condition know that as $x=0, \frac{dy}{dx} = 0$ and also as $x = x_i, \frac{dy}{dx} = 0$ using equation (3.12), we have two variables and two-equation here we can simply generalized that.

Case 1: If $x=0$

$$\begin{aligned} \sum_{n=1}^i m_n (x_{(2n-2)})^1 + \frac{1}{2L} \sum_{n=1}^i m_n (L - x_{(2n-2)})^2 + \frac{1}{2} \sum_{n=1}^i Rn(x_{(2n-2)})^2 - \\ \frac{1}{6L} \sum_{n=1}^i Rn(L - x_{(2n-2)})^3 = \frac{1}{2} \sum_{n=1}^i F(L - x_{(2n-2)})^2 - \frac{1}{6L} \sum_{n=1}^i F(L - x_{(2n-2)})^3 \end{aligned}$$

Case 2: If $x = x_i$

$$\begin{aligned} \frac{1}{2} \sum_{n=1}^i m_n (x_{2i} - x_{(2n-2)})^1 + \frac{1}{2L} \sum_{n=1}^i m_n (L - x_{(2n-2)})^2 + \frac{1}{2} \sum_{n=1}^i Rn(x_{2i} - x_{(2n-2)})^2 - \\ \frac{1}{6L} \sum_{n=1}^i Rn(L - x_{(2n-2)})^2 = \frac{1}{2} \sum_{n=1}^i F(x_{2i} - x_{(2n-2)})^2 - \frac{1}{6L} \sum_{n=1}^i F(L - x_{(2n-2)})^3 \end{aligned}$$

The matrix equation can be generated on the coefficient of moment reaction force and external force component. It can be represented by alphabet as follows

$$[c]\{m\} + [d]\{R\} = \{F\}$$

$$\begin{bmatrix} a_n & b_n & m_n \\ c_n & d_n \end{bmatrix} \{R_n\} = \{f_n - f_{n-1}\} \quad (3.14)$$

However, force components can be represented with a single expression after the following steps

➤ For case 1

$$\begin{aligned} F_1 &= F \frac{1}{2} x_1^2 + \frac{1}{6L} (L - x_1)^3 \\ F_2 &= F \frac{1}{2} x_3^2 + F \frac{1}{6L} (L - x_3)^3 + F_1 \\ F_n &= F \frac{1}{2} (x_{2n} - x_{(2n-1)})^2 + F \frac{1}{6L} (L - x_{(2n-1)})^3 + F_{n-1} \end{aligned} \quad (3.15)$$

➤ For case 2

$$\begin{aligned} F_1 &= \frac{1}{2} F (x_2 - x_1)^2 - \frac{1}{6L} F (L - x_1)^3 \\ F_2 &= \frac{1}{2} F (x_4 - x_3)^2 - \frac{1}{6L} F (L - x_3)^3 + f_1 \\ F_n &= F \frac{1}{2} (x_{2n} - x_{(2n-1)})^2 + F \frac{1}{6L} (L - x_{(2n-1)})^3 + f_{n-1} \end{aligned}$$

Equations (3.11) and (3.12) are the basic governing equation for the determination of bending and deflection of the horizontal moment on static load condition, however, equation (3.14) is used to determine the internal force moment of each joint.

3.1.2 Dynamic Modelling of the Vehicle

Mathematical model of dynamic analysis verified by two-equation of motion namely newton equation of motion and Euler equation of motion

Modeling of vehicle braking

The force and moment generating characteristics of the tires while the braking force generated at the tire's contact patch depends on the slip ratio as the wheel is braked from a free rolling. wheel with a slip ratio of zero to a fully locked wheel where the slip ratio is unity. In this section, it is not so much concerned with the tires. Rather addressing the modeling of the mechanisms used to apply a braking torque acting about the spin axis of the road wheel that produces the change in slip ratio and subsequent braking force.

Clearly, as the vehicle brakes, as shown in Figure below, there is weight transfer from the rear to the front of the vehicle. Given what we know about the tire behavior the change in the vertical loads acting through the tires will influence the braking forces generated. As such the braking model may need to account for real effects such as proportioning the braking pressures to the front and rear wheels or the implementation of anti-lock braking systems (ABS). Before any consideration of this, we need to address the mechanism to model a braking torque acting on a single road wheel. The braking torque M_T is given by

$$M_T = n\mu pARd$$

n = the number of friction surfaces (pads)

μ = the coefficient of friction between the pads and the disc

p = the brake pressure

A = the brake piston area

Rd = the radius to the center of the pad

Note that depending on the sophistication of the model the coefficient of friction may be constant or defined as a run-time variable as a function of brake rotor temperature.

Obtaining such data is usually relatively easy, but the calculation of rotor temperature can be a little more involved

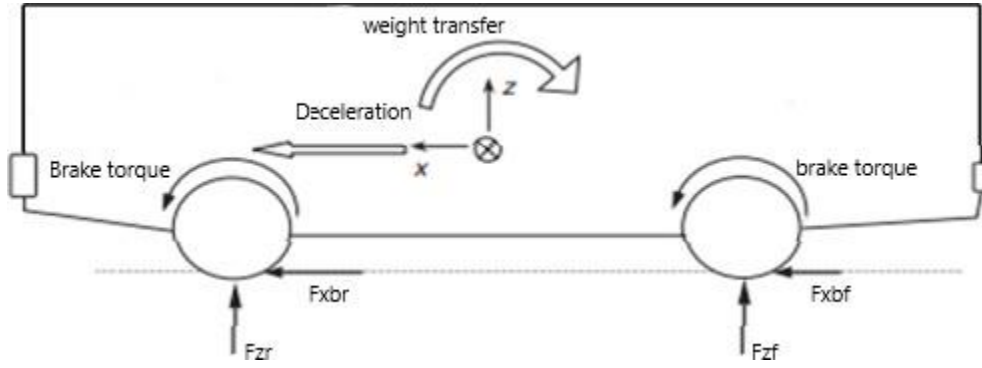


Figure 3. 3 Free body diagram of braking[49]

By the D’alembert principle, the sm of moments of forces that act on a wheel during braking is equal to zero.

$$M_b + M_r + M_{ar} - M_w - R_x r_d = 0 \quad (3.16)$$

Modelling of Vehicle Cornering

In the case of cornering, the constant vehicle speed is considered the rotational motion of the vehicle roll, pitch, and yaw are assumed to attain their steady-state in time. So the normal acceleration of the vehicle can be regarded as constant in time as well.

The equilibrium equation of the vehicle curvilinear motion under the normal inertia force of the magnitude $\frac{W}{g} \cdot \frac{v^2}{R}$ and the tangential one of magnitude $\frac{W}{g} \cdot \ddot{x}$ being applied at the vehicle center of gravity are obtained.

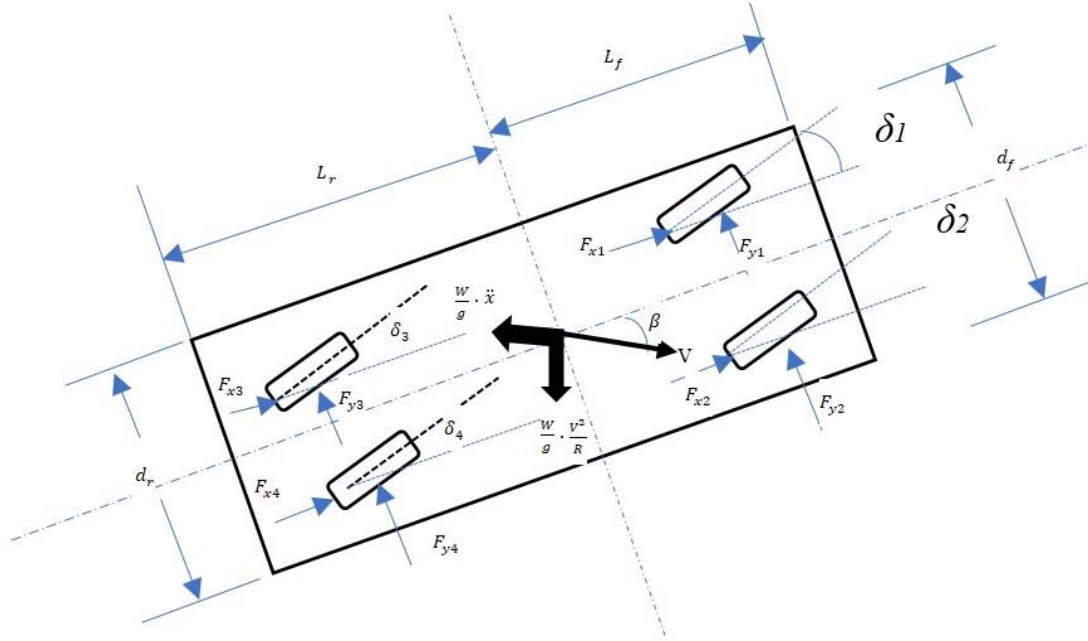


Figure 3. 4 bus cornering [50]

$$-\frac{W}{g} \cdot \ddot{x} + \sum \{F_{xi} \cos(\beta + \delta_i) - F_{yi} \sin(\beta + \delta_i)\} = 0 \quad (3.17)$$

$$-\frac{W}{g} \cdot \frac{V^2}{R} + \sum \{F_{yi} \cos(\beta + \delta_i) - F_{xi} \sin(\beta + \delta_i)\} = 0 \quad (3.18)$$

$$-W + \sum F_i = 0 \quad (3.19)$$

But the lateral and longitudinal acceleration transferred is

$$\text{But } \frac{V^2}{R} = (-\ddot{x} \sin \beta + \frac{V^2}{R} \cos \beta)$$

$$\ddot{x} = (-\ddot{x} \cos \beta + \frac{V^2}{R} \sin \beta)$$

The equilibrium in roll, pitch, and yaw are expressed by

Roll equation

$$\begin{aligned} \frac{W_s}{g}(-\ddot{x} \sin \beta + \frac{V^{\circ}}{R} \cos \beta)h_s + \frac{a_f}{2}(F_{z1} - F_{z2}) + \frac{dr}{2}(F_{z3} - F_{z4}) + h_f(F_{y1} + F_{y2}) \\ + h_r(F_{y3} + F_{y4}) = 0 \end{aligned} \quad (3.20)$$

Pitch equation

$$\frac{W_s}{g}(-\ddot{x} \cos \beta + \frac{V^{\circ}}{R} \sin \beta)h_s + L_f(F_{z1} + F_{z2}) + L_r(F_{z3} + F_{z4}) = 0 \quad (3.21)$$

Yaw equation

$$\begin{aligned} L_f(F_{x1} \sin \delta_1 + F_{y1} \cos \delta_1 + F_{x2} \sin \delta_2 + F_{y2} \cos \delta_2) - L_r(F_{x3} \sin \delta_3 + F_{y3} \cos \delta_3 \\ + F_{x4} \sin \delta_4 + F_{y4} \cos \delta_4) + \frac{d_f}{2}(-F_{x1} \cos \delta_1 + F_{y1} \sin \delta_1 + F_{x2} \cos \delta_2 - \\ F_{y2} \sin \delta_2) + \frac{d_f}{2}(-F_{x3} \cos \delta_3 + F_{y3} \sin \delta_3 + F_{x4} \cos \delta_4 - F_{y4} \sin \delta_4) = 0 \end{aligned} \quad (3.22)$$

3.2 Numerical modeling

3.2.1 Bus geometry

The modeling of the bus structure is made with data collected from Bishoftu Automotive Engineering Industry bus bodybuilding section. Before measuring the structure, a drawing of the bus structure is made. This helped for easy placement of the measured length on the corresponding members on the drawing. During the data collection of the structure, all members of the structure are measured with a length measuring tape. The modeling of the bus structure is made with ANSYS 2019(ANSYS 19.0). The bus structure is made with

steel beams of rectangular hollow sections (RHS), of different sizes. The sizes of RHS used are for example RHS 80×40×3, RHS 50×30×2, and 40×40×2.

This bus has a capacity of 61 passengers. The modeling of the bus body is a two-step process comprising, a first geometric model of the bus and a second, a finite element model. It would be good if both models are developed in the same CAD environment. Finite Element Analysis of the base model is carried out for strength, stiffness, and safety. It includes linear static analysis to identify strength criteria that include maximum stresses and deflections; analysis for dynamic behavior. The bus beam cross-sectional members are made of hollow rectangular mild steel beam shown in (Figure 4.7) with the material property in Table 3.2 Material selection for the existing bus body frame

Material selection plays a crucial part in providing the desired strength endurance, safety, and reliability to the vehicle. To choose optional material we need an extensive study on the property of different materials. The material for the existing bus body frame structure model is the structure steel DIN standard of St 37.2 with the following parameter shows in table 3.2.

Table3. 1 Material properties RHS (rectangular hollow section) structure.

No	Material	Tensile yield strength	Compressive yield strength	Tensile ultimate strength	Density	Young's modulus	Elon.	Poisons ratio
1	Structure steel	230 MPa.	230 Mpa	440 Mpa	7850 kg/m ³	200 Gpa	20%	0.3

3.2.1.1 For the original bus structure

Before going to the finite element analysis, the modeling of the bus structure should be made. The Figure given below shows the model of the bus made in solid work 2018 window. The structure parts are made with the real profiles and parts are made with the real profiles and dimensions used in the factory. The bus body is created by 3-D wireframe modeling as shown the dimension is 2.55-meter height, 11.89-meter length, and 3.27-meter width the total weight is 3046 kg. There are 328 elements mostly are T-joints. The

assembled model can be divided into six frames; driver side, passenger's side, floor side, roof side, rear side, and front side. The material type used is the DIN standard of St 37.2 with a variety of shapes.

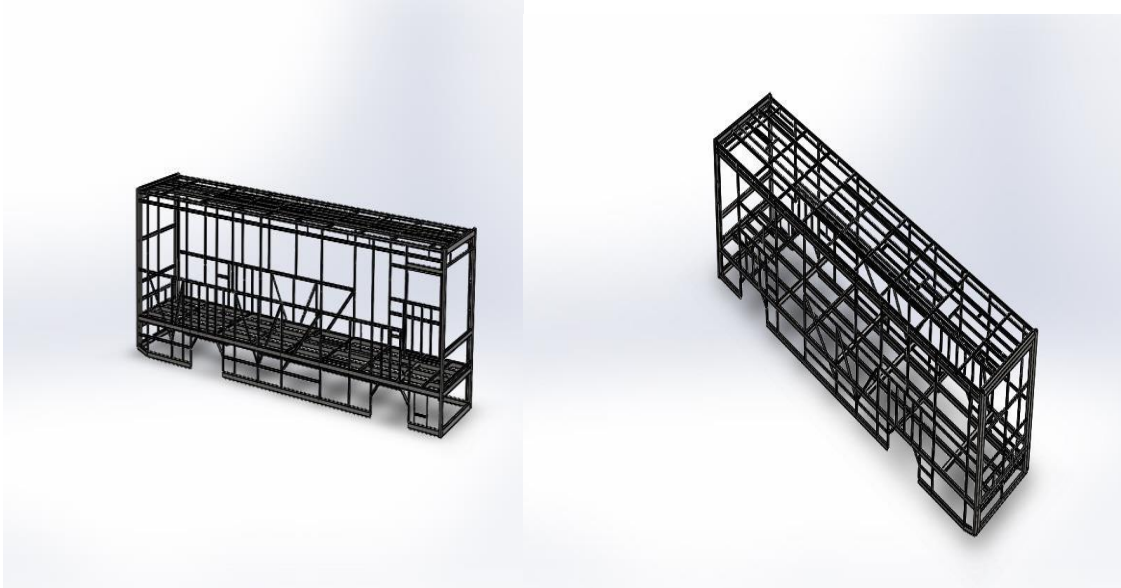


Figure 3. 5 solid work model of Bishoftu bus model.

3.2.1.2 For improved bus structure

Improvement Process

The main objective of the structure improvement was to reduce weight while maintaining the strength of the structure in a safe condition. As the results of the analysis of the original structure under bending load and torsional stiffness show, the efforts and displacements found are very low. Therefore, it is possible to improve the structure by identifying beams and elements that support less load and modify the structure.

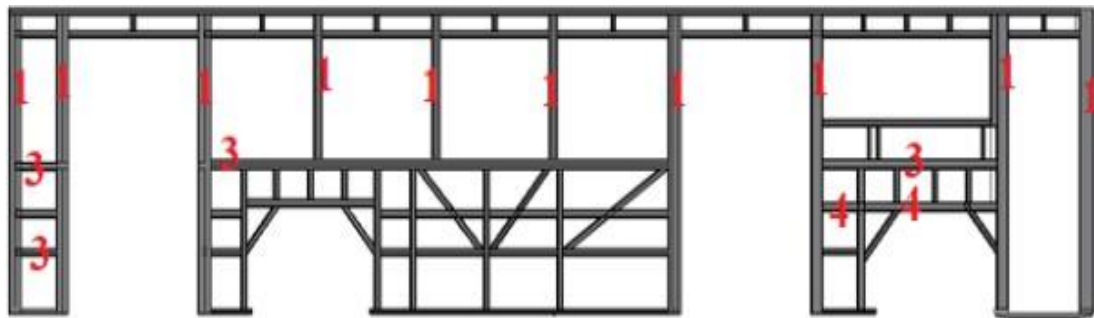


Figure 4.1 Passenger door side structure showing members which use the same RHS

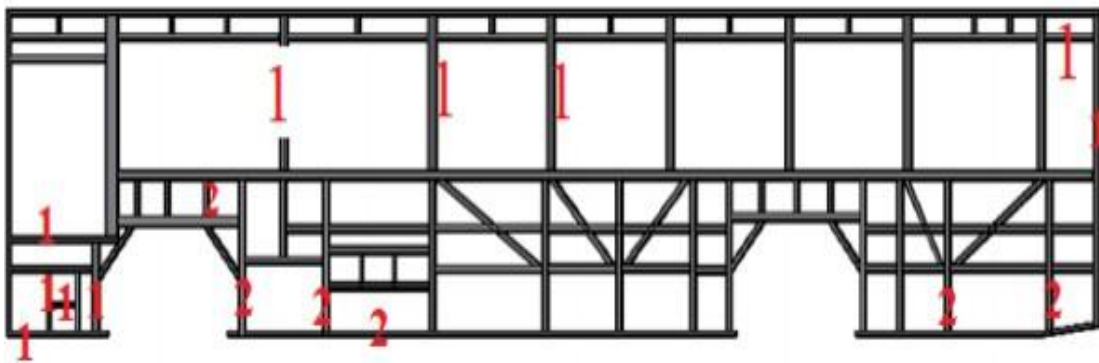


Figure 4.2:-Driver side door structure showing members which use the same RHS.

The improvement in the weight of the structure is mainly based on the braking load and the cornering results. The modified structure is analyzed again for both boundary conditions. The figures above show the components that have the same RHS size.

Those components of the structure that use RHS of size 80X40 and thickness of 2mm are assigned with number one(1), 60X52, and thickness of 2.5mm are assigned with number two(2). 75 X50 and thickness 2.5mm assigned with number three (3) whereas those members which use RHS of 70X50 and thickness of 2mm are assigned with number four. The above-stated sizes of RHS are used to build the existing bus structure at BAEI.

Changing the size of RHS

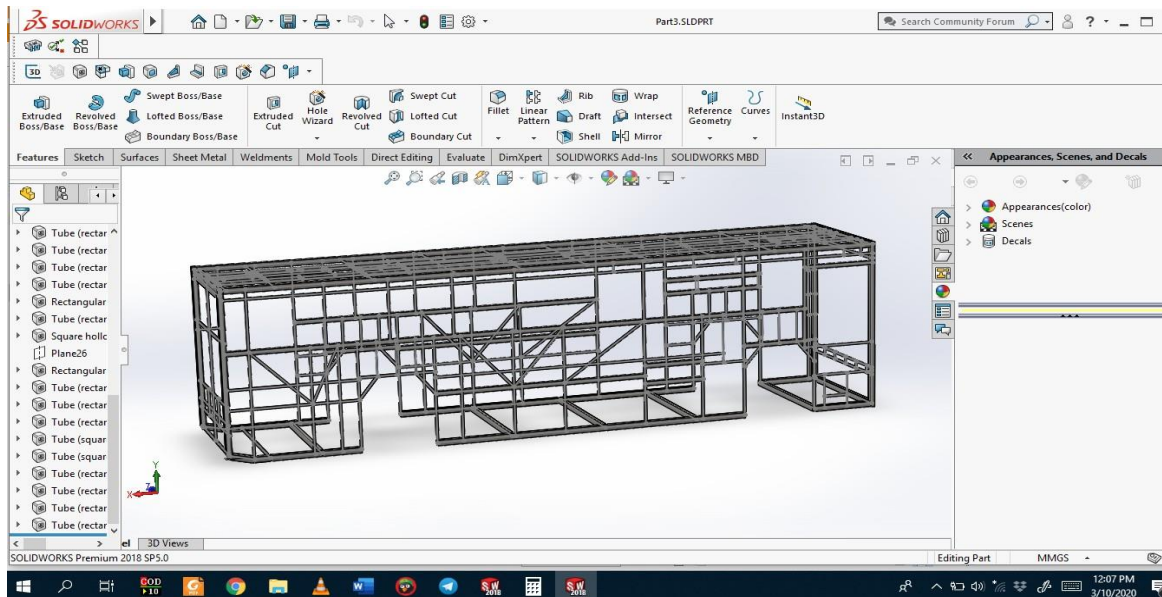
The results of the original structure analysis show that the structure is subjected to low-stress values. When we look at the results of the braking loading of the structure, the structure is subjected to lower stress compared to the cornering loading. The results of the torsional structure are higher in magnitude but generally, the structure is subjected to very low-stress values than the yield stress of the material. From this, it can be concluded that there is scope for reducing the size of the structural members.

Based on the above results some of the members can be replaced with lower size members as discussed below.

RHS size of 80X40X2mm is replaced by 60X40X2 mm, RHS size of 75X50X2.5 mm is replaced by 60X35X1.5 mm, RHS size of 70X50X2 mm is replaced by 40X40X2 mm, and

RHS size of 60X52X2 mm is replaced by 40X40X1.5 mm. A new vehicle body structure was generated using the new size members. The improved bus structure is shown in the below solid work environment.

Table3.2 Solid work model of improved structure



3.2.2 Finite element meshing of the bus body structure

Figure 3.15 shows Finite element modeling made with ANSYS 19 Workbench. The structure modeling is by SOLIDWORK software exported as SAT. Format and is imported to ANSYS 19.0 Workbench.

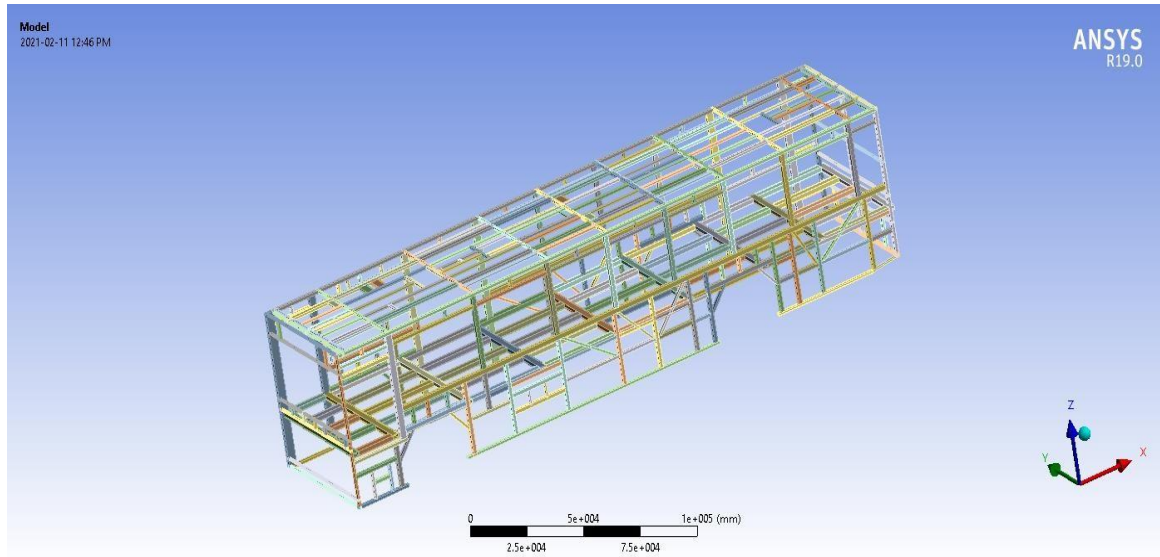


Figure 3.6 model imported to ANSYS workbench

Finite element meshing is made with ANSYS 19 workbench. Meshing is an integral part of the computer-aided engineering (CAE) simulation process. The mesh influences the accuracy, convergence, and speed of the solution. Furthermore, the time it takes to create a mesh model is often a significant portion of the time it takes to get results from a CAE solution. Tetrahedral mesh elements are used in the meshing of the bus structure.

In ANSYS 19 Workbench, the Tetra mesh method provides

- Support for 3D inflation
- Built-in growth and smoothness control. The mesher will try to create a smooth size that varies based on the specified growth factor[51].

The finite element model has 957545 nodes and 472261 elements.

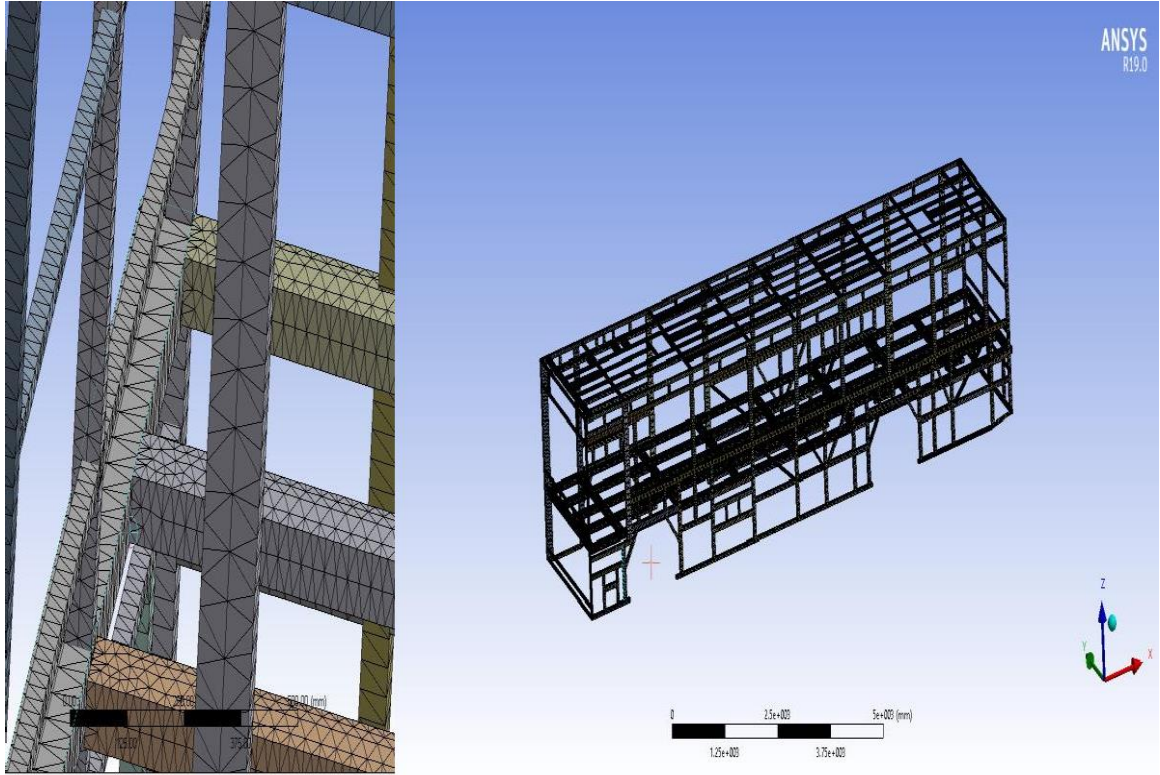


Figure 3.7 ANSYS meshed structure

3.2.3 Inputs for Finite Element Analysis

The inputs for the finite element analysis are all the loads carried by the bus. The loads carried by bus during operation are self-weight of the bus, passenger weight, luggage, engine weight, fuel weight, and extra tire weight. Different loading cases act on the bus structure. As shown in Figure 3.18 all the loads considered are applied to the structure. The applied loads are indicated by red color. The loads on the bed of the structure are lumped and placed on the respective nodes. The luggage weight carried on the bus structure on the rear and side section. Air conditioning weight carried on the bus structure is rear and front on the roof section.

Table3. 3 Total weight of the bus

No	Component	Amount in number	Average individual mass(Kg)	Total mass (Kg)	The total weight(N)
1	Passenger	61	65	3965	38,896.65
2	Seat	61	10.29	627.69	6157.64
3	Air conditioner(on roof)	2	100	200	2000
4	Luggage on rear and side	1	200	200	1962
5	Self- weight of structure	1	3046	3046	29881.26
6	Fuel tank	1	250	250	2452.5
7	Engine	1	900	900	8829
Total weight of the structure					90179.05

3.2.4 Boundary Conditions used in the analysis

The boundary condition used in the analysis is different according to the operating conditions of the bus. The two major loads considered are bending load and torsional stiffness. Both two loads are studied under the cornering and braking boundary condition of the structure.

3.2.4.1 The boundary condition for braking

On the braking case, the main loads that are considered are passenger weight, seat weight, luggage weight, and engine weight and self-weight of the bus which is taken into consideration by applying gravity as an inertial load which is gravitation acceleration i.e. $9.81m/s^2$. The passenger weight together with seat weight is acted as a lumped mass. The point of application is on the nodes of the passenger seat. The luggage is assumed to be on the roof serves as a load-bearing structure in addition to providing protection. Besides, the bus has a compartment on the rear side and right side which is used to carry luggage. The main boundary condition unique to braking load is braking deceleration in the direction

where friction happened in between tire and road surface. Therefore braking deceleration is applied with the whole structure i.e. $Bg=\mu g$ where μ is the friction coefficient between the tire and the road surface ($0 < \mu < 1$). nodal displacement on the right and left side should be applied as shown in figure 3.17.

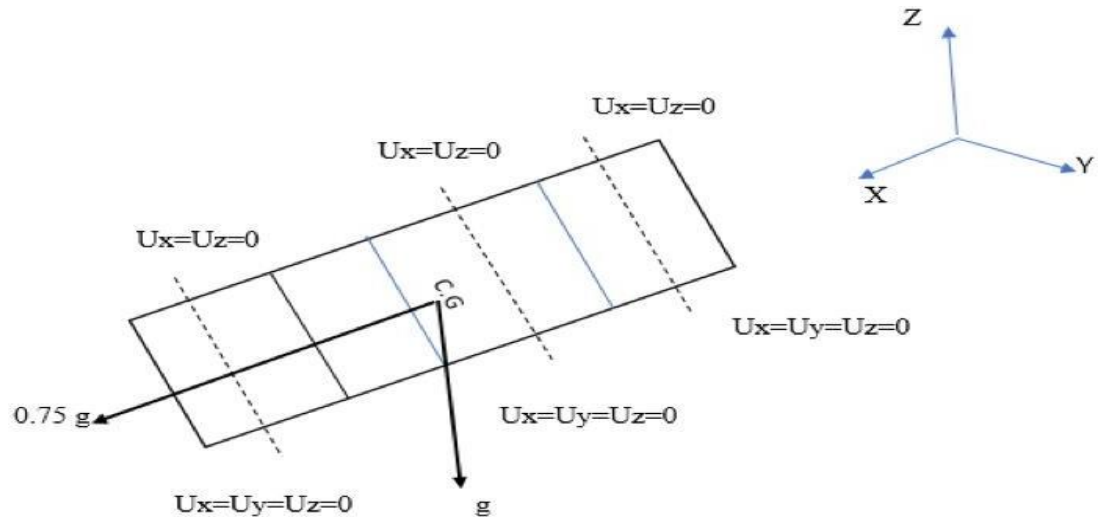


Figure 3.8 Braking boundary condition

The “g” value is used as a braking deceleration for the braking load case in the computational model used to simulate the braking maneuver.

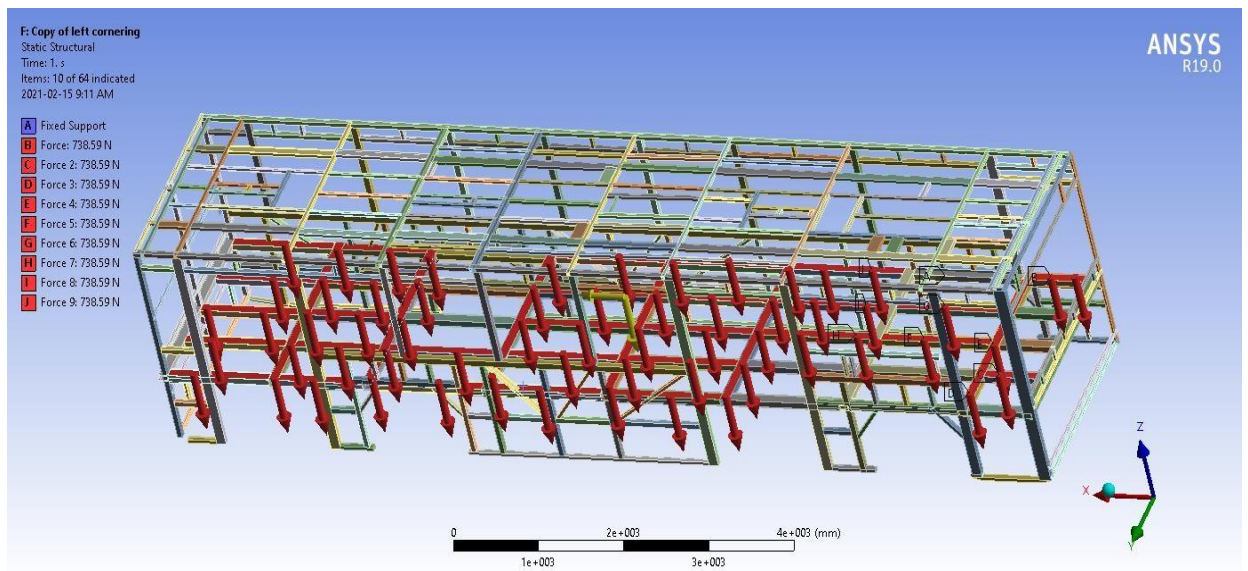


Figure 3.9 braking loads and boundary condition

3.2.4.2 Right cornering load case

This loading case is the same as the braking load case except that the cornering acceleration applied on the structure whereas on the braking case braking deceleration applied. The main loads that are considered are passenger weight, seat weight, luggage weight, and engine weight and self-weight of the bus which is taken into consideration by applying gravity as an inertial load which is gravitation acceleration i.e. 9.81m/s^2 .

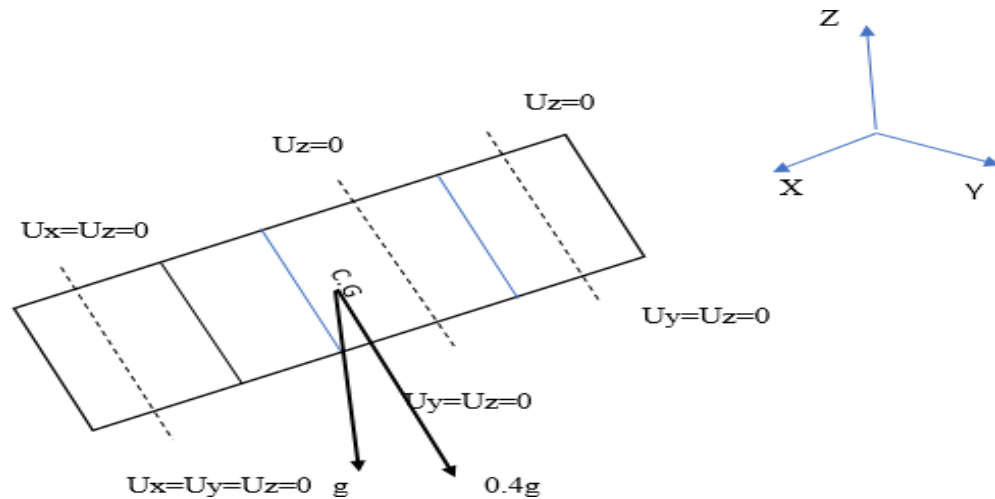


Figure 3.10 boundary condition for right cornering

The “g” value is used as a cornering load case in a computational model to simulate a cornering maneuver.

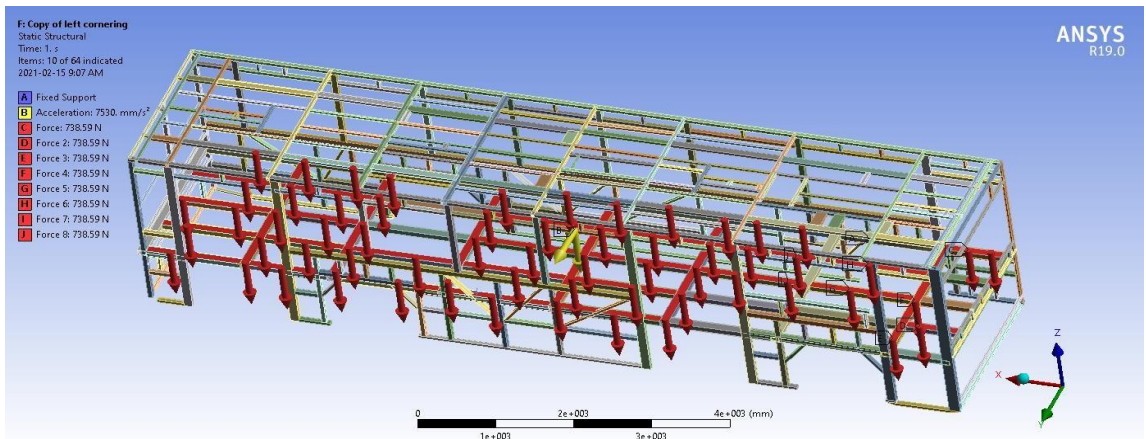


Figure 3.11 right cornering loads and boundary condition.

3.2.4.3 Left cornering load case

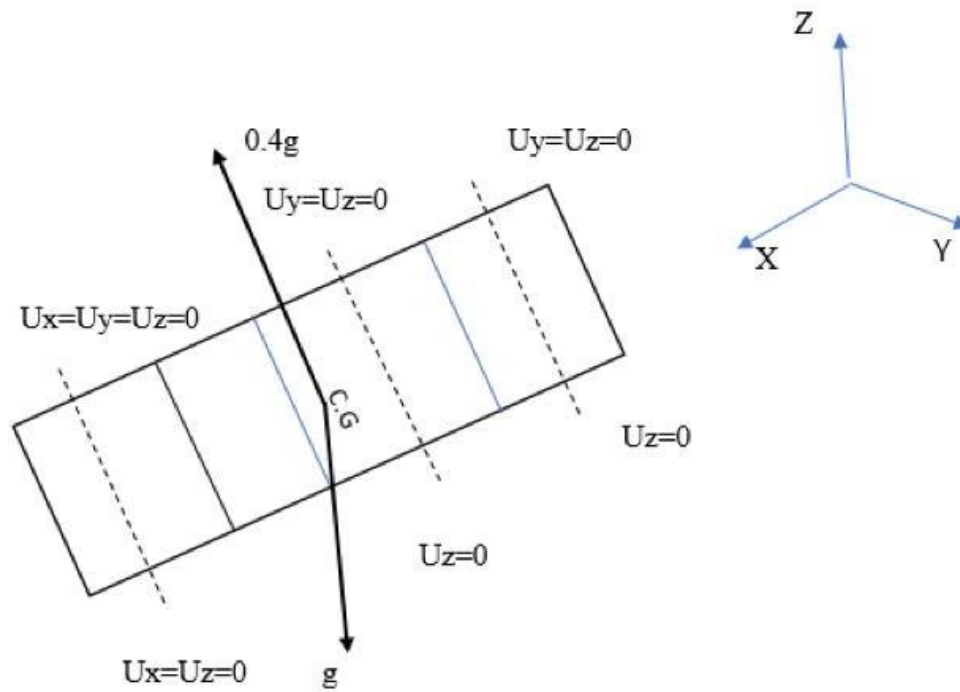


Figure 3.12 boundary condition for left cornering

The “g” value is used as a cornering load case in a computational model to simulate a cornering maneuver.

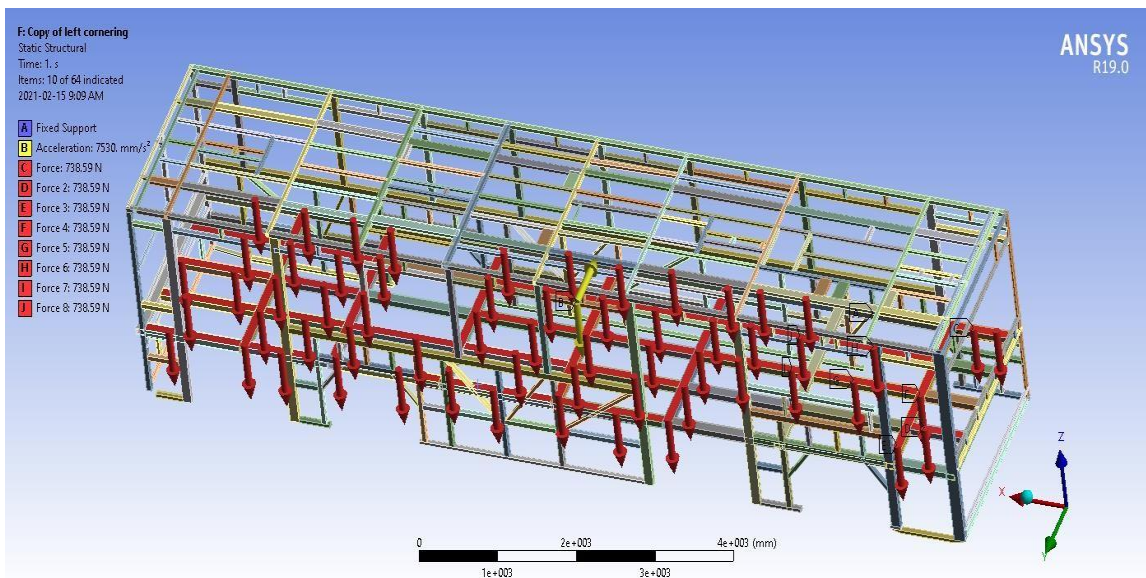


Figure 3.13 loads and boundary conditions for left cornering

3.3 Boundary conditions of the Modified structure

The Modified bus body structure was analyzed in the same way as the original structure was analyzed. The difference between the two analyses was the use of the new model generated by replacing some elements with low-size ones. All the boundary conditions used in the original structure analysis were used for the analysis of the new Modified structure. The load conditions considered for the original structure analyses applied for the improved structure also. The two major loads considered are braking and cornering for both the right and left steering condition of the structure.

3.4 Research Methodology

This research focuses on the dynamic analysis of bus body structure assembly in Ethiopia. For the data collection, the Bishoftu City bus assembled by BAEI (Bishoftu Automotive Engineering Industry) is selected as it is one of the buses having large customers and maximum market coverage. The factory uses different size RHS (rectangular hollow section) to build the city bus body structure. The required data on the structure for modeling was provided by BAEI.

The research focuses on the response of bus structure during cornering and braking for further improvement of bus structure contributing significantly to the stability and strength of the bus body frame structure. The analysis includes strength analysis, stiffness analysis, dynamic analysis, and simulation of bus frames. Strength and stiffness analysis is concerned with stress and deformation of bus frame and analysis is done using ANSYS 19 workbench finite element analysis. The dynamic analysis is also done while the bus is Turning and braking.

The research started by modeling the bus structure with the data collected from the bus manufacturer. The model is then analyzed for properties like strength i.e. stress and deformations. The result of the analysis gave the beams and elements which are underloaded and overload generally, the study of this paper is carried out through the following steps.

1. Literature Review: A lot of paper and journal has been read and a part of it is considered in this thesis, Also, different reliability websites and other relevant literature review are done.
2. Data collection: reading the previously designed manufactured Bishoftu city bus in Bishoftu automotive engineering industry (BAEI) and measuring each dimension components of the structure.
3. Modeling of the bus body frame structures: this is made by using the data recorded from the existing Bishoftu city bus built and collect data.SOLIDWORKS software is used to build the 3D model.
4. The Finite Element (FE) analysis: of structure for the required of the result using ANSYS Workbench 19.0 software. Finally, the vehicle structure is the analysis based on the ANSYS result of static and dynamic structural analysis .i.e. stress and displacement.
5. Developing the mesh model is an integral part of the computer-aided engineering (CAE) simulation process. The mesh influences the accuracy, convergence, and speed of the solution.
6. Dynamic analysis of the model using the proper finite element analysis and Simulation software to investigate the performance of the model.
7. Identify the critical points having the highest stress improved the bus structure.

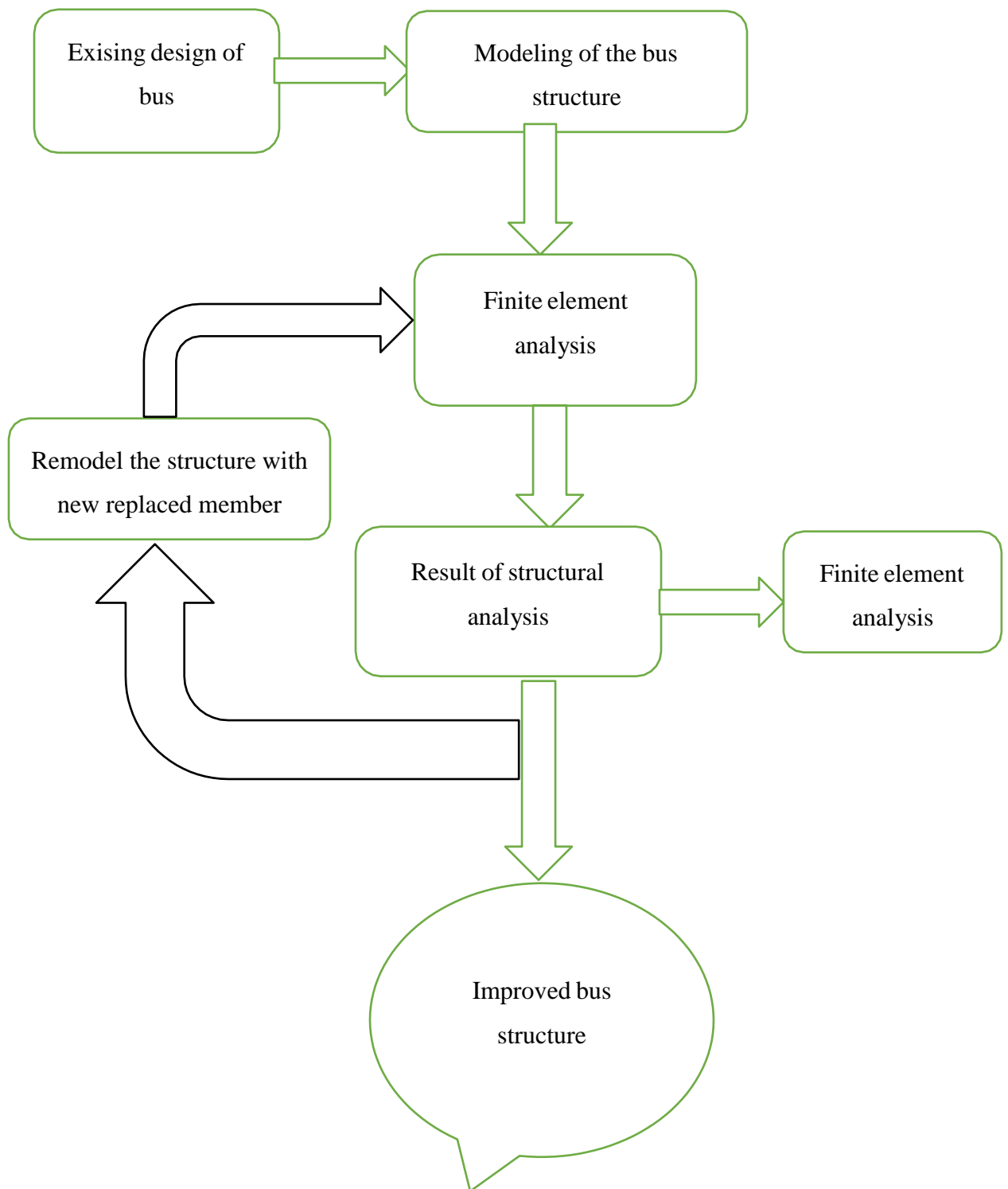


Figure 3.14 Analysis flow chart diagram

3.5 Data Collection

This section discusses the analysis of the workflow of the bus body structure assembly in Ethiopia. For the data collection, Bishoftu automotive engineering industry (BAEI) is selected. This company is selected based on its large market coverage both for private and governmental companies. The factory uses RHS (rectangular hollow section) to build the bus structure. Using the data found from the company the modeling is made. To easily understand, the body structure is divided into six parts, driver side consists of the driver door Figure 4.1 the passenger side consists of the passenger door (Figure 4.2), top structure (roof) (Figure 4.3), floor structure (Figure 4.4), vehicle front (Figure 4.5) and the rear side (Figure 4.6) Detailed description of individual parts considered is given in Appendix- A

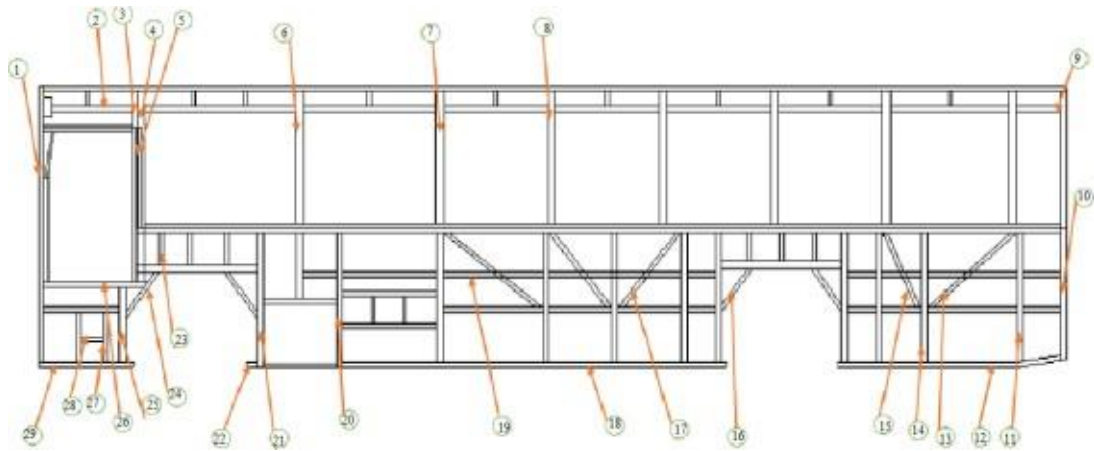


Figure 3.15 Bishoftu Bus left side frame structure

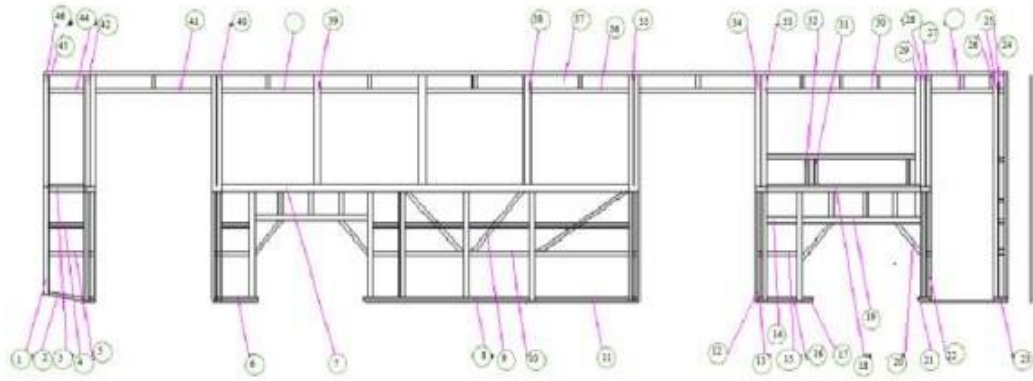


Figure 3.16 Bishoftu Bus right side frame structure

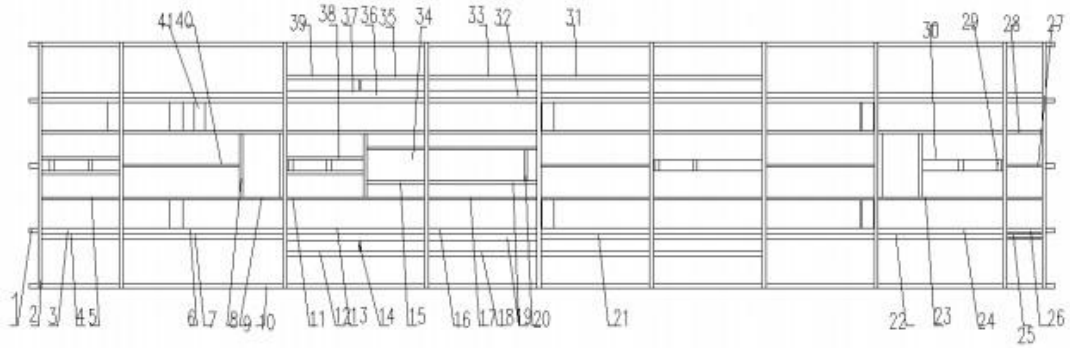


Figure 3.17 Bishoftu Bus Roof side frame structure

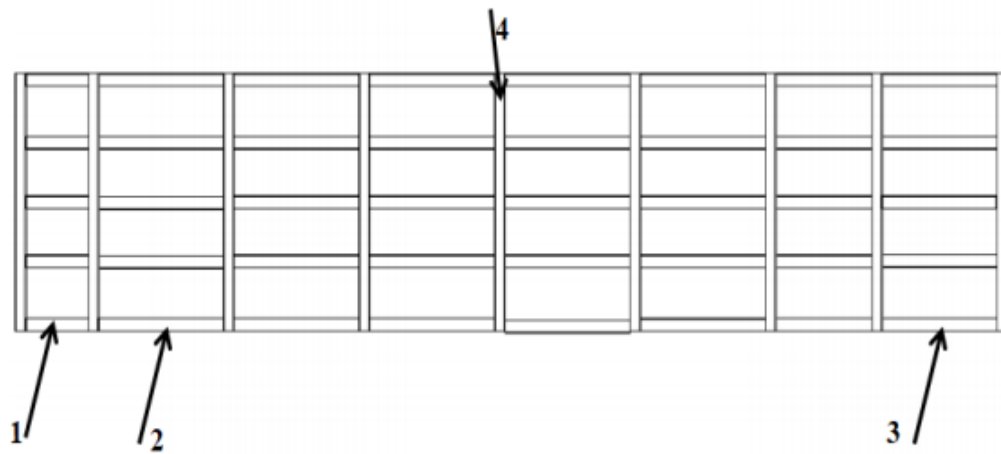


Figure 3.18 Bishoftu Floor side frame structure

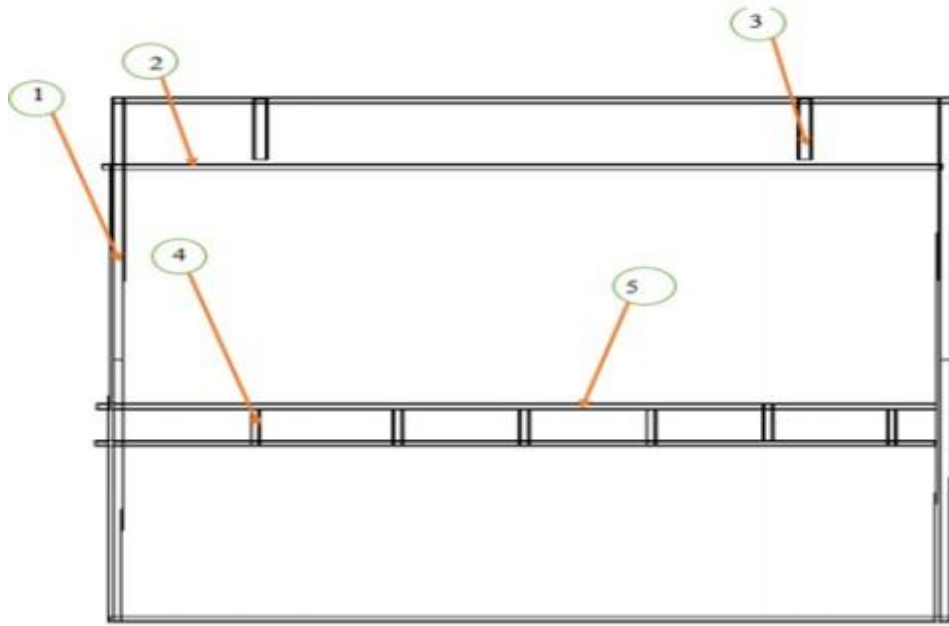


Figure 3.19 Bishoftu bus Front side frame structure

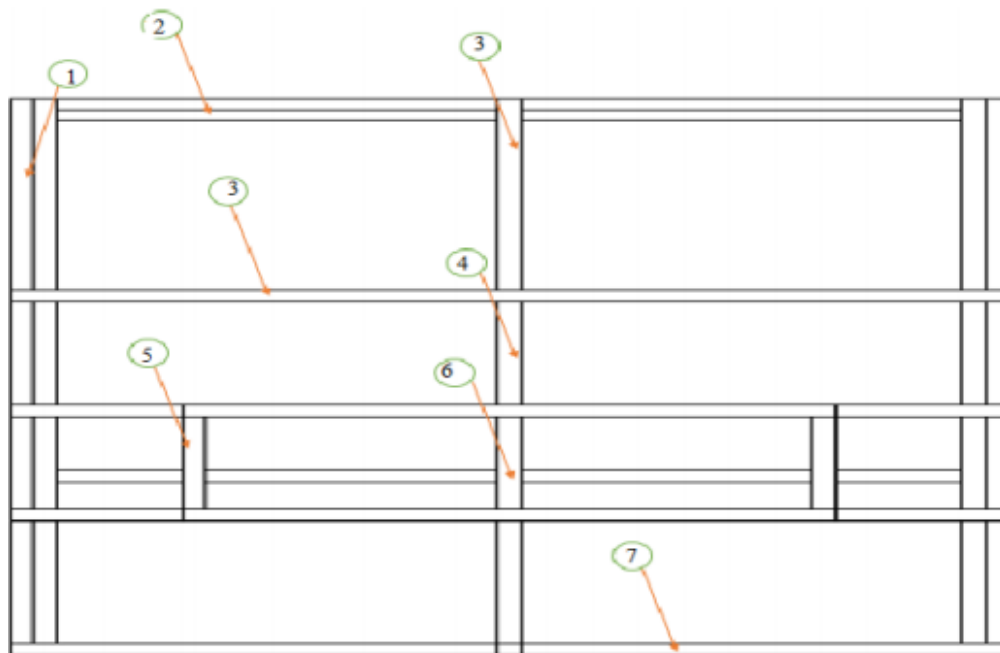


Figure 3.20 Bishoftu bus Rear side frame structure

Table3.4 Self structure weight of bus body

Component Name	Mass In Kg	No. of Elements
Driver Side Bus Frame	227.717	61
Passenger Side Bus Frame	1757.268	78
Roof Side Bus Frame	352.32	116
Floor Side Bus Frame	566.421	44
Front Side Bus Frame	32.711	15
Rear Side Bus Frame	109.586	14
	3046.023	328

4 RESULTS AND DISCUSSION

This chapter deals with computer-aided design, and analysis is needed to study the structural properties of vehicles and improve the design of vehicles. With this tool, one can easily determine vehicle structural strength and dynamic properties. Simulations are useful for examining and studying body behavior under various operating scenarios without the need for physical testing of a real vehicle. Also, the simulation results can be used to demonstrate and communicate the reliability of the vehicle to the certification approver. This procedure will be beneficial both for the manufacturers, as they will have confidence in what they are producing (provided that they produce the body to the design), and for the country as a whole, as they will have the advantages of reliable locally made vehicles.

4.1 Validation of the method used

The following method is used as validation of the method used. The method is verification by using a simple supported overhanging beam of cross-section used in the structure.

4.1.1 Deflection of the beam

Macaulay's method is used to find the bending moment at any general section X-X of the beam. Macaulay's method helps to find a single expression for bending moment throughout the complete span of the beam. It is used to cover all loading conditions. Figure Load applied on the beam

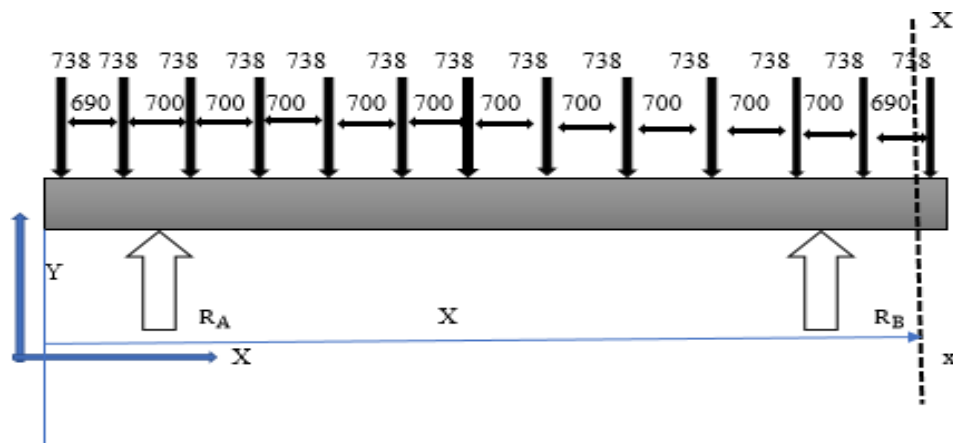


Figure 4.3 Reaction force on the beam

$$F_A = 4428 \text{ N} \quad F_B = 4428 \text{ N}$$

$$M_{xx} = -738x - 738(x - 690) + 4059(x - 690) - 738(x - 1390) - 738(x - 2090) - 738(x - 2790) - 738(x - 3490) - 738(x - 4190) - 738(x - 4890) - 738(x - 5590) - 738(x - 6290) - 738(x - 6990) + 4059(x - 6990).$$

But the bending moment is given by the following equation

From the mathematical model that applied in chapter three equation '3.1'

$$M = EI \frac{d^2y}{dx^2}$$

The second integration of this equation gives deflection (δ) of the beam

$$\delta = y$$

Therefore, integrating twice the above bending moment equation will provide the following deflection equation along the length of the beam.

$$y = \delta = \frac{1}{EI} \left[-738 \frac{x^3}{6} - 738 \frac{(x-690)^3}{6} + 4059 \frac{(x-690)^3}{6} - 738 \frac{(x-1390)^3}{6} - \frac{(x-2090)^3}{6} - \frac{(x-2790)^3}{6} - \frac{(x-3490)^3}{6} - \frac{(x-4190)^3}{6} - \frac{(x-4890)^3}{6} - \frac{(x-5590)^3}{6} - \frac{(x-6290)^3}{6} - \frac{(x-6990)^3}{6} + Ax + B \right]$$

Where A and B are integrating constants to be solved from the boundary conditions.

When $x=690$, $y=0$ and $x=6990$, $y=0$.

Therefore, the values of A and B is

$$A = -9.0688 \times 10^9 \quad = 6297.922 \times 10^9$$

$$EI = 200 \times 467971.99 \times 10^3 = 9.36 \times 10^{10} \text{ Nmm}^2$$

Substituting the value at different length

Table 4.1 deflection of the beam

Length of the beam(mm)	Deflection (mm)
0	67.29
690	0
1390	-68.67
2090	-129.64
2790	-174.78
3490	-198.72
3840	-201.76
4190	-198.72
4890	-174.78
5590	-129.63
6290	-68.67
6990	0
7680	67.29

4.1.2 Bending moment

The stress is given by

$$\sigma = \pm \frac{My}{I}$$

Where M=bending moment

I = the second moment of area y from the N.A of the beam cross-section.

The applied load are a load of passenger and seat weight

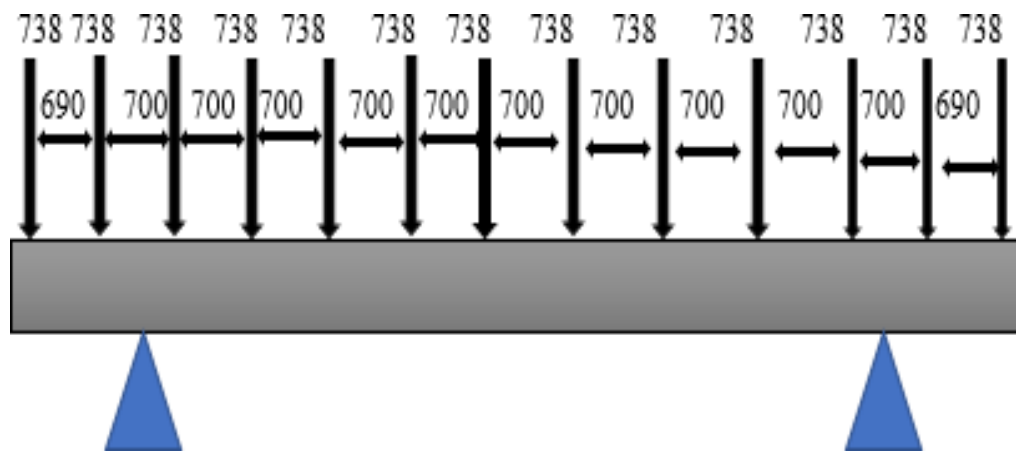


Figure 4.4 Load applied on the beam

Reaction force calculated as follows

$$R_A + R_B = 738 + 738 + 738 + 738 + 738 + 738 + 738 + 738 + 738 + 738 + 738 + 738 + 738$$

$$R_A + R_B = 8856 \text{ N}$$

$$\sum MA = 0$$

$$-738 \times 690 = 738 \times 700 + 738 \times 1400 + 738 \times 2100 + 738 \times 2800 + 738 \times 3500 + 738 \times 4200 + 738 \times 4900 + 738 \times 5600 - R_B \times 6300 + 738 \times 6990$$

$$R_A = 4428 \text{ N} \quad R_B = 4428 \text{ N}$$

The second moment of area for the hallow section is given by

$$I = \frac{b_2}{12} h_2^3 - \frac{b_1}{12} h_1^3$$

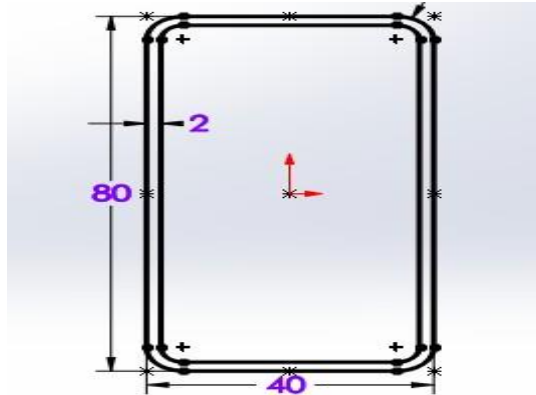


Figure 4.5 RHS from solid work welding profile.

$$b_2 = 40 \text{ mm}$$

$$b_1 = 36 \text{ mm}$$

$$h_2 = 80 \text{ mm}$$

$$h_1 = 76 \text{ mm}$$

$$I = \frac{40}{12} \times 80^3 - \frac{36}{12} \times 76^3$$

$$= 389738.67 \text{ mm}^4$$

- The maximum bending moment is calculated to be $M_{\max} = 4656780 \text{ Nmm}$.
- The maximum tensile stresses occur at the bottom periphery of the cross-section, i.e. $y = 40 \text{ mm}$.
- The maximum tensile stresses occur at the bottom periphery of the cross-section, i.e. $y = 40 \text{ mm}$.

$$\sigma = \pm \frac{My}{I} = \frac{4656780 \times 40}{389738.67} = \pm 477.93 \text{ Mpa.}$$

The compressive stress occurs at the top side of the cross-section and its value is calculated to be -477.93 Mpa . The tensile stress occurs at the bottom section of the beam's cross-section, and its value is found to be $+477.93 \text{ Mpa}$. Now to find the von miss stress (equivalent stress), we should first find the principal stresses.

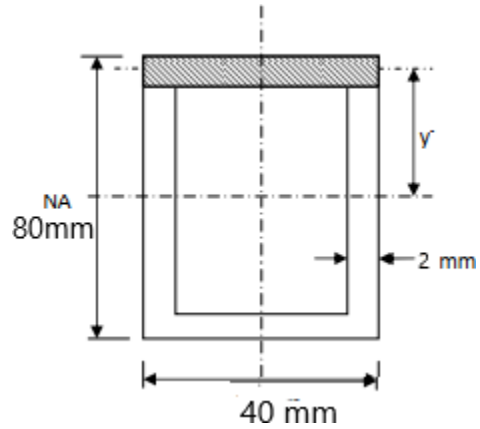


Figure 4.6 RHS cross-section

For the shear stress at section, considering the shaded area above

$$Q = y^- A'$$

Where y^- is the distance from the neutral axis to the centroid of the area considered and A' is the area of the considered section.

$$y^- = 76/2 + 1 = 39 \text{ mm}$$

$$A' = 40 \times 2 = 80 \text{ mm}$$

$$Q = 39 \times 80 = 3120 \text{ mm}^2$$

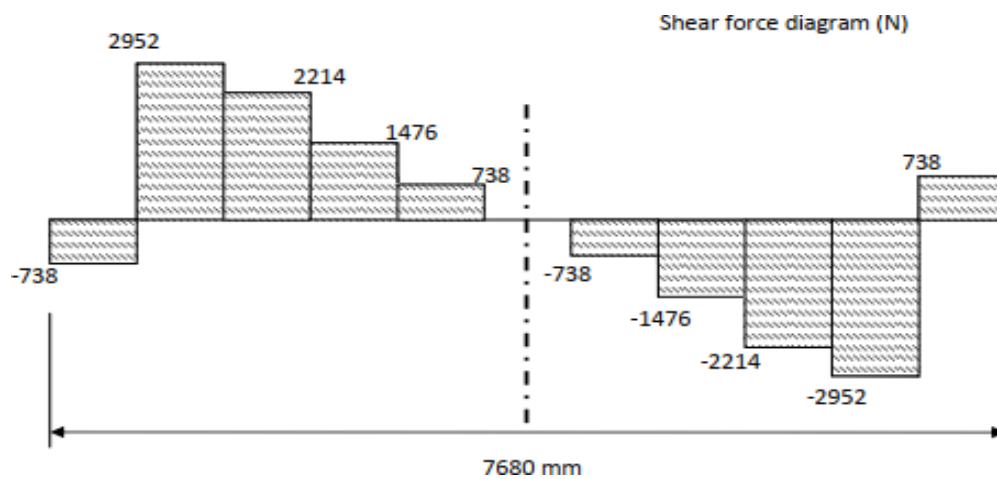


Figure 4.7 shear force diagram

Now shear force at the middle of the beam becomes zero.

The overall shear force becomes zero $r_{xy}=0$

To find the principal stress, the below equation is used.

$$\sigma_1, \sigma_2 = \frac{\sigma_x + \sigma_y}{2} \pm \sqrt{\left(\frac{\sigma_x - \sigma_y}{2}\right)^2 + r_{xy}^2}$$

$$\sigma_x = -477.93 \text{ Mpa}, \quad \sigma_y = 0$$

$$\sigma_1 = 0, \sigma_2 = 0 \quad \sigma_3 = -477.93 \text{ Mpa.}$$

$$\sigma_{von-miss} = \left[\frac{(\sigma_1 - \sigma_2)^2 + (\sigma_2 - \sigma_3)^2 + (\sigma_3 - \sigma_1)^2}{2} \right]^{1/2}$$

$$\sigma_{von-miss} = 477.93 \text{ Mpa.}$$

4.1.3 Verification of manual analysis of the beam with ANSYS Workbench

The following figure shows the finite element mesh of the beam.

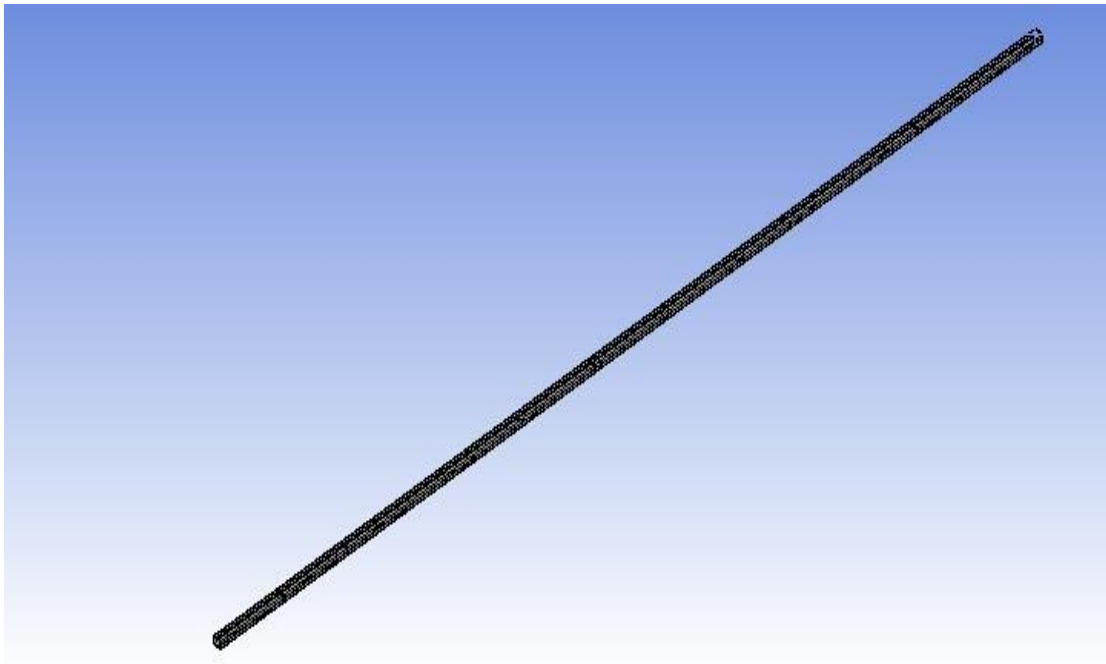


Figure 4.8 the meshed structure of the beam

The loads on the beam are applied to the structure in the places where they are applied on the structure.

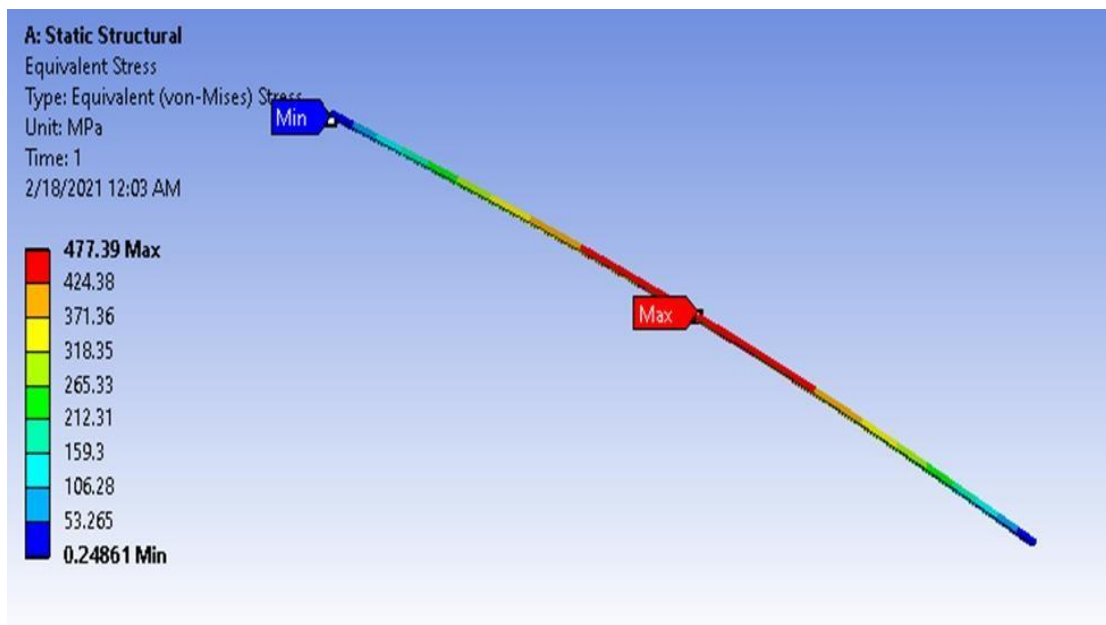
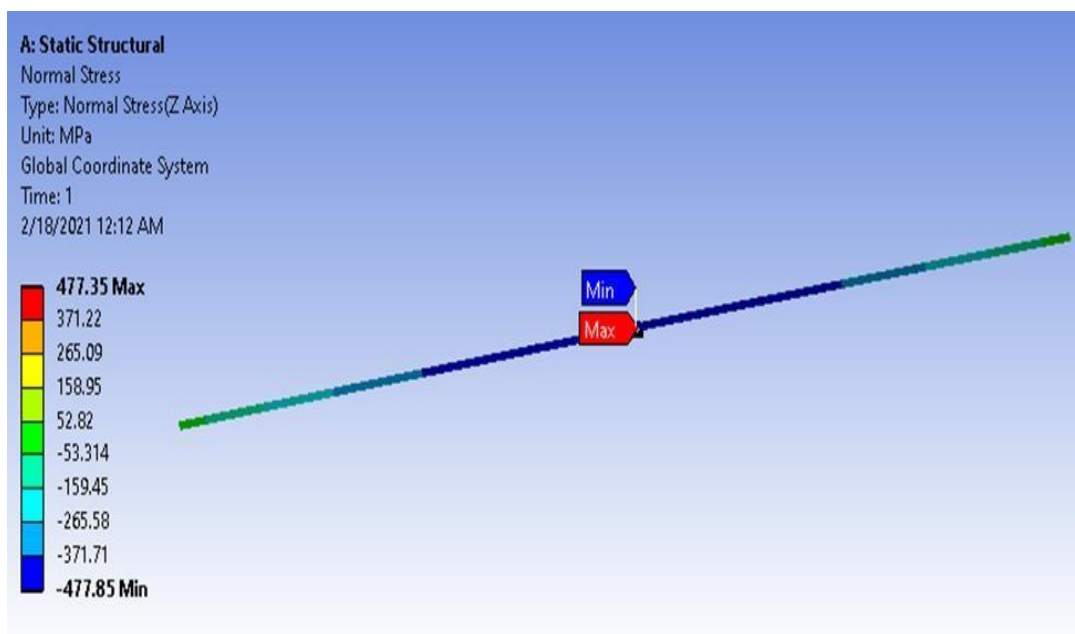


Figure 4.9 equivalent stress distribution



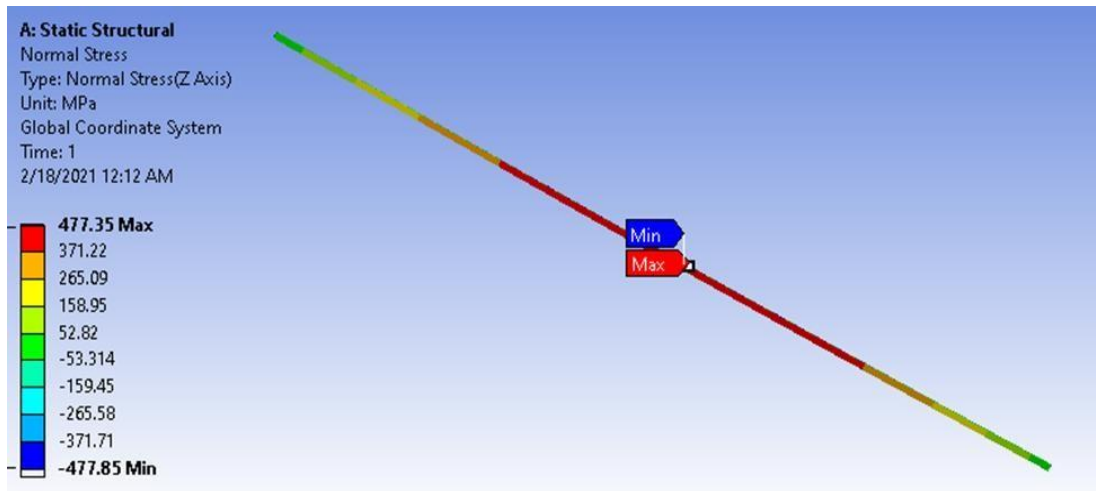


Figure 4.10 normal stress distribution at the upper and bottom periphery of the beam

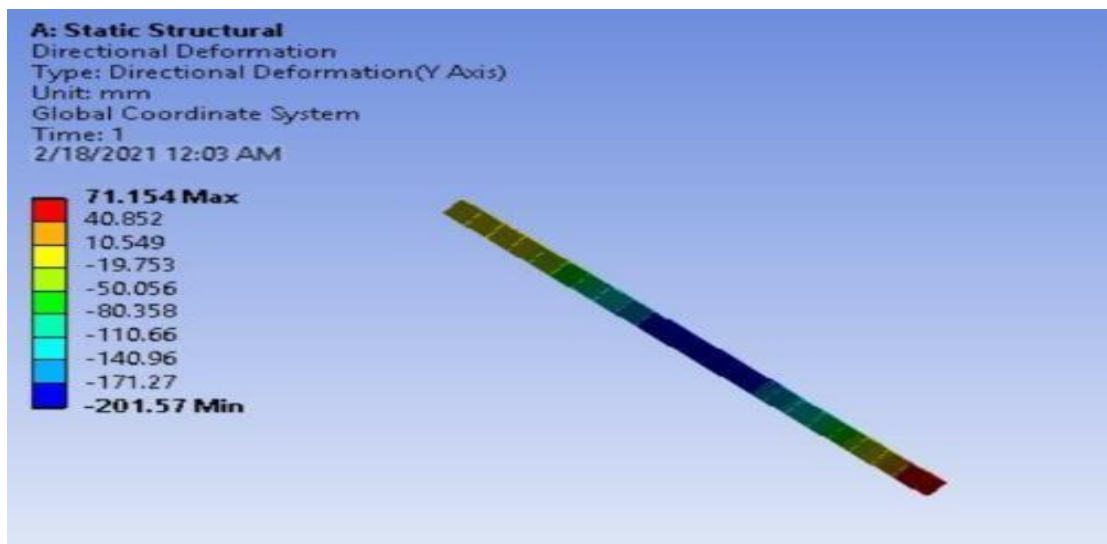


Figure 4.11 deformation of the beam

The above figures show the stress and deformation values of the beam. The maximum tensile stress is 477.35Mpa and the maximum compressive stress is -477.85Mpa. As we observe from the analytical and software analysis of the beam, there is a close similarity in equivalent, maximum tensile, maximum compressive stress, and deformation. As we observe from the analytical and software analysis of the beam, there is a close similarity in bending and deflection results. This shows the procedure used in the analysis of the bus structure is correct. The maximum Calculated error between analytical calculation and numerical methods is 5.2 % by comparing the maximum deformation value.

4.2 Dynamic analysis of original bus structure

4.2.1 Braking Load Condition

The boundary condition for the case of braking load - both front and rear wheels (left and right wheel) must be constrained in three main directions at the nodes, and the offsets in the x, y, and z directions are specified as explained in figure 4.12. By applying these boundary conditions to the finite element model, the stresses and displacements on critical structural elements were calculated from the ANSYS 19.0 desktop. In the case of a braking load, the structure experiences both bending loads and torsional rigidity.

Figure 4.12 shows the normal stress distribution in the frame structure of a bus during braking, with critical stress occurring at the front of the body due to the shift in vehicle weight. The maximum normal stress is 49.545 MPa in section 160, and the minimum normal stress is 61.95 MPa in section 68. The elements were subjected to both compressive and tensile stresses from -61.95 MPa to 49.545 MPa.

Figure 4.13 shows the equivalent stress on the front part of the body frame has more value than the remaining part, the maximum equivalent stress is 115.99Mpa at part 160 and the minimum equivalent stress occurs at part 90. The maximum equivalent stress that occurred at part 160 (115.99Mpa) is less than the maximum allowable stress of steel structure which is 230Mpa. The rare side of the bus body experience the least von misses stress.

The braking effect also showed on the deformation counter plot obtained from the analysis workbench tool, the bus structure frontal area got a high displacement value. Part 170 has the total deformation value of 2.3961mm and the minimum total deformation creates at part 90 as shown in figure 4.14. Figure 4.15 shows the distribution of directional deformation along the x-axis, the maximum directional deformation is 0.45183mm and 0.27303mm along the positive x-axis and negative x-axis respectively. The negative sign in displacement shows the direction of deformation. Figure 4.16 shows the shear stress distribution of the XY plane, the minimum shear stress is -11.614Mpa at part 137 and the maximum shear stress is 26.376Mpa at part 160.

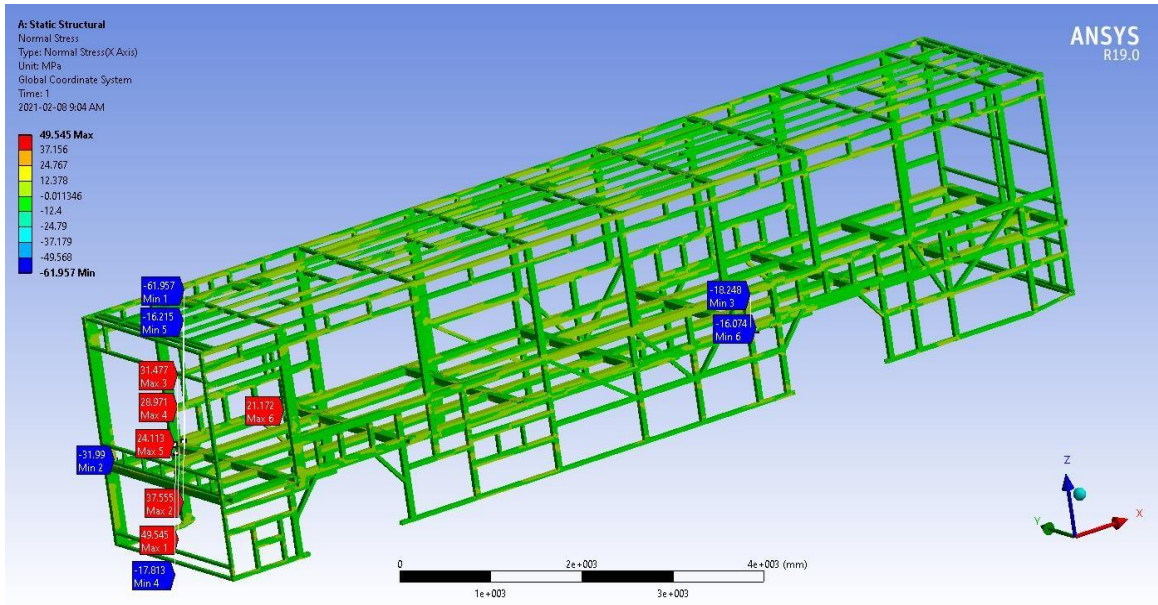


Figure 4. 12 normal stress of original structure for braking load case

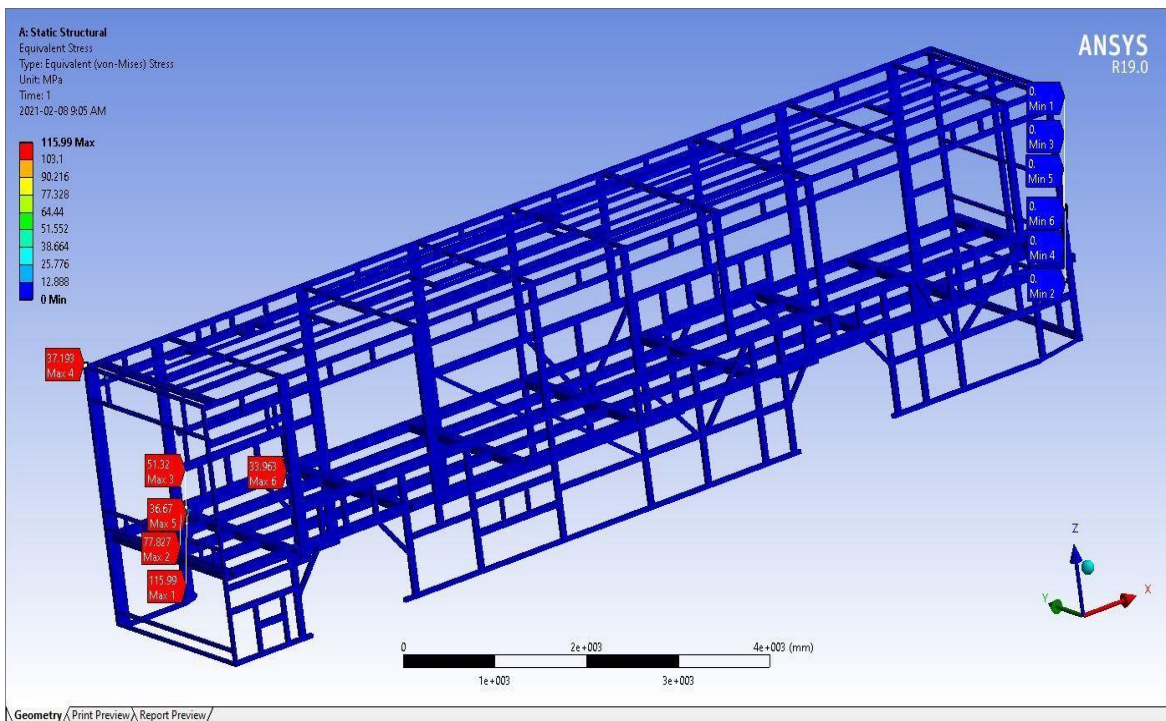


Figure 4.13 von-mises stress of original structure for braking load case.

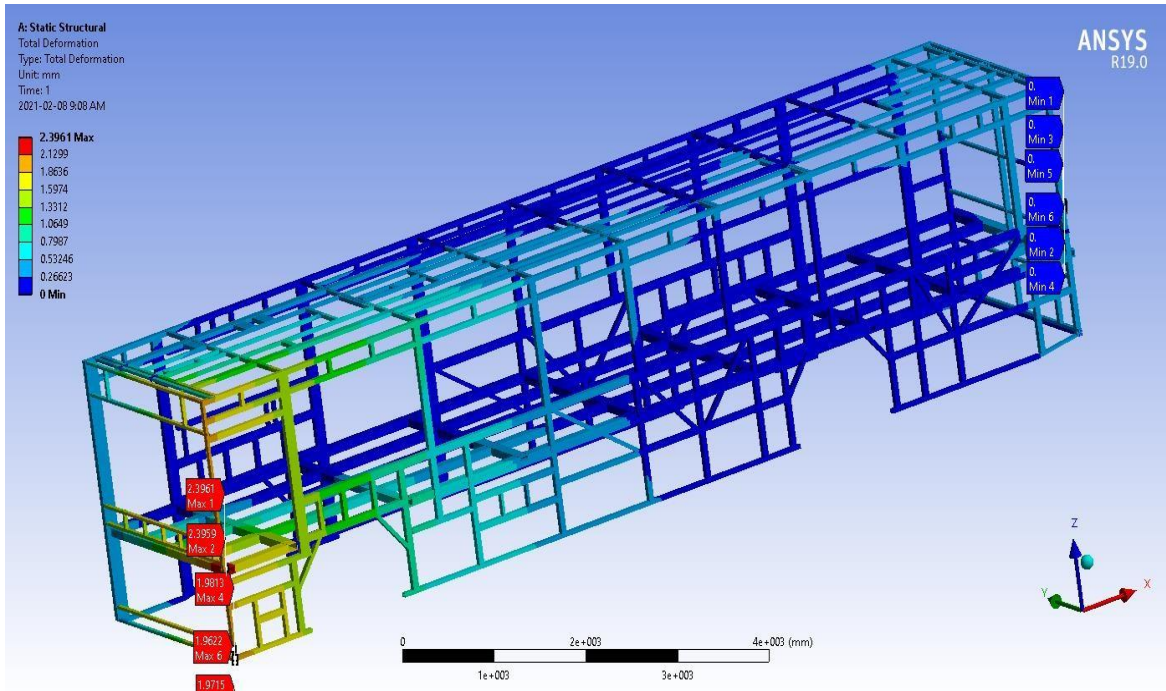


Figure 4.14 total deformation of the original structure for braking load case.

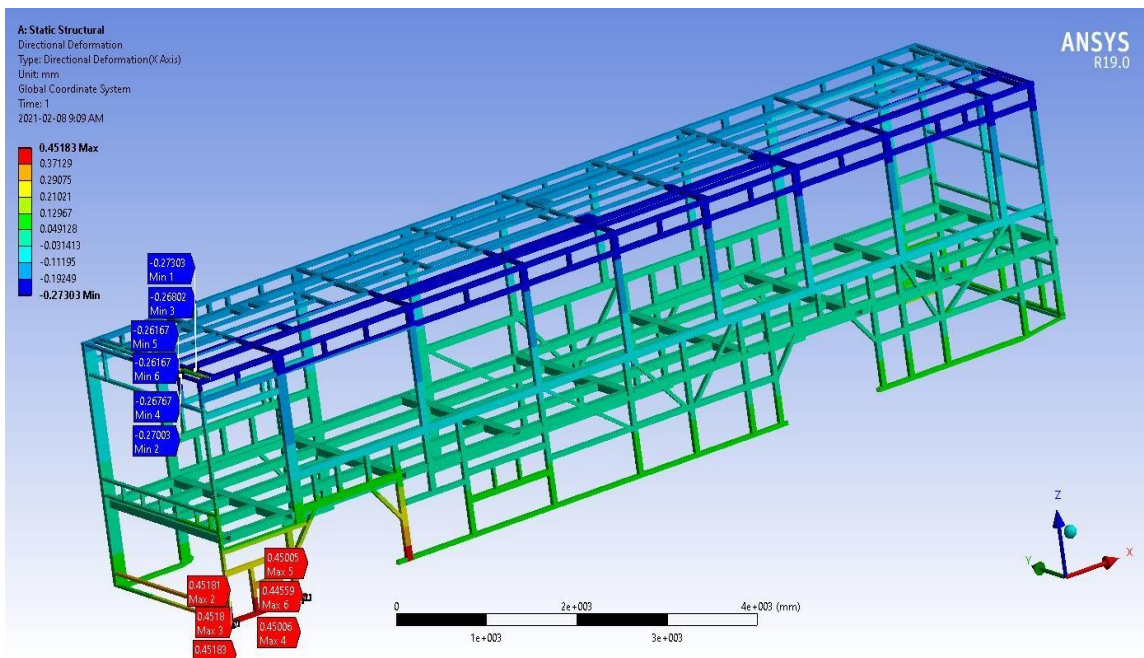


Figure 4.15 directional deformation of the original structure for the braking load case.

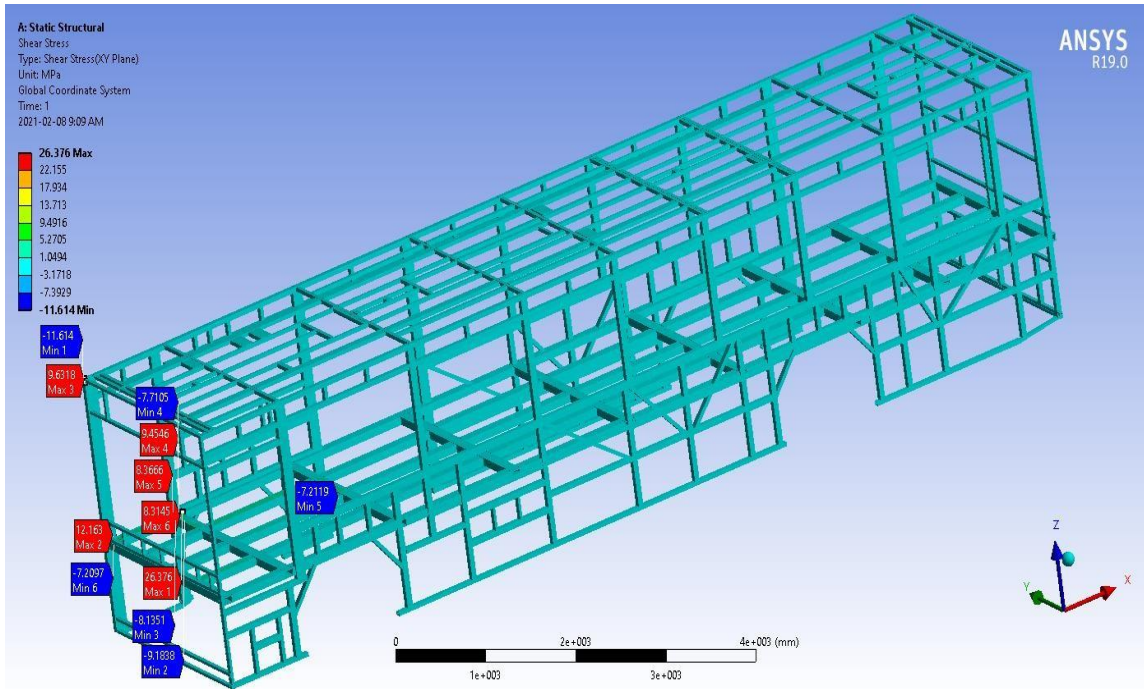


Figure 4.16 shear stress (XY plane) of the original structure for the braking load case.

Table 4.2 summary result of bus structure during braking

Braking I	Normal stress	Equivalent stress	Total displacement	Directional displacement	Shear stress
Maximum	49.545Mpa at part160	115.99 Mpa at part 160	2.3961mm at part 170	0.45183mm at part	26.376Mpa at part 137
Minimum	-61.95Mpa at part 68	0	0	-0.273 mm at part.	-11.62Mpa at part160

4.2.2 Cornering Load

Right cornering load cases

The boundary condition for the right cornering load case is both front and the rear wheels (left and right side wheel) are to be constrained in the three principal directions at the nodes and the displacements in x, y, and z directions are set as explained at the figure 3.19.

Applying these boundary conditions on the finite element model, calculated the stresses and displacements on the critical members of the structure.

The result below is obtained from the ANSYS result contour by applying the right cornering load cases and boundary conditions. Normal stress distribution during right cornering clearly shows the critical stress values that occurred at the junction point between the side frame and the bed structure. It is due to weight transformation from the outer wheel to the inner wheel. Figure 4.17 shows normal stress along the x-axis, the sidewall structure experience the maximum tensile stress of 91.586Mpa at part 26 and the minimum compressive stress of – 46.006Mpa at part 306.

Figure 4.18 shows von misses stress of bus structure during the right cornering. The total effect of stress on the bus structure is mainly expressed by the equivalent stress of the structure. On the contour plot, the maximum equivalent stress is 139.46Mpa, which is less than the allowable stress of a steel structure. The minimum stress 0Mpa at part 306 and the maximum equivalent stress occurred at part 313.

Figure 4.19 shows the total deformation of the structure, the maximum total deformation occurs at the part by which minimum equivalent stress is obtained and the minimum total deformation occurs on the part that the maximum equivalent stress recorded. The maximum total deformation is 38.123mm and the minimum total deformation is 0mm.

The negative sign in displacement shows the direction of deformation. Figure 4.20 shows the distribution of directional deformation along x-axis, the maximum directional deformation is 0.5932 mm (part146) along positive x-axis and - 0 .6371mm (part326) along Negative x-axis.

Figure 4.21 shows the shear stress of the structure, the maximum shear stress is 26.387 Mpa occurs at part 306 and the minimum shear stress is -43.988Mpa recorded at part 6. The body structure can stand the maximum shear load along the XY plane. The shear stress is directly related to the torsional rigidity of the structure.

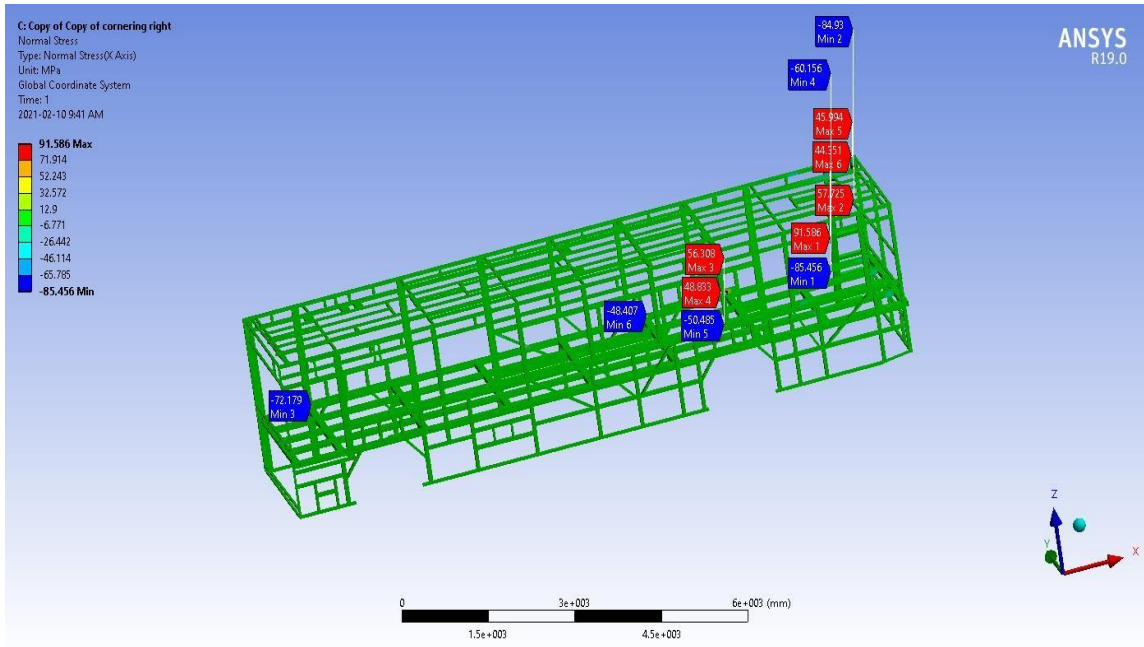


Figure 4.17 normal stress of original structure for the right cornering load case.

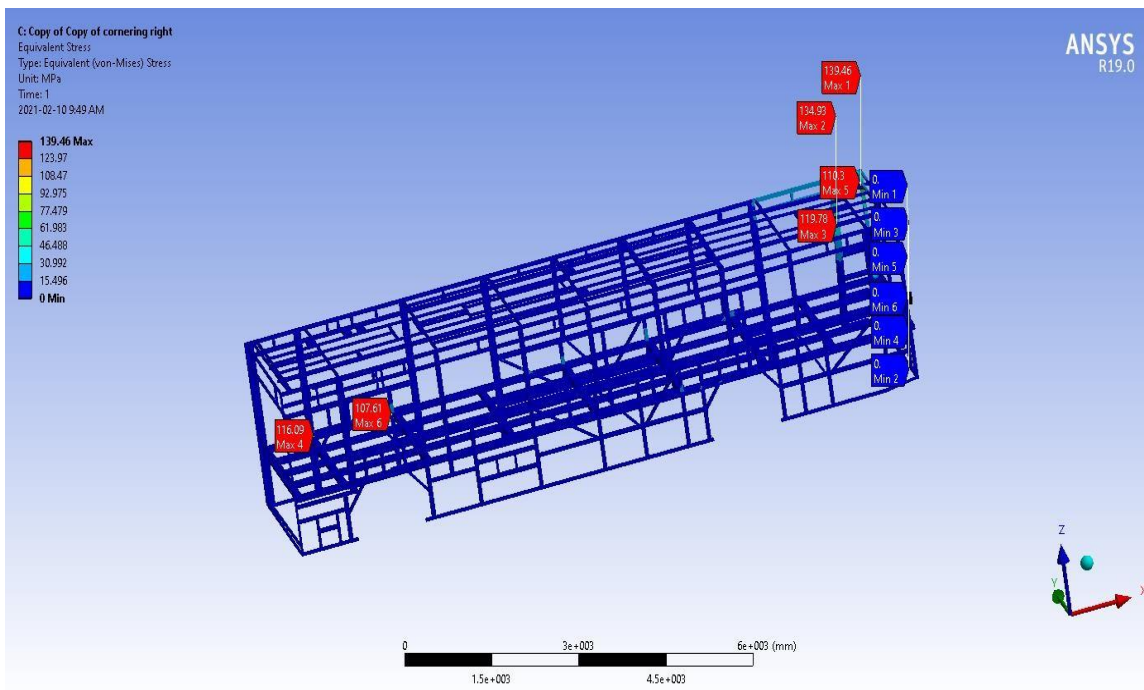


Figure 4.18 von-misses stress of original structure for right cornering load case.

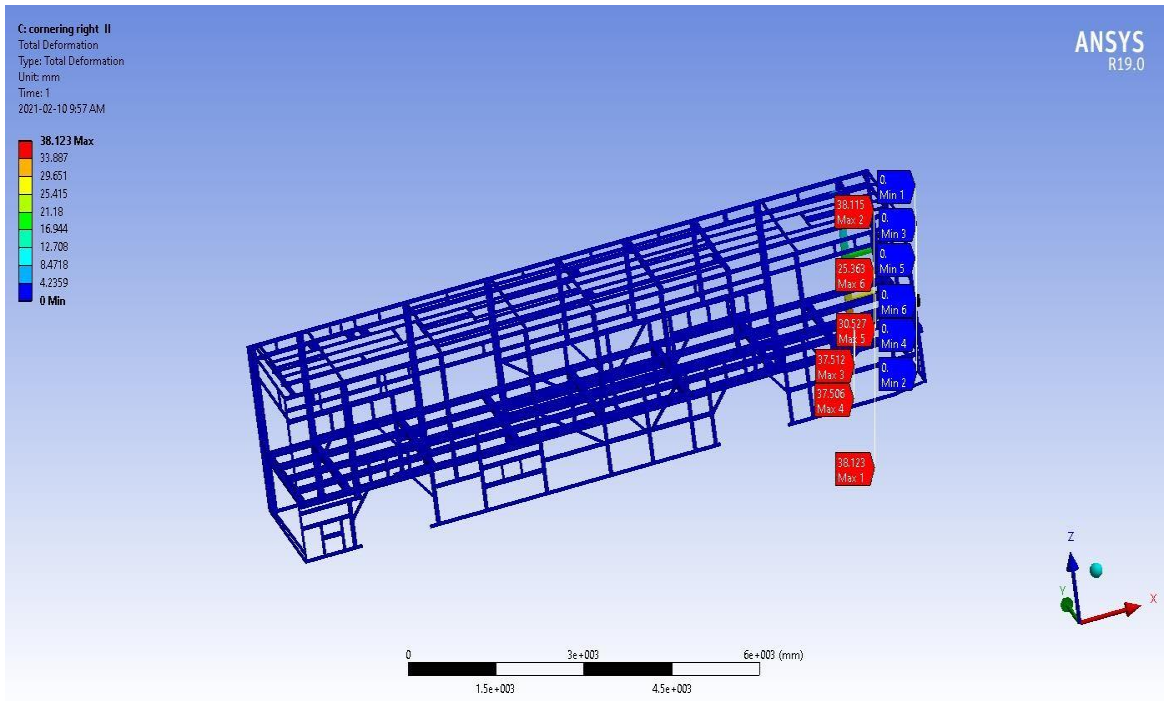


Figure 4.19 total deformation of the original structure for the right cornering load case.

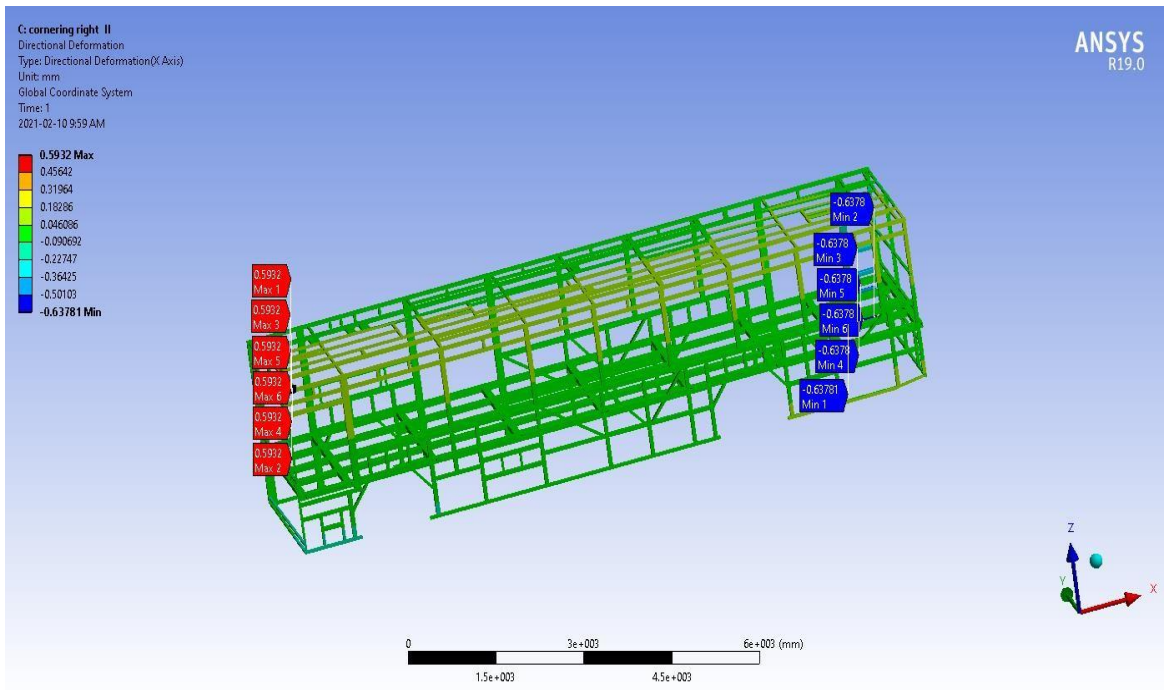


Figure 4.20 directional deformation of the original structure for right cornering load case.

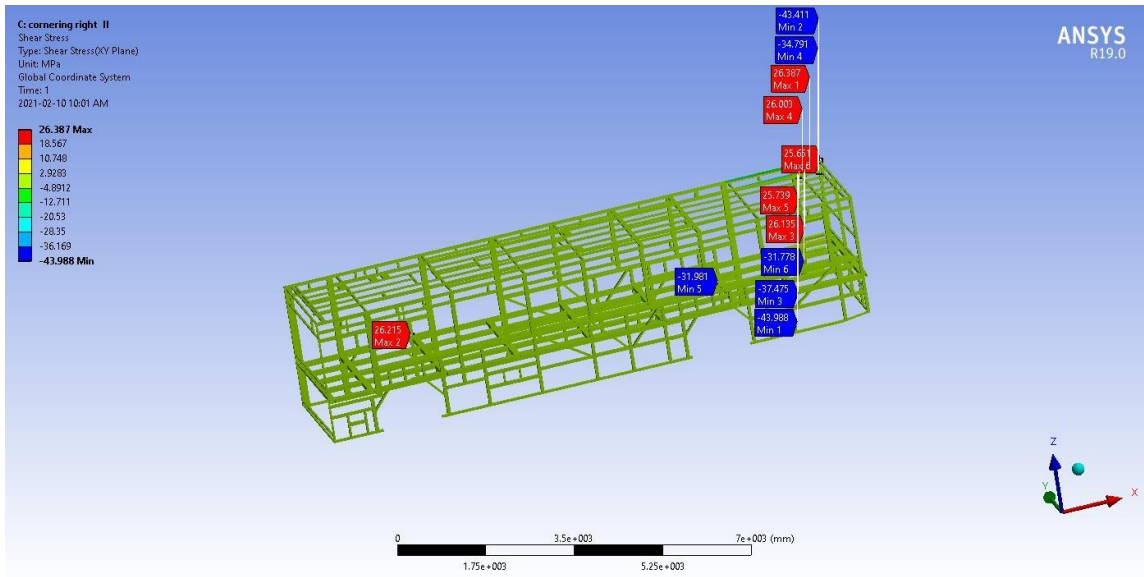


Figure 4.21 shear stress (XY plane) of the original structure for the right cornering load case.

Table 4.3 Summary table of stress and displacement for right cornering

Right cornering I	Normal stress	Equivalent stress	Total displacement	Directional displacement	Shear stress
Maximum	91.586Mpa at part 26	139.46 Mpa at part 313	38.123mm at part	0.5922mm at part 146	26.387Mpa at part 306
Minimum	-46.01Mpa at part 306	0	0	-0.6371 mm at part326	-43.99Mpa at part6

Left cornering loading result

The boundary condition used in left cornering is the same as the boundary condition on right cornering except for the position of nodal displacement and the direction of steering acceleration, all the nodal displacement shift the position from left to right and vice versa. Fixed support is also applied to the position of wheel mounted.

During left cornering; the structure experience both tensile stress (106Mpa) and compressive stress (-40.84Mpa) occurs at part 145 and part 99 respectively. The junction

point between the side and bed structure developed the critical stress as shown in figure 4.22.

Figure 4.23 shows the equivalent stress of the bus structure; maximum stress is 153.33 Mpa occurs at part 15 and the minimum equivalent stress is zero. The rare side structure more likely to develop minimum von-misses stress values. The members on the sidewall and front side structure relatively develop higher equivalent stress values. The maximum equivalent that occurs is less than the maximum yield stress of steel structure so the structure is in the safe range.

As shown in Figure 4.24 the maximum total deformation values of 6.3194mm. Here also the minimum total deformation develops at the backside of the frame structure and the maximum total deformation comes along the frontal area of the structure.

Figure 4.25 shows the distribution of directional deformation along the x-axis, the maximum directional deformation is 4.6852mm along the positive x-axis and – 0.34662mm along the Negative x-axis.

Figure 4.26 shows the shear stress of the structure, the maximum shear stress is 15.149Mpa occurs at part 41 and the minimum shear stress is -32.866Mpa recorded at part 22. The body structure can stand the maximum shear load along the XY plane.

Table 4.4 Summary table for left cornering

Left cornering I	Normal stress	Equivalent stress	Total displacement	Directional displacement	Shear stress
Maximum	106Mpa at part145	153.33 Mpa at part 15	6.3194mm at part 99	4.6852mm at part 99	15.149Mpa at part 41
Minimum	-40.84Mpa at part 99	0	0	-0.34662 mm at part1.	-32.86Mpa at part22

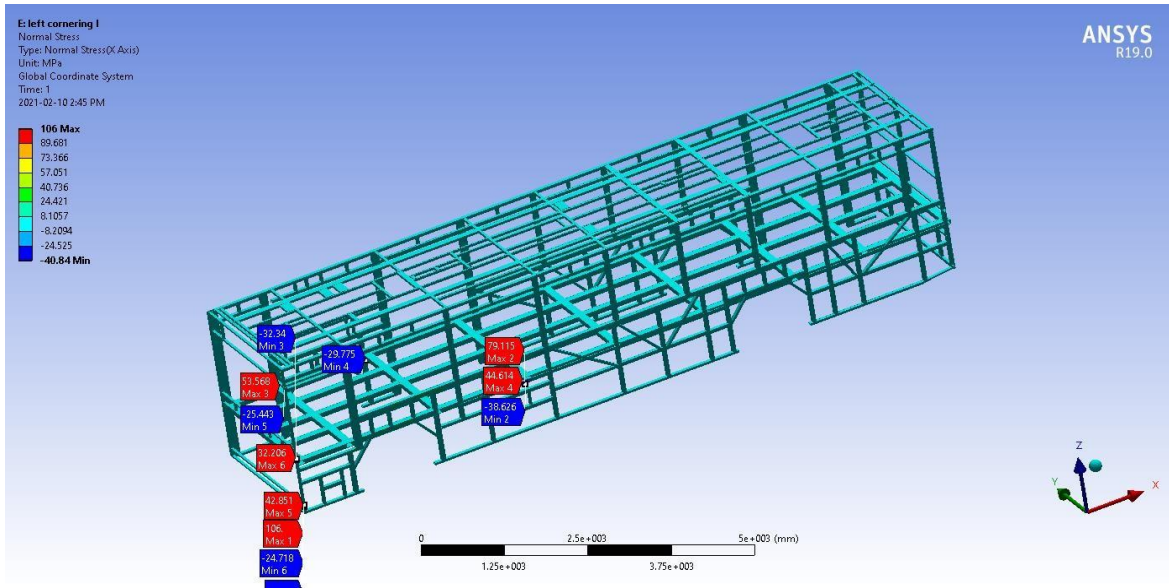


Figure 4.22 normal stress of original structure for the left cornering load case.

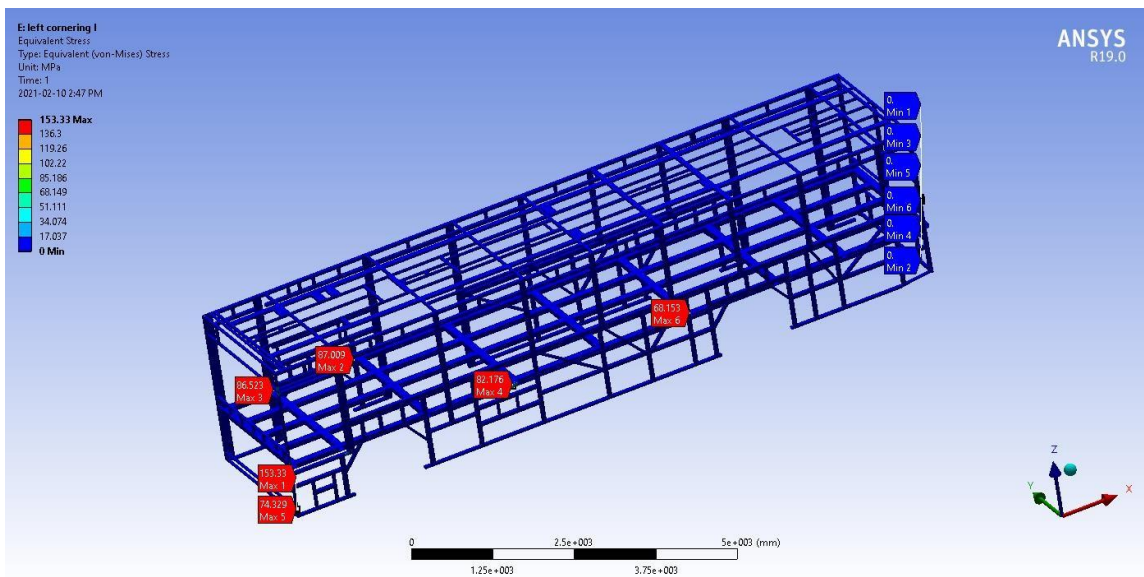


Figure 4.23 von –misses stress of original structure for the left cornering load case.

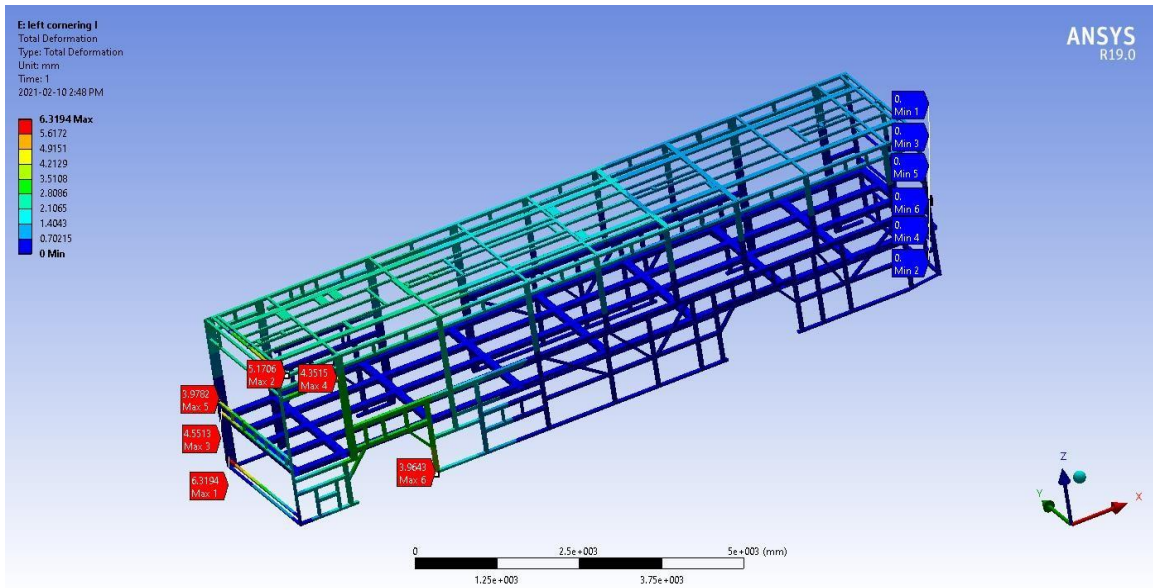


Figure 4.24 total deformation of original structure for left cornering load case.

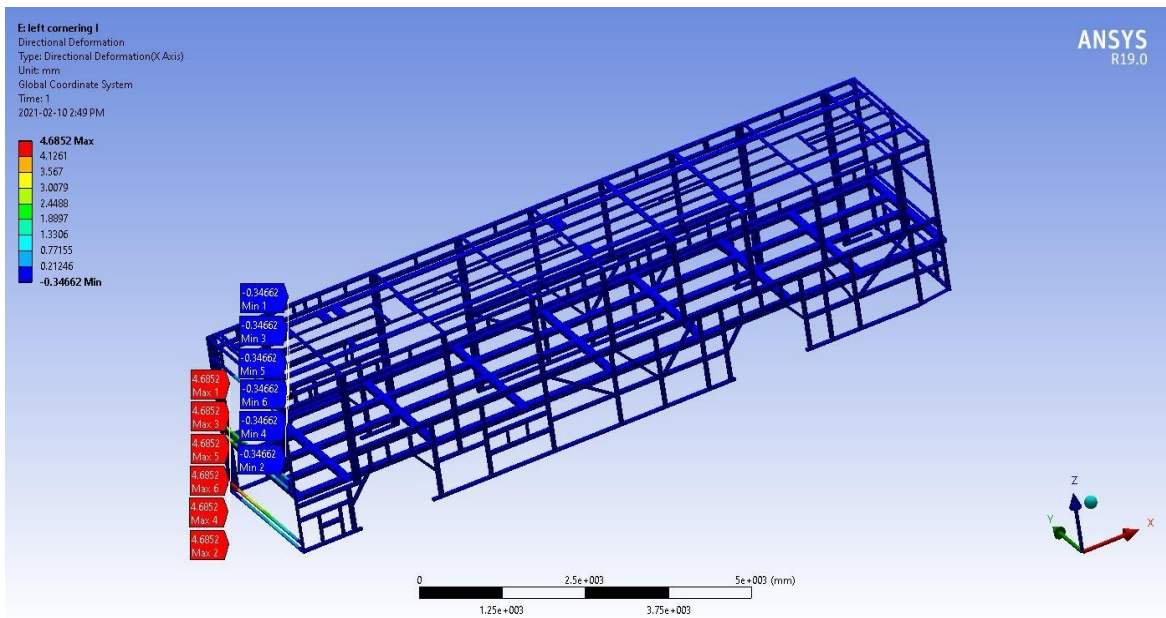


Figure 4.25 directional deformation of the original structure for the left cornering load case.

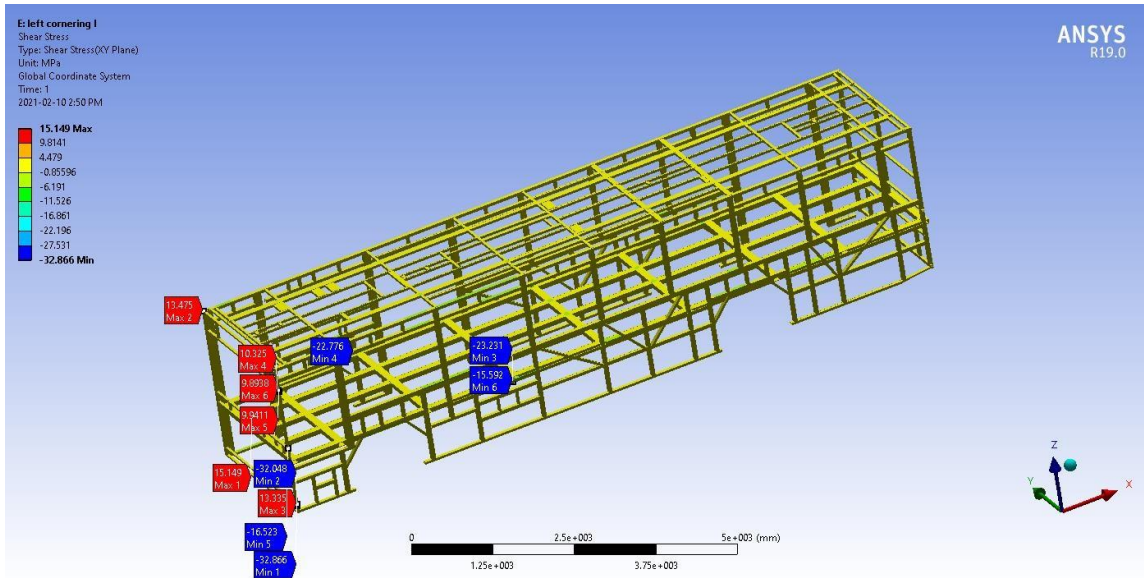


Figure 4.26 shear stress (XY plane) of the original structure for the left cornering load case.

4.3 Dynamic analysis of improved bus structure

4.3.1 Braking load condition

Figure 4.17 shows the normal stress distribution of the bus frame structure while it is braking, the critical stress occurs at the front part of the body due to the weight shifting behavior of the vehicle during braking. The maximum normal stress is 85.5Mpa at part 157 and the minimum normal stress is – 138.82Mpa at part 236. The members experienced both compressive and tensile stresses from -61.95Mpa to 49.545Mpa.

Figure 4.28 shows the equivalent stress on the front part of the body frame has more value than the remaining part, the maximum equivalent stress is 219.14Mpa at part 157 and the minimum equivalent stress occurs at part 90. The maximum equivalent stress that occurred at part 157 (219.14Mpa) is less than the maximum allowable stress of steel structure which is 230Mpa. The rare side of the bus body experience the least von misses stress.

The braking effect also showed on the deformation counter plot obtained from the analysis workbench tool, the bus structure frontal area got a high displacement value. Part 165 has

the total deformation value of 8.4926mm and the minimum total deformation creates at part 90 as shown in figure 4.29.

Figure 4.30 shows the distribution of directional deformation along the x-axis, the maximum directional deformation is 1.1251mm and -1.0678mm along part 100 and part 35 respectively. The negative sign in displacement shows the direction of deformation.

Figure 4.31 shows the shear stress distribution of the XY plane, the minimum shear stress is -28.996Mpa at part 194 and the maximum shear stress is 31.722Mpa at part 157.

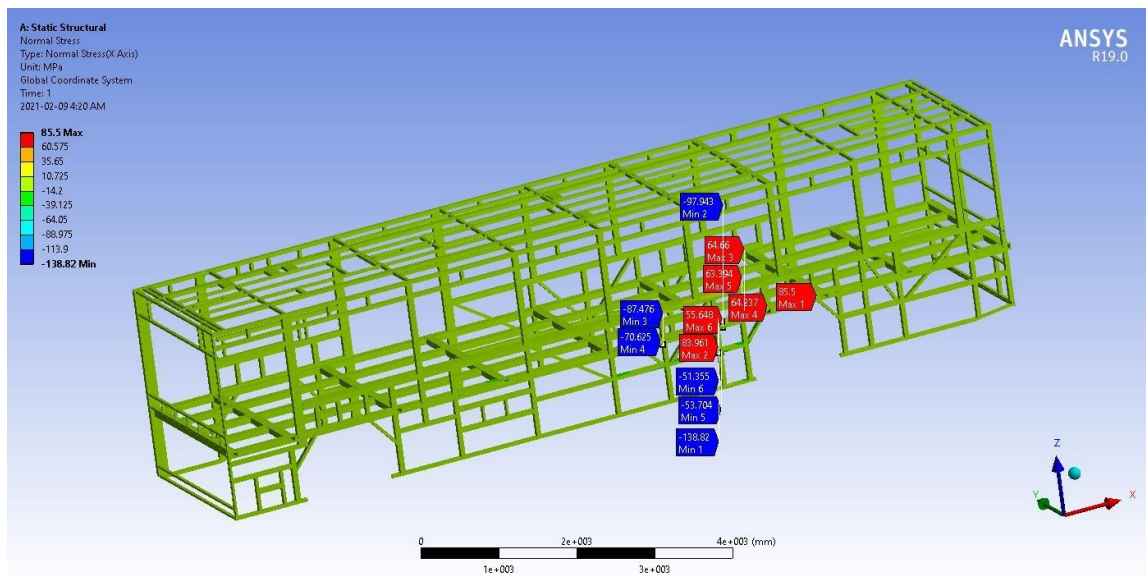


Figure 4.27 normal stress of improved structure for braking load case.

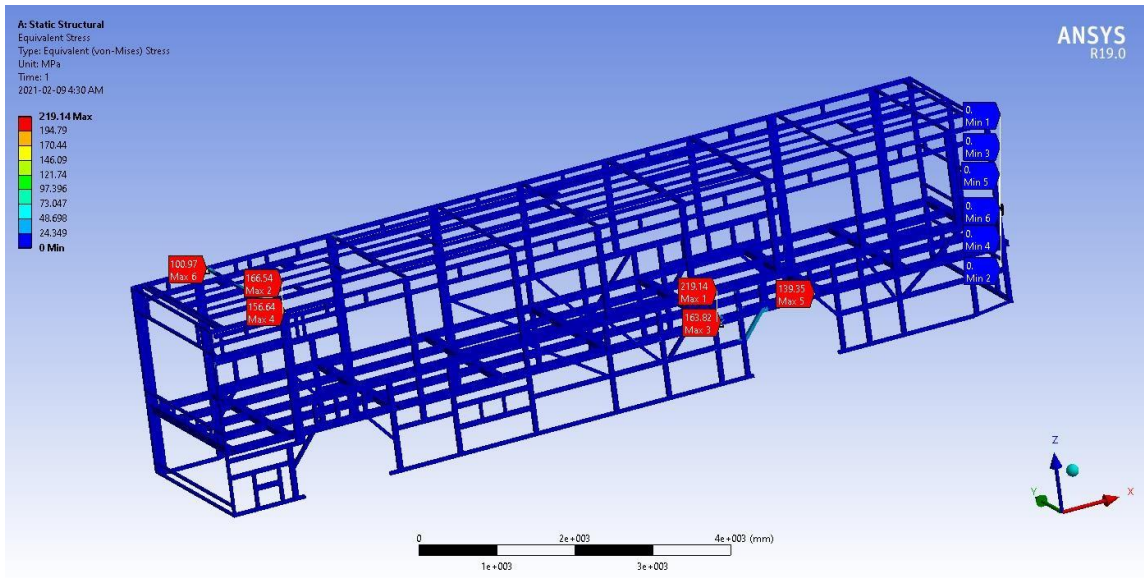


Figure 4.28 von-misses stress of improved structure for braking load case.

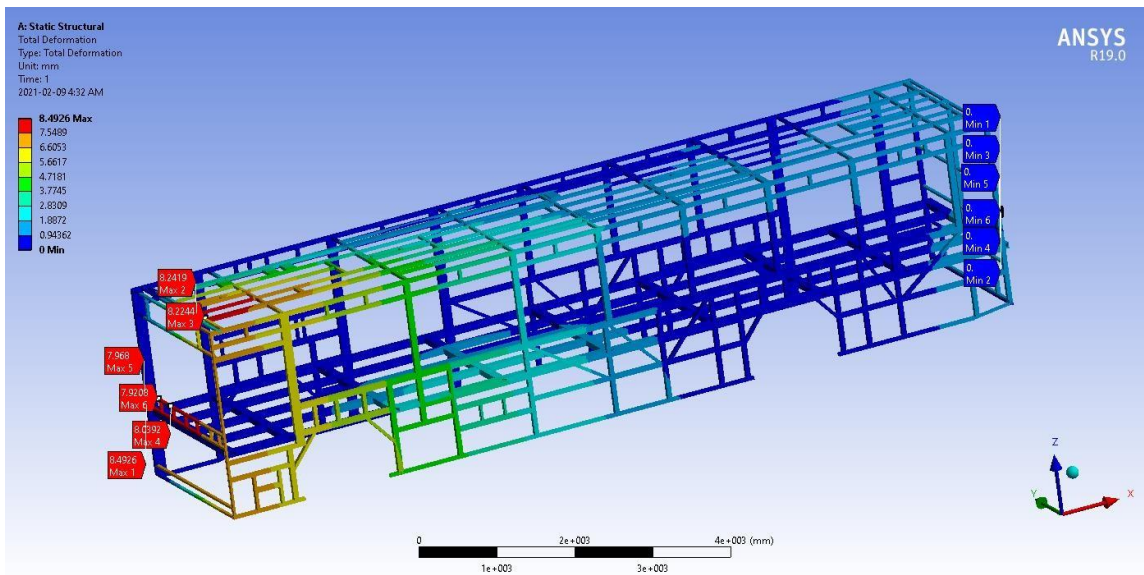


Figure 4.29 total deformation of improved structure for braking load case.

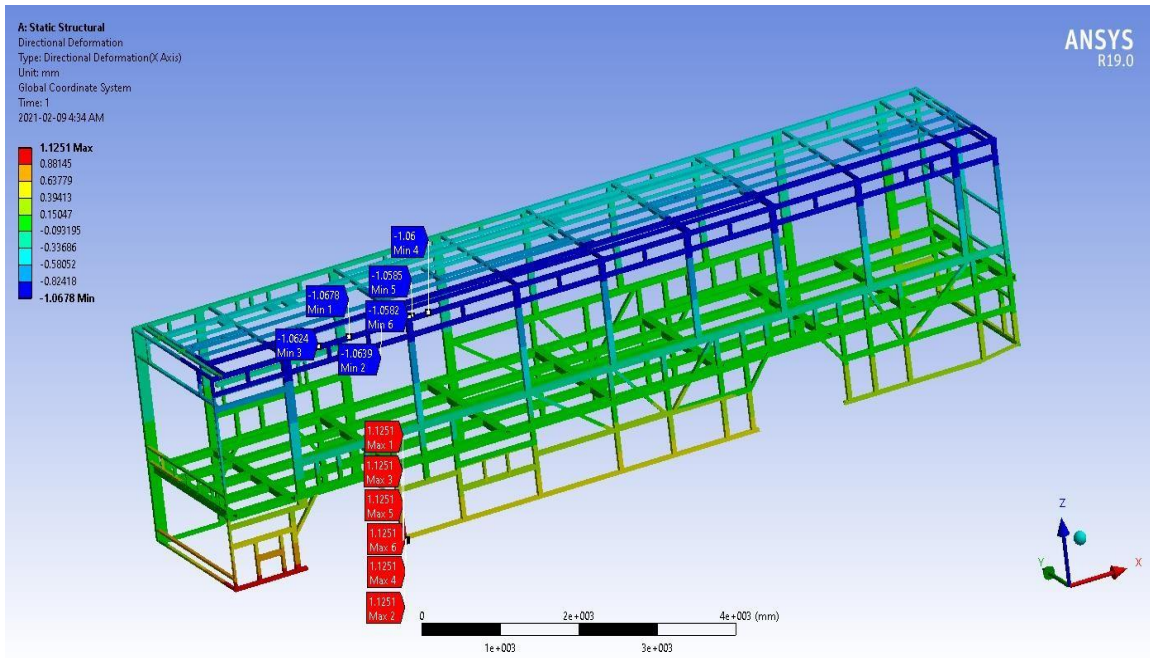


Figure 4.30 directional deformation of improved structure for braking load case.

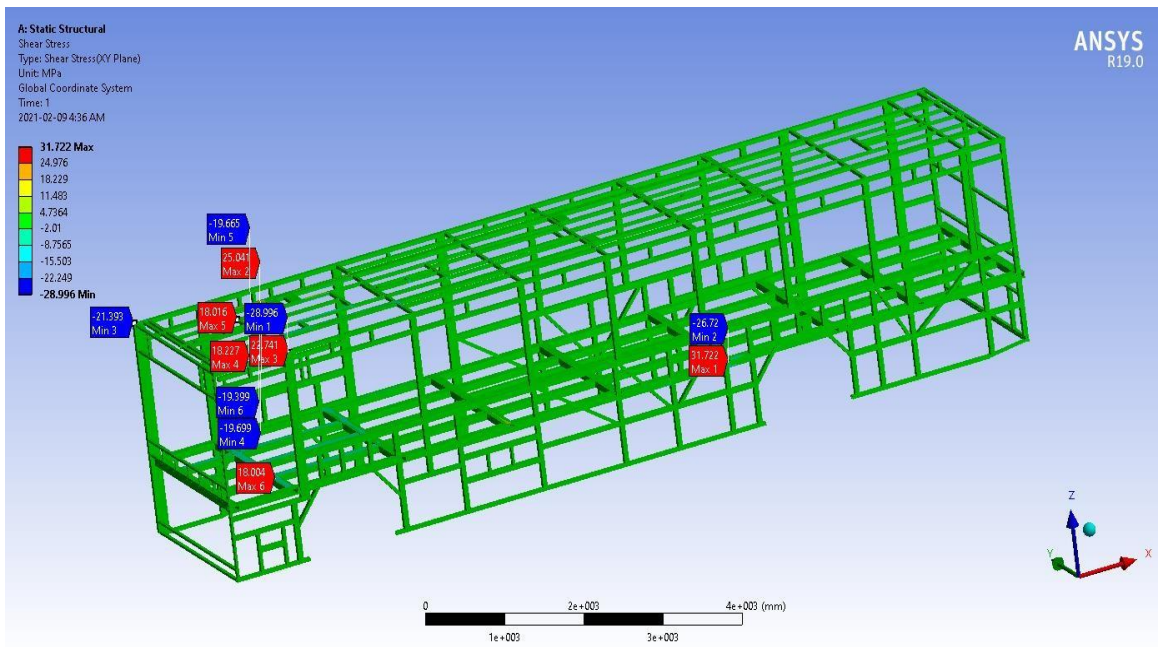


Figure 4.31 Shear stress (XY plane) of improved structure for braking load case.

Table 4.5 Summary table for displacement and stress values for braking load case after improvement.

Braking II	Normal stress		Equivalent stress		Total displacement		Directional displacement		Shear stress	
Maximum	85.5Mpa at part157	at	219.14Mpa at part 157	at	8.492mm at part 165	at	1.1251mm at part 100	at	28.996Mpa at part 194	
Minimum	-138.82Mpa at part 236	at	0	at	0	at	-1.0679mm at part35.	at	-31.72Mpa at part157	

4.3.2 Cornering load condition

Right cornering load

The boundary condition for the right cornering load case is both front and the rear wheels (left and right side wheel) are to be constrained in the three principal directions at the nodes and the displacements in x, y, and z directions are set as explained at the figure 3.19. Applying these boundary conditions on the finite element model, calculated the stresses and displacements on the critical members of the structure.

The result below is obtained from the ANSYS result contour by applying the right cornering load cases and boundary conditions. Normal stress distribution during right cornering clearly shows the critical stress values that occurred at the junction point between the side frame and the bed structure. It is due to weight transformation from the outer wheel to the inner wheel. Figure 4.32 shows normal stress along the x-axis, the sidewall structure experience the maximum tensile stress of 122.73Mpa at part 166 and the minimum compressive stress of -46.006Mpa at part 12.

Figure 4.33 shows the von misses stress of bus structure during the right cornering. The total effect of stress on the bus structure is mainly expressed by the equivalent stress of the structure. On the contour plot, the maximum equivalent stress is 183.28, which is less than the allowable stress of a steel structure. The minimum stress 0Mpa at part 90 and the maximum equivalent stress occurred at part 166.

Figure 4.34 shows the total deformation of the structure, the maximum total deformation occurs at the part by which minimum equivalent stress is obtained and the minimum total deformation occurs on the part that the maximum equivalent stress recorded. The maximum total deformation is 7.8018mm and the minimum total deformation is 0mm.

The negative sign in displacement shows the direction of deformation. Figure 4.35 shows the distribution of directional deformation along the x-axis, the maximum directional deformation is 5.1048 mm along the positive x-axis and - 0.37266 mm along the Negative x-axis.

Figure 4.36 shows the shear stress of the structure, the maximum shear stress is 15.356 Mpa occurs at part 141 and the minimum shear stress is -36.061Mpa recorded at part 166. The body structure can withstand the maximum shear load along the XY plane. The shear stress is directly related to the torsional rigidity of the structure.

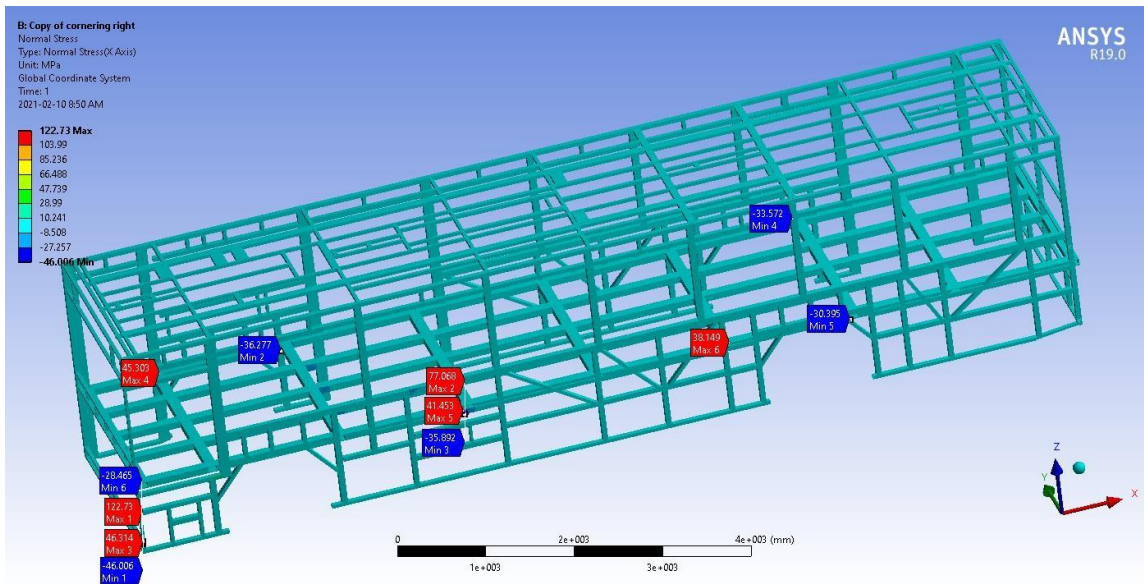


Figure 4.32 normal stress of improved structure for the right cornering load case.

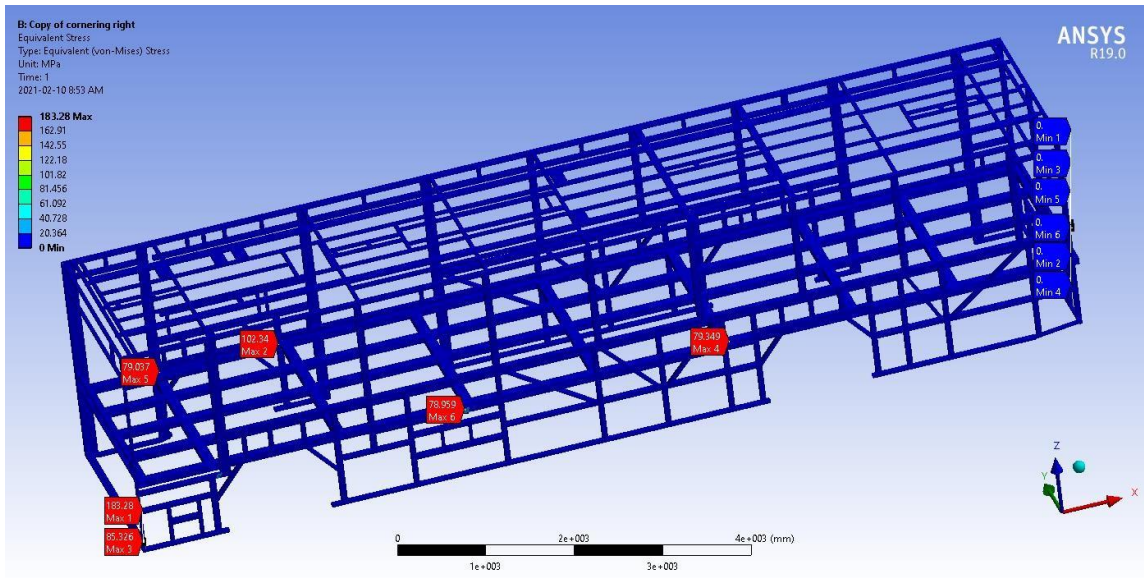


Figure 4.33 von-misses stress of improved structure for right cornering load case.

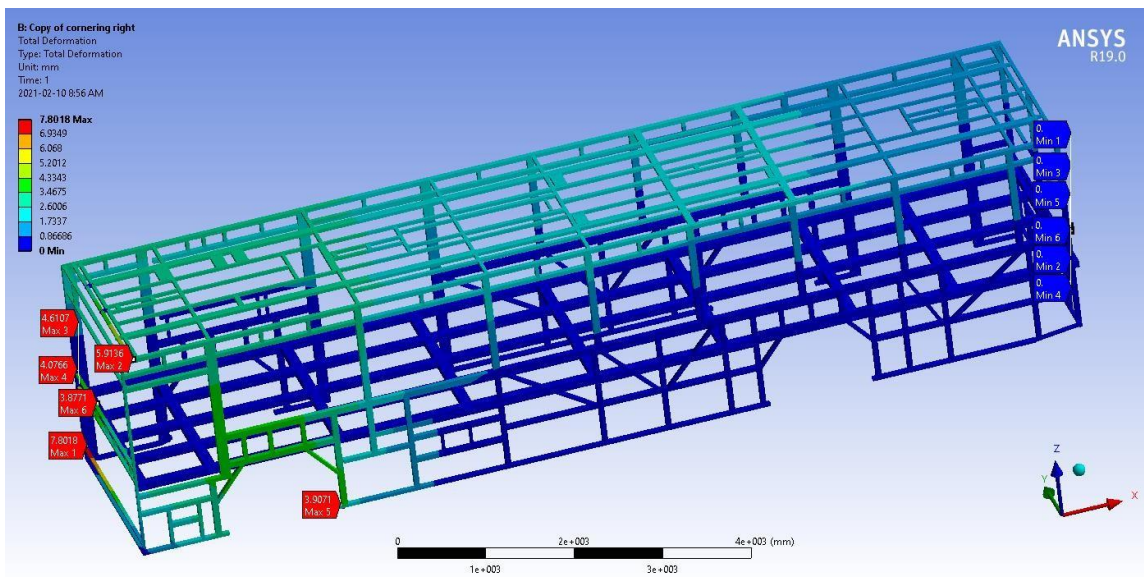


Figure 4.34 total deformation of improved structure for the right cornering load case.

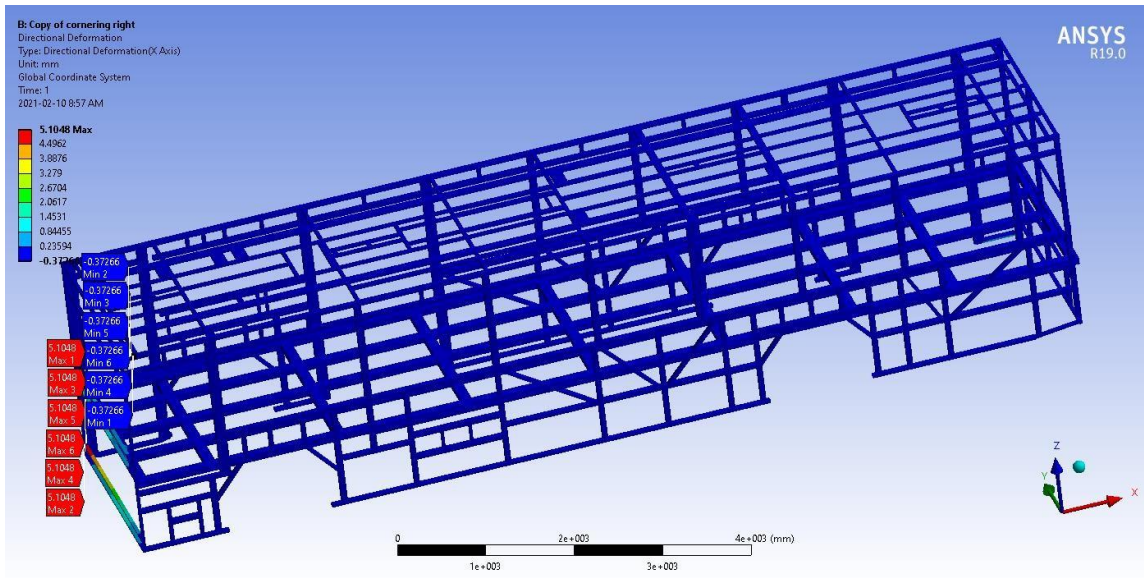


Figure 4.35 directional deformation of improved structure for the right cornering load case.

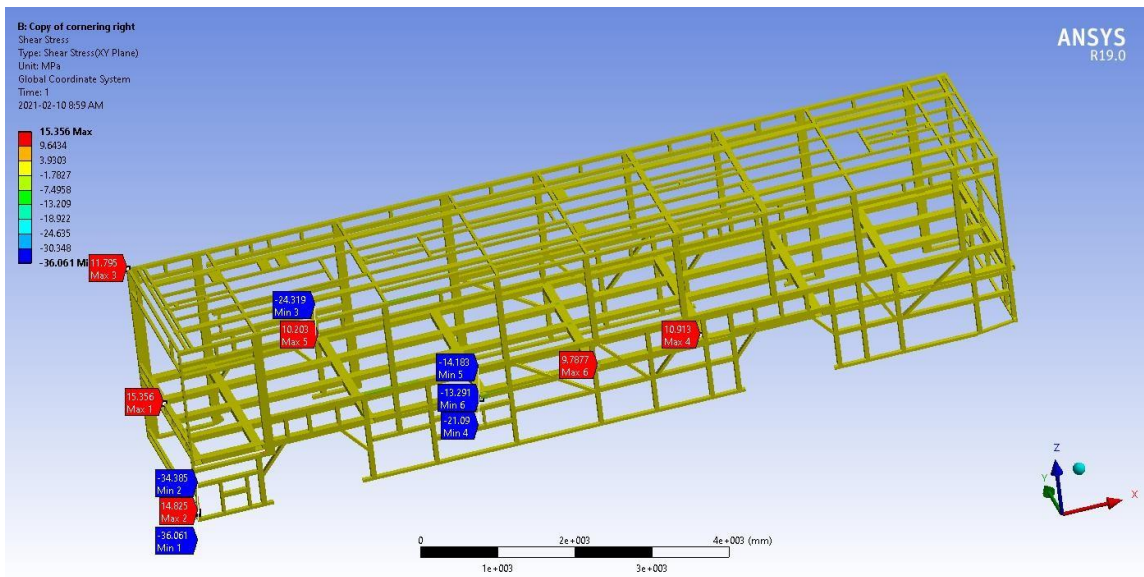


Figure 4.36 shear stress (XY plane) of improved structure for the right cornering load case.

Table 4.6 Summary table for displacement and stress values for the right cornering load case after improvement.

Right cornering II	Normal stress	Equivalent stress	Total displacement	Directional displacement	Shear stress
Maximum	122.73Mpa at part166	183.28 Mpa at part 166	7.8018mm at part	5.1048mm at part	15.356Mpa at part 141
Minimum	-46.006Mpa at part 99	0	0	-0.37266mm at part.	-36.06Mpa at part166

Left cornering load case

The boundary condition used in left cornering is the same as the boundary condition on right cornering except for the position of nodal displacement and the direction of steering acceleration, all the nodal displacement shift the position from left to right and vice versa. Fixed support is also applied to the position of wheel mounted.

During left cornering; the structure experience both tensile stress (144.75Mpa) and compressive stress (-56.3155Mpa) occurs at part 122 and part 12 respectively. The junction point between the side and bed structure developed the critical stress as shown in figure 4.37.

Figure 4.38 shows the equivalent stress of the bus structure; maximum stress is 210.88Mpa occurs at part 122 and the minimum equivalent stress is zero. The rare side structure more likely to develop minimum von-misses stress values. The members on the sidewall and front side structure relatively develop higher equivalent stress values. The maximum equivalent that occurs is less than the maximum yield stress of steel structure so the structure is in a safe range.

As shown in Figure 4.39 the maximum total deformation value of 8.6891mm, is the highest deformation value recorded on the whole analysis. Here also the minimum total deformation develops at the backside of the frame structure and the maximum total deformation comes along the frontal area of the structure.

4.40 shows the distribution of directional deformation along the x-axis, the maximum directional deformation is 0.71971mm along the positive x-axis and – 5.9709mm along the Negative x-axis.

Figure 4.41 shows the shear stress of the structure, the maximum shear stress is 20.83 Mpa occurs at part 141 and the minimum shear stress is -45.191Mpa recorded at part 122. The body structure can withstand the maximum shear load along the XY plane.

Table 4.7 Summary table for displacement and stress values for left cornering load case after improvement.

Left cornering II	Normal stress	Equivalent stress	Total displacement	Directional displacement	Shear stress
Maximum	144.75Mpa at part122	210.88 Mpa at part 122	8.689mm at part	0.7197mm at part	20.83Mpa at part 41
Minimum	-56.32Mpa at part 12	0	0	-5.97 mm at part1.	-45.2Mpa at part122

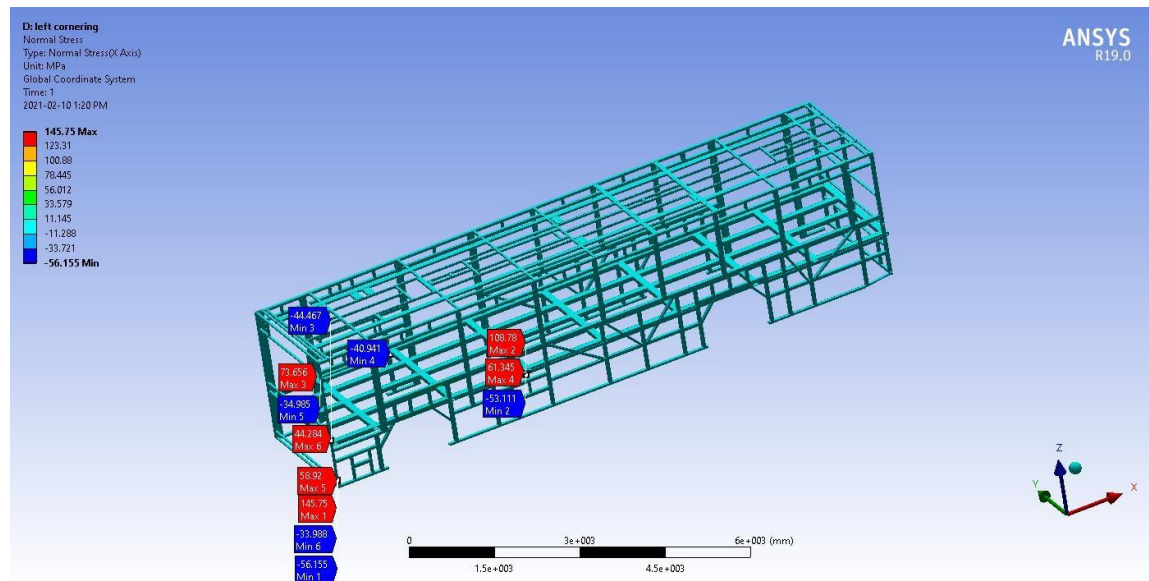


Figure 4.37 normal stress of the original structure for the left cornering load case.

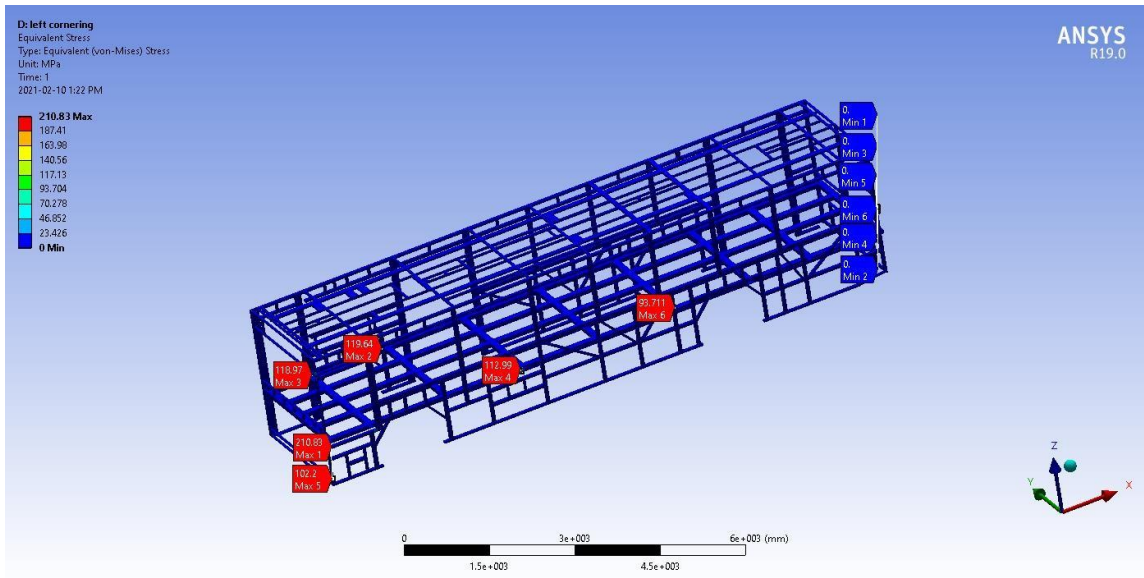


Figure 4.38 von- misses stress of improved structure for the left cornering load case.

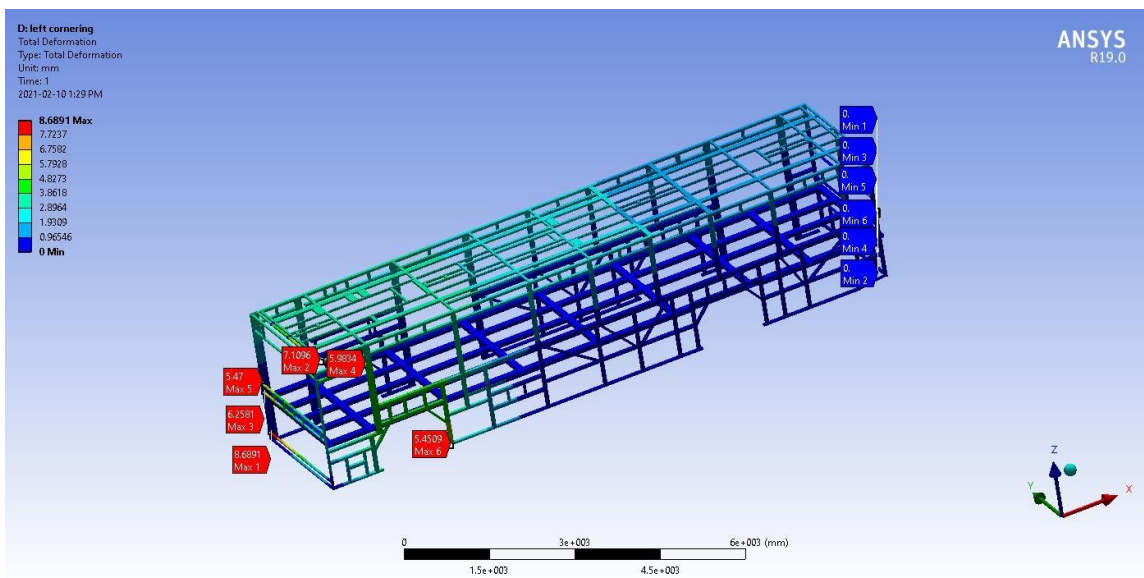


Figure 4.39 total deformation of improved structure for the left cornering load case.

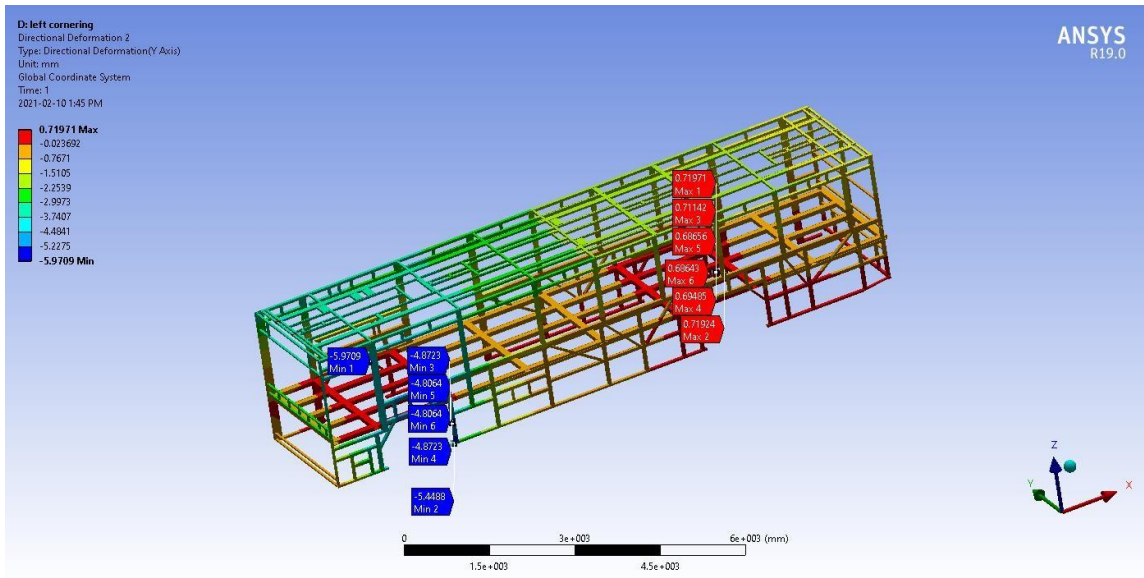


Figure 4.40 directional deformation of improved structure for the left cornering load case.

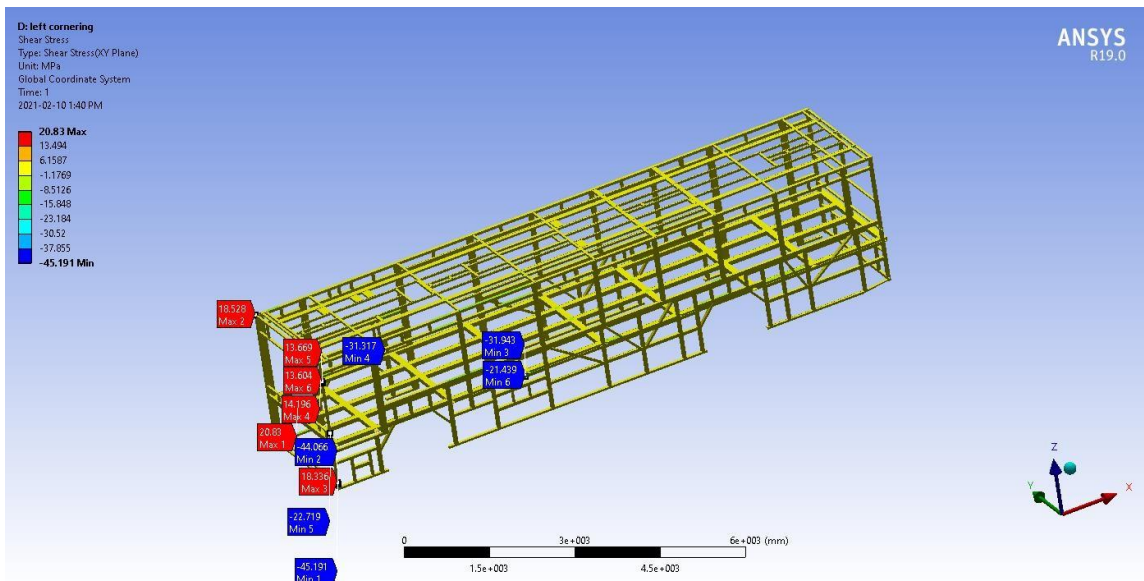


Figure 4.41 shear stress (XY plane) of improved structure for the left cornering load case.

4.4 Comparison of the original structure and improved bus structures.

4.4.1 Mass of the structure

The total amount of steel structure reduced from the original bus structure is summarized in Table 4.11

Table 4.8 Previous RHS used and New RHS used

No	Previous RHS used(mm)	New RHS used(mm)
1	80 X 40 X 2	60 X 40 X 2
2	75 X 50 X 2.5	60 X 35 X 1.5
3	70 X 50 X 2	40 X 40 X 2
4	60 X 52 X 2	40 X 40 X 1.5

To estimate the amount of steel hollow structure, we need to find the total length of RHS steel used in the bus structure.

Table 4.9 Total length of RHS 80X40X2mm used in driver door side structure.

No.	member	Length (mm)	Amount in number	Total length(mm)
1	6(Table A.1)	1203.5	1	1203.5
2	7(Table A.1)	1203.5	2	2407
3	8(Table A.1)	1203.5	7	8424.5
4	9(Table A.1)	2424	1	2424
5	10(Table A.1)	1197	1	1197
6	25(Table A.1)	681	1	681

6	26(Table A.1)	453	2	906
7	27(Table A.1)	253	1	253
8	28(Table A.1)	1162	1	1162
9	29(Table A.1)	1024	1	1024
Total			18	19682

Table 4.10 Total length of RHS 60X52X2mm used in driver door side structure.

No.	Member	Length	Amount in member	Total length(mm)
1	11(Table A.1)	1,165.5	1	1,165.5
2	14(Table A.1)	1,167.5	12	14,010
3	20(Table A.1)	1,207.5	2	2,415
4	21(Table A.1)	1,207.5	2	2,415
5	22(Table A.1)	5,188	2	10,376
6	23(Table A.1)	9,926	1	9,926
Total			20	40,307.5

Table 4.11 Total length of RHS 80X40X2mm used in passenger door side structure.

No	Member	Length (mm)	Amount in member	Total length(mm)
1	39(Table A.2)	1205	2	2,410
2	40(Table A.2)	1205	7	8,435
Total			9	10,845

Table 4.12 Total length of RHS 75X50X2.5mm used in passenger door side structure.

No	Member	Length (mm)	Amount member	Total length(mm)
1	3(Table A.2)	423.8	1	423.8
2	4(Table A.2)	423.8	1	423.8
3	7(Table A.2)	1291.9	1	1,291.9
4	18(Table A.2)	1782.7	1	1,782.7
	Total		4	3922.2

Table 4.13 Total length of RHS 70X50X2mm used in passenger door side structure.

No	Member	Length (mm)	Amount member	Total length(mm)
1	14(Table A.2)	353.9	1	353.9
2	19(Table A.2)	1358.9	1	1,358.9
	Total			1,712.8

Length of RHS saved

Table 4.14 Total length and weight of the Original structure

No	Types RHS used	Length(mm)	Mass kg
1	80×40×2mm	30,527	109.55
2	75×50×2.5mm	3,922.2	17.37
3	70×50×2mm	1,712.09	6.14
4	60×52×2mm	40,307.5	134.5178
	Total		267.5778

Table 4.15 Total length and weight of the Modified structure

No	Types RHS used	Length(mm)	Mass kg
1	60×40×2mm	30,527	90.37
2	60×35×1.5mm	3,922.2	8.3789
3	40×40×2mm	1,712.09	3.993
4	40×40×1.5mm	40,307.5	71.869
Total			174.6109

Mass reduced = 267.5778Kg-174.6109Kg

=93.5778Kg

% reduction in weight = $\frac{93.8778}{3046} \times 100\% = 3.07\%$

It was found that the modified bus body structure weighs 93.5778 kg less than the original body structure weight. The amounts to a 3.07% improvement in the weight without compromising the safety and performance of the vehicle.

4.4.2 Braking loading condition

Table 4.16 Comparison of displacement and stress values of the original structure with modified braking load case.

Normal stress(Mpa)	Σ_{max}	σ_{1max}	49.545
		σ_{2max}	85.5
	Σ_{min}	σ_{1min}	-61.95
		σ_{2min}	-138.82

Equivalent stress(Mpa)	σ_{vmax}	σ_{v1max}	115.99
		σ_{v2max}	219.14
	σ_{vmin}	σ_{v1min}	0
		σ_{v2min}	0
Total deformation(mm)	E_{max}	ϵ_{t1max}	2.3961
		ϵ_{t2max}	8.492
	E_{min}	ϵ_{t1min}	0
		ϵ_{t2min}	0
Directional deformation(mm)	ϵ_{xmax}	ϵ_{x1max}	0.45183
		ϵ_{x2max}	1.1251
	ϵ_{xmin}	ϵ_{x1min}	-0.273
		ϵ_{x2min}	-1.0679
Shear stress(Mpa)	T_{max}	τ_{1max}	26.376
		τ_{2max}	28.996
	T_{min}	τ_{1min}	-11.62
		τ_{2min}	-31.72

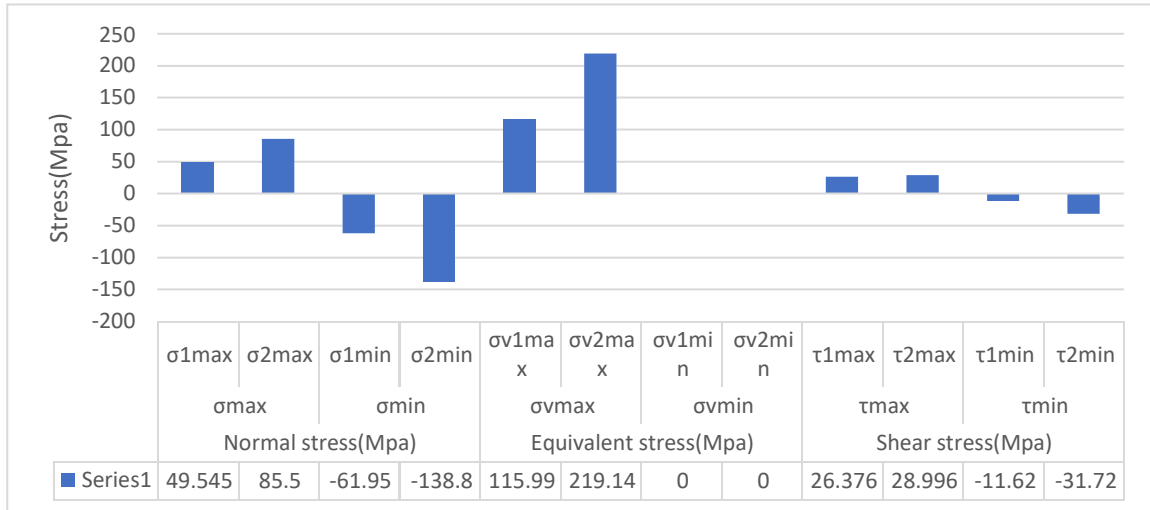


Figure 4. 42 stress comparison of the original structure with improved structure.

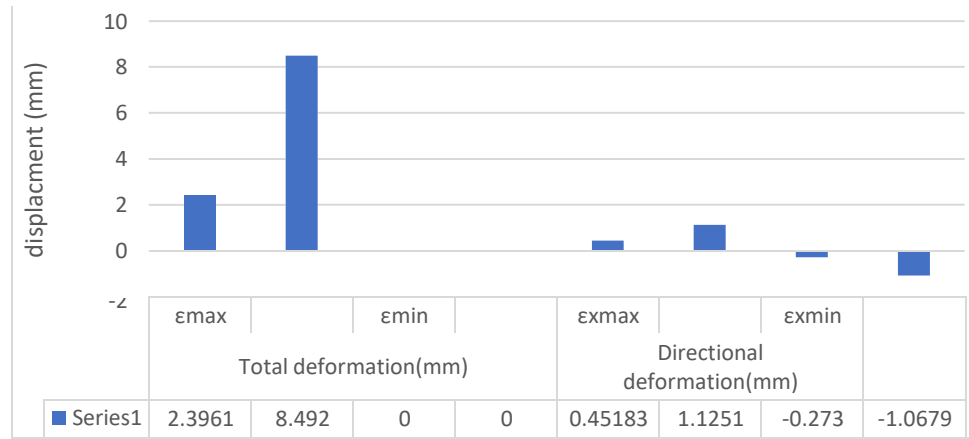


Figure 4.43 displacement comparison of the original structure with an improved one

4.4.3 Right cornering

Table 4.17 Comparison of displacement and stress values of the original structure with modified on the right cornering load case.

Normal stress(Mpa)	σ_{max}	σ_{1max}	91.586
		σ_{2max}	122.73
	σ_{min}	σ_{1min}	-46.1
		σ_{2min}	-46.006
Equivalent stress(Mpa)	σ_{vmax}	σ_{v1max}	139.46

		σ_{v2max}	183.28
		σ_{v1min}	0
		σ_{v2min}	0
Total deformation(mm)	ϵ_{max}	ϵ_{t1max}	38.123
		ϵ_{t2max}	7.8018
	ϵ_{min}	ϵ_{t1min}	0
		ϵ_{t2min}	0
Directional deformation(mm)	ϵ_{xmax}	ϵ_{x1max}	0.5922
		ϵ_{x2max}	5.1048
	ϵ_{xmin}	ϵ_{x1min}	-0.6371
		ϵ_{x2min}	-0.37266
Shear stress(Mpa)	τ_{max}	τ_{1max}	26.387
		τ_{2max}	15.356
	τ_{min}	τ_{1min}	-43.09
		τ_{2min}	-36.06

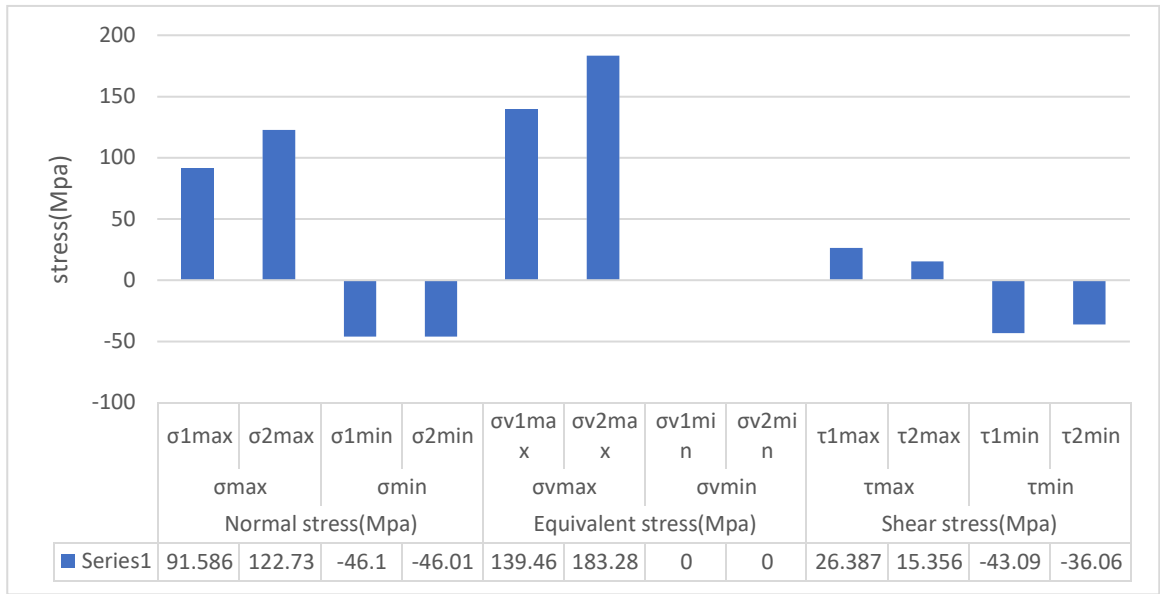


Figure 4.44 right cornering stress comparison of the original structure with improved structure

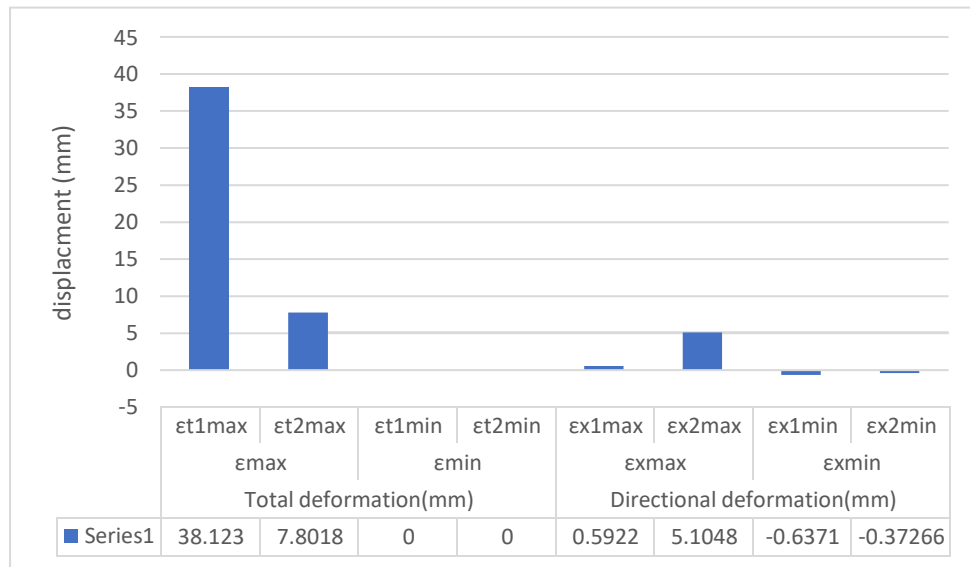


Figure 4.45 right cornering displacement comparison of the original structure with improved structure

4.4.4 Left cornering

Table 4.18 Comparison of displacement and stress values of the original structure with modified on left cornering analysis.

Normal stress(Mpa)	Σ_{\max}	$\sigma_{1\max}$	106
		$\sigma_{2\max}$	144.75
	Σ_{\min}	$\sigma_{1\min}$	-40.84
		$\sigma_{2\min}$	-56.32
Equivalent stress(Mpa)	$\Sigma_{v\max}$	$\sigma_{v1\max}$	153.33
		$\sigma_{v2\max}$	210.88
	$\Sigma_{v\min}$	$\sigma_{v1\min}$	0
		$\sigma_{v2\min}$	0
Total deformation(mm)	E_{\max}	$\epsilon_{t1\max}$	6.3194
		$\epsilon_{t2\max}$	8.689
	E_{\min}	$\epsilon_{t1\min}$	0
		$\epsilon_{t2\min}$	0
Directional deformation(mm)	$E_{x\max}$	$\epsilon_{x1\max}$	4.6852
		$\epsilon_{x2\max}$	0.71974
	$E_{x\min}$	$\epsilon_{x1\min}$	-0.34662
		$\epsilon_{x2\min}$	-5.97
Shear stress(Mpa)	T_{\max}	$\tau_{1\max}$	15.149
		$\tau_{2\max}$	20.83
	T_{\min}	$\tau_{1\min}$	-32.86

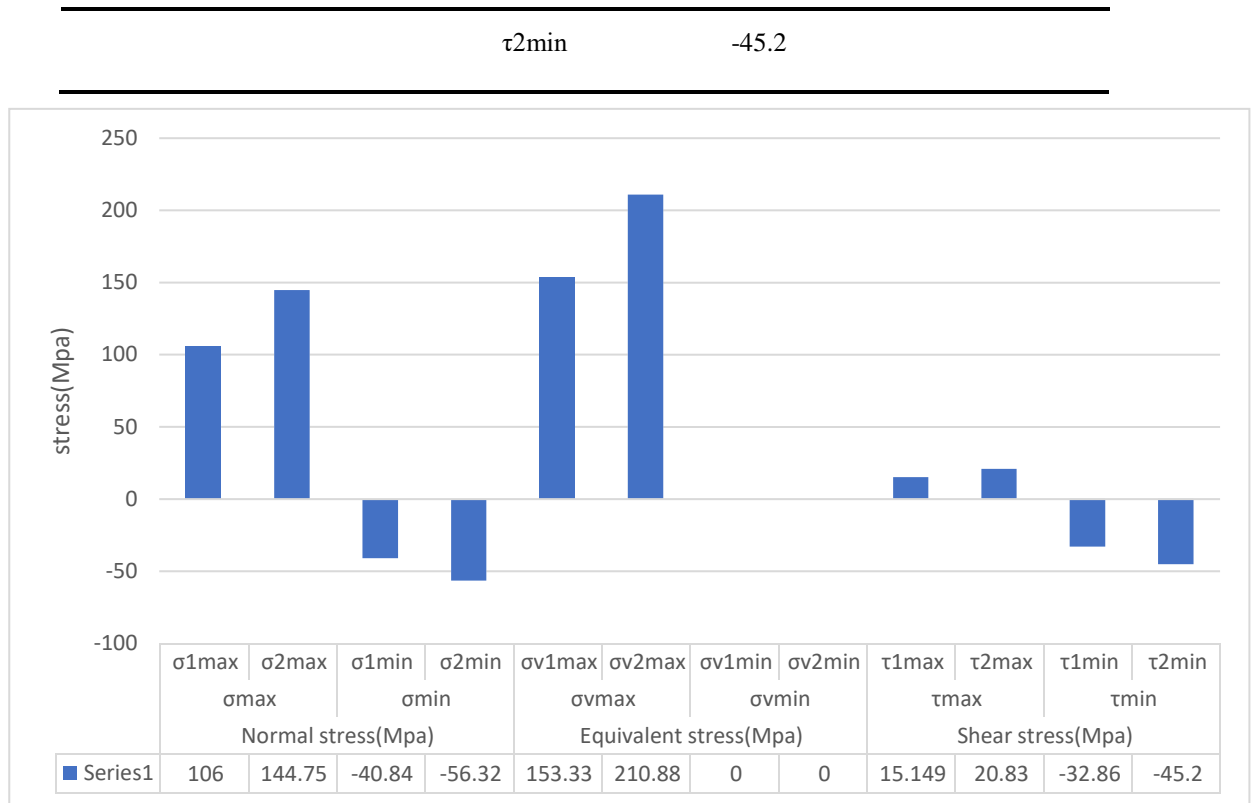


Figure 4. 46 left cornering stress comparison of the original structure with improved structure

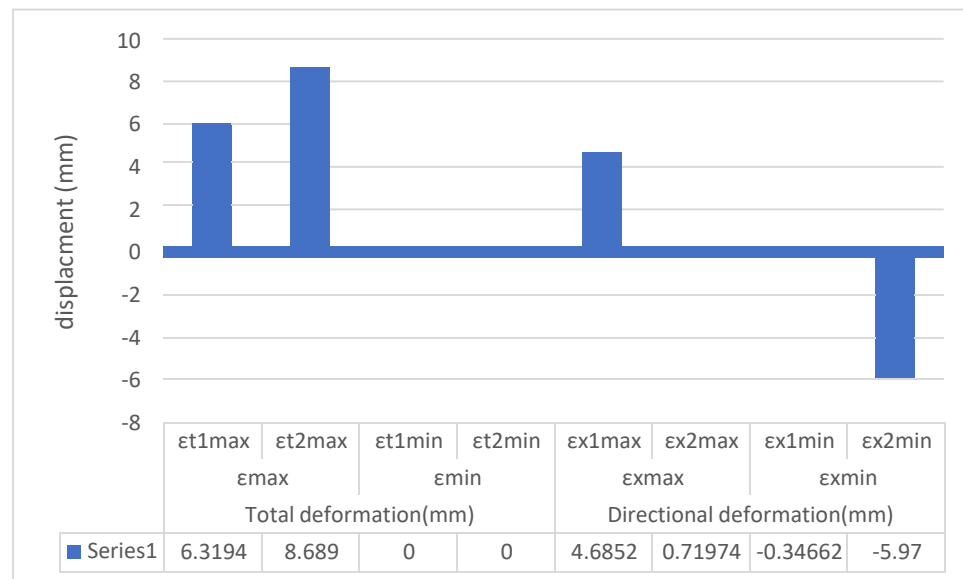


Figure 4.47 left cornering displacement comparison of the original structure with improved structure

5 CONCLUSION AND RECOMMENDATION

This chapter discussed the summary of works on present work, the conclusion drawn from the analysis, and the scope of future works.

5.1 Conclusion

In this research work, modeling and analysis of the metal body structure of Bishoftu City Bus were carried out and identified the possibility of a reduction in weight by optimization of the structure. The research work started with the measurement of the complete dimensions of the bus body, and from that, a model was created in Solid work for further analysis using ANSYS software. Through the analysis identified strong and weak points in the structure. The analysis is done through the longitudinal and lateral performance of braking and cornering loads and boundary conditions of the bus structure. The results obtained from the analysis give us room to further improve the bus structure by redesigning. In the improvement process, the members of the original structure are replaced with reduced thickness and cross-section profile. Accordingly, a new model was recreated using the reduced size elements and again analysis was carried out under the same loading conditions. The result of the analysis confirmed that the modified structure is safe in all aspects. Further, the total weight of the modified structure was calculated and compared with the weight of the original structure. It was found that the modified bus body structure weighs 93.577 kg less than the original body structure weight. The amounts to a 3.07% improvement in the weight without compromising the safety and performance of the vehicle. Based on the previous works of literature analogy, it is expected to reduce 2.4% fuel consumption and a 1.2 % reduction in emission. The procedure used for the analysis is validated using analytical calculations on a simply supported overhanging beam because the normal stresses and equivalent stress of the beam have close similarities in both numerical and analytical methods used.

5.2 Recommendation

The finding through this research is important to recommend to the automotive company which builds the bus structure. Worked with the newly improved structure helped the bus system with low consumption of fuel and efficiency due to weight decrement. Further improvement can make with removing some structure or welding effects of the structure by considering safe design consideration. At the company level, the cost of a newly improved structure is significantly lower, so it is recommended to use an improved structure. On an annual basis, the company will reduce its cost of production.

The analysis performed in this research is based on the existing shape and size of the bus. However, complete structural analysis and, thus, understanding of dynamic behavior of the vehicle in every situation required further analysis. Therefore, the following are recommended for future work as extensions and elaborations of this research:

- The shape of the structure is to be analyzed which has an aerodynamic effect on the structure.
- Welding quality while assembling the structure members is to be analyzed.
- The dynamic behavior of the structure during the rollover condition of the bus needs to be analyzed.
- The effects of the windshield and door structures on the overall stiffness characteristics of the vehicle structure also to be studied.
- Further redesign of the bus structure considering individual members.

REFERENCE

- [1] G. Heppeler, M. Sonntag, and O. Sawodny, "*Fuel Efficiency Analysis for Simultaneous Optimization of the Velocity Trajectory and the Energy Management in Hybrid Electric Vehicles*," IFAC, 2014, vol. 47, pp.375-381.
- [2] X. Tag, "Fuel consumption and CO₂ emissions from passenger cars in Europe À Laboratory versus real-world emissions I," *Prog. Energy Combust. Sci.*, 2017, vol. 60, pp. 97–131.
- [3] J. Benajes, A. García, J. Monsalve-serrano, and S. Martínez-boggio, "Optimization of the parallel and mild hybrid vehicle platforms operating under conventional and advanced combustion modes," *Energy Convers. Manag.*, vol. 190, no. February 2019, pp. 73–90.
- [4] L. Pelkmans and G. Lenaers, "Emissions and fuel consumption of natural gas-powered city buses versus diesel buses in real- city traffic Emissions and fuel consumption of natural gas-powered city buses versus diesel buses in real- city traffic," no. January 2015, pp 152-160.
- [5] M. Gupta Introduction, "Chapter 4 Static Structural Analysis," 2009, pp. 1–49.
- [6] M. Ross, "emissions : Effects of Vehicle and Driving Characteristics," 1994, pp. 75–112.
- [7] X. Jin, G. Yin, and N. Chen, "Advanced Estimation Techniques for Vehicle System Dynamic State : A Survey," 2019, pp. 1–26.
- [8] P. Taylor, K. Guo, D. Lu, S. Chen, W. C. Lin, and X. Lu, "Vehicle System Dynamics : International Journal of Vehicle Mechanics and The UniTire model : a nonlinear and non-steady-state tire model for vehicle dynamics simulation," no. May 2013, pp. 37–41.
- [9] V. Franc, G. Foucault, J. Cuilli, and R. Maranzana, "Adaptation of CAD model topology for finite element analysis," vol. 40, , 2008, pp. 176–196.

- [10] T. W. Soziales, "lecture notes Prof. Dr. Georg Rill © October 2003," no.FEB 2019.pp 16-19.
- [11] D. Singh, "Ride comfort analysis of passenger body biodynamics in active quarter car model using adaptive neuro-fuzzy inference system based super twisting sliding mode control," no. March 2019, pp 163-172.
- [12] S. Vaidya and C. Kulkarni, "Aerodynamic Development of a Formula Sae Car : Initial Design Stage," vol. 6, no. 12, 2017, pp. 14–18.
- [13] D Vanish "Essentials of Vehicle Dynamics" *vol 2, Feb 2015 pp. 141-152.*
- [14] A. You, M.Beuy, "Static load simulation analysis on chassis of the electric minibus integrated with the support frame of the removable battery pack by using Static Load Using FEA," vol. 06, 2019, pp 152-162.
- [15] N. Duarte, S. Alvarenga, V. R. Roso, and M. T. C. Faria, "Review of engine journal bearing tribology in start-stop applications," *Eng. Fail. Anal.*, vol. 108, no. November 2019, p. 104-344.
- [16] M. Lukac, F. Brumerick, L. Krzywonos, Z. Krzysiak, and M. E. Faculty, "Transmission system power flow model," vol. 19, 2017,pp. 27–31.
- [17] S. A. Gebremeskel, "Design, Simulation, and Prototyping of Single Composite Leaf Spring for Light Weight Vehicle," vol. 12, 2012 no. 7.pp 121-130.
- [18] G. Minak, "Structural Design and Manufacturing of a Cruiser Class Solar Vehicle," no. January 2019.pp 102-111
- [19] W. Hall, J. T. Mottram, and R. P. Jones, "Finite element simulation of a rolling automobile tire to understand its transient macroscopic behavior," vol. 218,2015. pp. 1393–1408
- [20] K. Daryabeigi, "AIM 99-1044 Analysis and Testing of High-Temperature Fibrous Insulation for Reusable Launch Vehicles 37th AIAA Aerospace Sciences Meeting" and Exhibit January ii -14, 1999 pp 245-251.

- [21] S. Kongwat, P. Jongpradist, and H. Hasegawa, “lightweight bus body design and optimization,” vol. 21, no. 4, 2020, pp. 981–991.
- [22] S. Kumar, A. K. Gupta, and P. Chandna, “static, dynamic and impact stress analysis of a bus body,” vol. 8, no. 1, 2018, pp. 733–744.
- [23] I. O. P. C. Series and M. Science, “Mode Shape Analysis of EV-Bus Chassis with Reverse Engineering Method Mode Shape Analysis of EV-Bus Chassis with Reverse Engineering Method,” 2019, pp 251-263.
- [24] F. Rebaïne, M. Bouazara, A. Rahem, and L. St-georges, “Static and Vibration Analysis of an Aluminium and Steel Bus Frame,” 2018 pp. 112–135.
- [25] Y. Ren, Y. Yu, B. Zhao, C. Fan, and H. Li, “Finite Element Analysis and Optimal Design for the Frame of SX360 Dump Trucks,” vol. 174, 2017, pp. 638–647.
- [26] K. Chinnaraj, M. S. Prasad, and C. L. Rao, “Experimental Analysis and Quasi-Static Numerical Idealization of Dynamic Stress on a Heavy Truck Chassis Frame Assembly,” vol. 14, 2008, pp. 271–280.
- [27] M. Seyedi, “Numerical assessment of occupant responses during the bus rollover test : A finite element parametric study,” 2019, pp 136-149.
- [28] K. Ashok, “dynamic analysis and design optimization of ladder chassis,” vol. 04, no. 12, 2020, pp. 10–21.
- [29] E. Sundberg, “Weight Optimization of a Composite Chassis for a Multimodal Lightweight Vehicle,” 2014pp. 152-169.
- [30] Y. Jung, S. Lim, J. Kim, and S. Min, “Lightweight design of electric bus roof structure using multi-material topology optimization,” 2019, pp 158-211.
- [31] F. Lan, J. Chen, and J. Lin, “Comparative analysis for bus side structures and lightweight optimization,” vol. 218, ,2017 pp. 1067–1075.
- [32] Z. Yang, B. Deng, M. Deng, and G. Sun, “A Study on Finite Element Analysis of Electric Bus Frame for Lightweight Design,” vol. 03049, 2018, pp. 1–4.

- [33] S. Lu, H. Ma, L. Xin, and W. Zuo, "Lightweight design of bus frames from multi-material topology optimization to cross-sectional size optimization," vol. 0273, 2018, pp 258-269.
- [34] J. Ahokas and S. Kosonen, "Dynamic Behaviour of a Tractor-trailer Combination during Braking," vol. 85, 2003, pp. 29–39.
- [35] F. Lan, J. Chen, and J. Lin, "Comparative analysis for bus side structures and lightweight optimization," no. October 2004, pp 165-198.
- [36] I. Journal, M. E. Issn, and P. Publishing, "No Title," vol. 14, no. 2, 2017, pp. 4196–4210.
- [37] V. R. Deulgaonkar, "International Journal of Vehicle Structures & Systems Finite Element Analysis and Experimental Simulation of Chassis Mounted Platform for Off-Road Wheeled Combat and Transport Utility Vehicles," vol. 10, no. 1, 2018, p. 4273.
- [38] L. Venkata and V. Gopala, "A New Design and Analysis of BUS Body Structure," no. August 2020, pp 89-98.
- [39] H. Zhang, G. Huang, and D. Yu, "Numerical modeling for the frame structure of light van-type electric truck," vol. 103, no. 2, 2020, pp. 1–27.
- [40] M. R. Chandra, S. Sreenivasulu, and S. A. Hussain, "Modeling and Structural analysis of heavy vehicle chassis made of polymeric composite material by three different cross-sections," vol. 2, no. 4, 2012, pp. 2594–2600.
- [41] H. Mohamed and A. Harrich, "bus-cad," no. August 2014, pp 356-369.
- [42] P. Kunakorn-ong, K. Ruangjirakit, P. Jongpradist, and S. Aimmanee, "Design and optimization of electric bus monocoque structure consisting of composite materials," vol. 0, no. 01, 2020, pp. 1–18.
- [43] Marco Cavazzuti and Luca Splendi "structural optimization of automotive chassis : theory, set up, design" Nov 2018 pp 96-124

- [44] T. A. Abegaz, "Weight optimization of bishoftu city bus (model zk6118hga) body frame structure," 2019 pp 1-121.
- [45] I. Iturrioz, "structural optimization of a bus in the rollover," 2018, pp 16-89.
- [46] K. Kamalakkannan, "Design and analysis of a bus body side frame 1," no. 4, 2016, pp. 8–10.
- [47] D. S. Kumar, "Rollover Analysis of Bus Body Structure as Per AIS 031 / ECE R66," 2018 pp. 1–7.
- [48] J.worth K. bruce "bus system analysis "mar 2015vol 01 pp 151-163
- [49] H. Wallentowitz, "Lecture Longitudinal Dynamics of Vehicles." vol 02 Feb 2014, pp 145-163
- [50] Thomas D. Gillespie "Fundamentals of Vehicle Dynamics ." 2011 pp 265-287.
- [51] T. D. Canonsburg, "ANSYS Mechanical APDL Structural Analysis Guide," vol. 3304, no. November 2013 pp. 724–746.

APPENDIX-A

Table A. 1 Part list of Bishoftu bus left side body frame

n o	Part number	Description	Q	length	total	kg
1	A5401-11100359	Front left end post J50X30X2.0/Q235-B	2	2539	5078	12.118
2	A5401- 14000035	Driver side fixture assemble J30*10*1-B	1	924	924	2.205
3	A5401-11100361	Post J60× 40×2 /Q235-B	2	1715	3430	9.262
4	A5401-11100362	Cushion pipe J30*10*1/235-B	1	1378.5	1378.5	0.822
5	A5401-11100363	Cushion pipe J30*10*1/235-B	1	893	893	0.533
6	A5401-12000033	Window post J80*40*2/235-B	1	1203.5	1203.5	4.384
7	A5401-12000035	Window post J80*40*2/235-B	2	1203.5	2407	8.767
8	A5401-12000034	Window post J80*40*2/235-B	7	1203.5	8424.5	30.685
9	A5401-11000269	Rear left side fixture post J80*40*2	1	2427	2427	8.84
10	A5401-14100532	U-Chanel cold rolled steel J80*40*2	1	1197	1197	4.36
11	A5401-11100378	Bottom post J60*52*2/235-B	1	1165.5	1165.5	3.952
12	A5401-15000041	Subordinate ridge F40*40*1.5- B	1	2422	2422	8.213

1 3	A5401-13100280	Bracing F40*40*1.5/235-B	1	1163.5	1163. 5	2.11
1 4	A5401-11100367	Bottom post J60*52*2/235-B	12	1167.5	14010	47.511
1 5	A5401-13100279	Oblique support F40*40*1.5/235-B	1	778	778	1.411
1 6	A5401-13100276	Bracing F40*40*1.5/235-B	4	515	2060	3.736
1 7	A5401-13100282	Oblique support F40*40*1.5/235-B	3	953	2859	5.184
1 8	A5401-15000042	Subordinate ridge J50*40*2/235-B	1	4144	4144	11.19
1 9	A5401-13100274	Oblique support F40*40*1.5/235-B	2	1255.5	2511	4.553
2 0	A5401-11000271	Bottom post J60*52*2/235-B	2	1207.5	2415	8.19
2 1	A5401-11000270	Front bottom post J60*52*2/235-B	2	1207.5	2415	4.09
2 2	A5401-15000040	Subordinate ridge J60*52*2/235-B	2	5188	10376	37.794
2 3	A5401-15000043	Left fixture beam J60*52*2/235-B	1	9926.5	9926. 5	33.663
2 4	A5401-13100273	Oblique support F50*40*2/235-B	3	553	1659	4.48
2 5	A5401-11100366	Window post J80*40*2/235-B	1	681	681	2.48
2 6	A5401-11100365	Short bottom post front J80*40*2/235-B	2	453	906	3.3
2 7	A5401-14100419	Ingle iron cold roll steel J80*40*2/235-B	1	253	253	0.922

2 8	A5401-15100400	Driving door frame beam J80*40*2/235-B	1	1162	1162	4.232
2 9	A5401-15000030	Subordinate ridge J80*40*2/235-B	1	1024	1024	3.73
				61	89293	272.71

Table A. 2 Part list of Bishoftu bus right side body frame

S/N	Part No.	Description	QT Y	length mm	Total .length	kg
1	A5401-14100537	Grooved cold rolled steel plate2.0/Q235-B	1	2472.6	2472.6	6.54
2	A5401-15100411	Lower beamJ50X40X2.0/Q235-B	1	472.8	472.8	1.25
3	PA33-00424M1	P75x50x25Q235-B Right middle waist beam	1	423.8	423.8	1.96
4	U040060010- 00424M1	Seat pre-buried plate cold rolled steel plat75x50*2.5/Q235-B	1	423.8	423.8	3.02
5	F020050050- 00424M1	beam F50X50X2.0/Q235-B	1	423.8	423.8	1.25
6	A5401-15000048	Side beam assemblyJ50X40X2.0/Q235-B	1	540.3	540.3	1.43
7	A5401-15100410	Right middle waist beam (2P75x50x25x10x2/Q235-B	1	1291.9	1291.9	5.98
8	A5401-15000047	Side beam assembly J50X40X2.0/Q235-B	1	3185.7	3185.7	1474

9	A5401-13100284	Diagonal supportF40X40X1.5/Q235-B	1	565	565	1.01
10	A5401-15100409	beam F50X50X2.0/Q235-B	1	2959.5	2959.5	5.97
11	J020030020- 01087M1	Battery door lower beamJ30X20X2.0/Q235- B	1	1087	1087	1.51
12	A5401-11100373	PadJ30X10X1.0/Q235-B	8	2489	19912	11.61
13	J010030010- 00060M1	PadJ30X10X1.0/Q235-B	4	1209	4836	2.885
14	J020070050- 00354M1	beamJ70X50X2.0/Q235-B	1	353.9	353.9	1.27
15	F020050050- 00354M1	beamF50X50X2.0/Q235-B	1	353.9	353.9	1.05
16	J020050040- 00354M1	Lower beamJ50X40X2.0/Q235-B	1	353.9	353.9	0.94
17	A5401-15000040	Side beam assembly J50X40X2.0/Q235-B	2	114.4	228.8	0.61
18	A5401-15000046	Right middle waist beam P75x50x25x10x2/Q235-B	1	1782.7	1782.7	8.25
19	J020070050- 01358M1	beamJ70X50X2.0/Q235-B	1	1358.9	1358.9	4.88
20	A5401-13100283	Wheel braceJ50X40X2.0/Q235-B	1	298.6	298.6	0.79
21	A5401-15000045	Side beam assembly J50X40X2.0/Q235-B	1	148.5	148.5	0.39
22	A5401-11100385	PadJ30X10X1.0/Q235-B	2	1169	2338	1.36

23	A5401-15000044	Side beam assemblyJ50X40X2.0/Q235-B	1	997.5	997.5	2.64
24	F020050050- 00060M1	Connecting pipeF50X50X2.0/Q235-B	6	2499	14994	44.4
25	A5401-11100384	Front door front pillaJ60X50X2.0/Q235-B	1	2499	2499	8.18
26	J015040020- 00139M1	Connecting pipeJ40X20X1.5/Q235-B	1	728	728	0.96
27	J020050040- 00728M1	beamJ50X40X2.0/Q235-B	1	2449	2449	6.49
28	A5401-11000283	Front door rear pillar assemblyJ60X40X2.0/Q235-B	1	2449	2449	7.25
29	A5401-11100382	Front door rear pillarJ60X40X2.0/Q235-B	1	2449	2449	7.25
30	A5401-12100048	Window columnJ60X40X2.0/Q235-B	1	1722.7	1722.7	5.1
31	J020050040- 01722M1	beamJ50X40X2.0/Q235-B	2	280	560	1.48
32	A5401-14000040	Side sign fixed square assembly cold rolled steel plate70X50X 3.0/Q235-A	2	1722.7	3445.4	18.89
33	F020040040- 00280M1	Connecting pipeF40X40X2.0/Q235-B	1	1205	1205	2.81
34	A5401-11100381	Front doorJ60X40X2.0/Q235-B	1	1205	1205	3.54

35	A5401-11000282	Middle door front column assemblyJ60X40X2.0	1	1205	1205	3.54
36	A5401-11000275	Front door rear pillar assemblyJ60X40X2.0/Q235-B	1	1129.5	1129.5	3.34
37	J020050040- 01139M1	beamJ50X40X2.0/Q235-B	1	1205	1205	3.19
38	U010137010- 00548M1	Sealed plate cold rolled steel plate60X40*2.0/Q235-B	2	1205	2410	7.13
39	A5401-12000035	Window column assemblyJ80X40X2.0/Q235-B	2	1205	2410	8.65
40	A5401-12000034	Window column assembly J80X40X2.0/Q235- B	7	1205	8435	30.27
41	J020050040- 01059M1	beamJ50X40X2.0/Q235-B	1	1339.9	1339.9	3.55
42	A5401-11000278	Rear door front column assemblyJ60X40X2.0/Q235-B	1	1205	1205	3.57
43	J020050040- 01340M1	beamJ50X40X2.0/Q235-B	2	1059.6	2119.2	5.61
44	A5401-11000274	Front door rear pillar assemblyJ60X40X2.0/Q235-B	4	423.8	1695.2	3.02
45	J020050040- 00424M1	beam J50X40X2.0/Q235-B	1	10972.5	10972. 5	29.05
46	J020050040- 10972M1	Right side beam J50X40X2.0/Q235-B	1	2422.6	2422.6	6.542

47	A5401-11000279	Right rear pillar assembly J50X40X2.0/Q235-B	1	1059.6	1059.6	2.861
				78	118123 .5	1757.8

Table A. 3 Part list of Bishoftu bus roof of the body frame

S/ N	Part No.	Name	QTY	length mm	To- length	kg
1	J020050040- 00098M1	Shelf beamJ50X40X2.0/Q235B	5	100	500	1.35
2	A5701-11000013	Top cover curved beam assembly 40*40*2.0/Q235B	10	2390	23900	57.035
3	A5701-00100174	StringerJ50X40X2.0/Q235B	2	832	1664	4.493
4	A5701-12100502	Groove cold rolled steel plate2.5/Q235B	2	832	1664	5.552
5	A5701-00100179	StringerJ50X30X1.5/Q235B	2	832	1664	3.409
6	A5701-00100175	StringerJ50X40X2.0/Q235B	2	1725	3450	9.316
7	A5701-12100503	Groove cold rolled steel plate2.5/Q235B	2	1725	3450	11.51
8	A5701-11100227	Top wind window curved beam J50X40X1.5/Q235B	5	615	3075	6.3
9	A5701-00100180	StringeJ50X30X1.5/Q235B	2	1725	3450	7.069

10	F020040040- 11037M1	Side beamF40X40X2.0/Q235B	2	1725	3450	8.233
11	A5701-00100181	StringerJ50X30X1.5/Q235B	2	1480	2960	5.368
12	A5701-13100103	Air conditioning fixed plate cold rolled steel plate3.0/Q235B	1	1480	1480	5.158
13	A5701-00100176	StringerJ50X40X2.0/Q235B	2	1480	2960	3.997
14	J015050030- 00100M1	Shelf beamJ50X30X1.5/Q235B	2	100	200	0.363
15	U015050030- 00620M1	Grooved cold rolled steel plate1.5/Q235B	2	620	1240	2.249
16	A5701-00100177	StringerJ50X40X2.0/Q235B	8	1170	9376	3.348
17	A5701-00100182	StringerJ50X30X1.5/Q235B	8	1170	9376	17.002
18	A5701-13100105	Air conditioning fixed plate cold rolled steel plate3.0/Q235B	1	1170	1170	4.078
19	U015050030- 01168M1	Grooved cold rolled steel plate1.5/Q235B	4	1170	4680	4.486
20	J015050030- 00300M1	Shelf beamJ50X30X1.5/Q235B	1	300	300	0.544
21	A5701-12100504	Groove cold rolled steel plate2.5/Q235B	6	1170	7020	20.665
22	A5701-12100505	Groove cold rolled steel plate2.5/Q235B	2	1340	2680	7.889
23	A5701-00100183	StringerJ50X30X1.5/Q235B	2	1340	2680	4.86

24	A5701-00100178	StringerJ50X40X2.0/Q235B	2	1340	2680	7.237
25	A5701-12100506	Groove cold rolled steel plate2.5/Q235B	2	380	760	2.536
26	J020050040- 00378M1	Shelf beamJ50X40X2.0/Q235B	2	380	760	2.052
27	U015050030- 00378M1	Grooved cold rolled steel plate1.5/Q235B	1	380	380	1.557
28	J015050030- 00378M1	Shelf beamJ50X30X1.5/Q235B	2	380	760	1.378
29	B0200050-00106M1	Fixed plate cold rolled steel plate50*106*2.0/Q235B	8	106	848	4.047
30	A5701-12100501	Groove cold rolled steel plate1.5/Q235B	2	865	1730	6.233
31	A5701-12100500	Groove cold rolled steel plate1.5/Q235B	4	1170	4680	16.863
32	A5701-13100107	Air conditioning fixed plate cold rolled steel plate3.0/Q235B	2	1170	2340	16.532
33	A5701-13100106	Air conditioning fixed plate cold rolled steel plate3.0/Q235B	2	1170	2340	16.532
34	Z020040015- 01168M1	Square cold rolled steel plate2.0/Q235B	2	1170	2340	11.168
35	A5701-13100104	Air conditioning fixed plate cold rolled steel plate3.0/Q235B	1	1170	1170	8.266

36	Z020040015-01478M1	Square cold rolled steel plate2.0/Q235B	2	1480	2960	14.127
37	A5701-12100499	Groove cold rolled steel plate1.5/Q235B	2	1480	2960	10.665
38	A5701-12100498	Groove cold rolled steel plate1.5/Q235B	2	820	1640	5.909
39	A5701-13100102	Air conditioning fixed plate cold rolled steel plate3.0/Q235B	1	1480	1480	10.456
40	B0400120-00270M1	Fixed plate hot rolled steel plate4.0/Q235B	2	1240	2480	17.521
41	A5701-12100497	Groove cold rolled steel plate120×270×1.5/Q235B	2	272.5	545	4.967
			116		125242	352.32

Table A. 4 Part list of Bishoftu bus floor body frame

S/N	Part No.	description	QTY	length mm	Total length	Mass Kg
1	9412- 015050050232	115×80×3	5	700	3500	31.157
2	9412- 015050050991	115×40×2	5	900	4500	26.988
3	9412- 015050050299	115×80×3	25	1400	35000	311.566
4	5101-38322	120×40×2	9	2392	21528	196.71
Total			44		64528	566.421

Table A. 5 Part list of Bishoftu bus front side body frame

S/N	Part No.	description	QTY	length mm	To length	Kg
1	6129s23-5301033	40×30×2.0	2	2503	5006	10.374
2	6129s23-5301027	40×30××2.0	3	2403	4806	4.98
3	6129s23-5301028	40×30×1.5	2	283	560	0.447
4	6129s23-5301029	20×40×1.5	6	143.9	8634	11.59
5	6129s23-5301030	30×20×1.5	2	2403	4806	5.32
Total			15	7735.9	23812	32.711

Table A. 6 Part list of Bishoftu bus rear side body frame

S/N	Part No.	Description	QTY	length mm	To-length	Kg
1	6129S01F-5801028	120×80×3.0	2	2900	5800	52.997
2	6129S01F-5801027	120×80×2.0	1	2361	2361	7.858
3	6129S01F-5801026	60×50×2.0	3	1000	3000	9.985
4	6129S01F-5801025	60×50×2.0	3	2361	7061	23.502
5	6129S01F-5801024	60×50×2.0	1	540	540	1.797
6	6129S01F-5801023	60×50×2.0	1	480	480	1.598
7	6129S01F-5801022	60×50×2.0	2	480	960	3.195
8	6129S01F-5801021	60×50×2.0	1	2600	2600	8.654
Total			14		22802	109.586

APPENDIX-B

Bus specification

- Overall dimension Width =2.55m Length=11.89m Height=3.27m
- Capacity including driver 61
- Wheel driver 4×2
- Wheelbase 6.4
- Maximum speed 80 k/h
- Fuel tank capacity 250L
- Engine type Diesel in line 6 cylinder
- Maximum torque 119 kg.m/1500rpm
- Maximum hours power 250 Hp/2300 rpm
- Gross vehicle weight 18000 kg